2018

# POLAR GIGANTISM AND SEA SPIDERS: A STUDY OF RESPIRATORY SCALING

Steven Joseph Lane

## Let us know how access to this document benefits you.

Follow this and additional works at: https://scholarworks.umt.edu/etd

Part of the Ecology and Evolutionary Biology Commons

POLAR GIGANTISM AND SEA SPIDERS: A STUDY OF RESPIRATORY SCALING

By

STEVEN JOSEPH LANE

M.S. Biology, Central Michigan University, Mt. Pleasant, Michigan, 2013
B.A. Biology, Spring Arbor University, Spring Arbor, Michigan, 2010

Dissertation

presented in partial fulfillment of the requirements
for the degree of

Doctor of Philosophy
In Organismal Biology, Ecology, and Evolution

The University of Montana
Missoula, MT

May 2018

Approved by:

Scott Whittenburg, Dean of The Graduate School
Graduate School

Dr. H. Arthur Woods, Chairperson
Division of Biological Sciences

Dr. Doug J. Emlen
Division of Biological Sciences

Dr. Scott R. Miller
Division of Biological Sciences

Dr. Amy L. Moran
University of Hawai'i, Department of Biology

Dr. Bret W. Tobalske
Division of Biological Sciences

ABSTRACT

*Lane, Steven, Ph.D., Spring 2018*          *Organismal Biology, Ecology and Evolution*

Polar Gigantism and Sea Spiders: A Study of Respiratory Scaling

Chairperson: Dr. H. Arthur Woods

  All animals must breathe to survive. The types of primary respiratory structures vary across the metazoa, and the overall size and components of these structures scale with body size. The scaling of respiratory structures has been well studied in vertebrate lungs and gills, but very few, if any studies, have looked at it in terms of cutaneous gas exchange, the process where oxygen moves across the outer integument via diffusion. My dissertation has sought to fill this gap in knowledge by studying animals that use cutaneous respiration, and my work has determined both how the components of their respiratory surfaces function and how they scale with body size. Using sea spiders as a model for cutaneous respiration, I answered these three specific questions: 1) How does a major but poorly studied group of marine arthropods exchange respiratory gases (Ch 1)? 2) How does the physiology and morphology underlying gas exchange scale with body size (Ch 2)? And 3) How do communities of organisms living on the surface of sea spiders (i.e., epibionts) affect their gas exchange and biomechanics (Ch 3 & 4)?
  Sea spiders (pycnogonids) are a globally distributed group of marine arthropods that span over five orders of magnitude in body size (Arnaud and Bamber, 1987). They lack gills and rely entirely on cutaneous respiration, which may be facilitated by pores in the cuticle (Davenport et al., 1987). The largest species live in the deep sea and around the poles, which also makes them a common and charismatic example of polar gigantism (Dell 1972), a biogeographic pattern describing the observation that taxa living near the poles often reach unusually large sizes. Sea spiders are an excellent group for studying the scaling of respiratory structures and gas exchange because they have a simple, tractable respiratory system, and there is great variation in body size across the group. Sea spiders have been studied for over a century, yet we still do not know the functional aspects of how they breathe nor how their respiratory surfaces have evolved to allow them to reach such large sizes.
  In chapter one, using a combination of empirical measurements and mathematical modeling, I show conclusively that sea spiders take up oxygen across pores in their cuticle. Furthermore, larger species obtain sufficient fluxes of oxygen not by increasing the number of pores in their cuticle, but rather by increasing the total pore volume across their body.
  In chapter two, I show that the scaling of respiratory components in sea spiders sets upper limits to body size. Cuticle porosity increases with body size, but it cannot increase indefinitely as a cuticle that is too porous may collapse due to external forces. Additionally, internal oxygen concentration decreases with increasing body size, but this concentration physically cannot go below zero. In addition, when levels of internal oxygen fall low enough, the animal likely fuels metabolism using anaerobic pathways, which is unsustainable for long periods. Therefore, these two variables constrain body

size, and the constraints cannot be overcome without some other innovation in the way that sea spiders exchange gases.

Finally, in chapters three and four, I show that the costs and benefits of epibionts vary with ambient conditions. When sea spiders are illuminated by sunlight, photosynthetic epibionts increase external oxygen levels, which may benefit their hosts by increasing the rate of oxygen flux into the sea spider's body. In the dark, encrusting epibionts reduce external oxygen levels and greatly reduce how quickly oxygen can diffuse into the sea spider, which will reduce the total inward flux of oxygen. These epibionts have no effect on host locomotion, but they increase the drag the animals experience, which likely increases the sea spider's risk of dislodgement or reduces their behavior during periods of high flow.

The surface of animals that exchange gases across their outer integument often serves two primary functions: gas exchange and structural support. These animals must balance a trade-off in which the integument is thin and porous enough to allow sufficient gas exchange but strong enough to withstand external forces. My dissertation shows that this trade-off can limit the maximum body size of these animals in multiple ways. Additionally, sea spiders are an important part of the Antarctic benthos and a common model for polar gigantism, yet little is known about their physiology and role in the ecosystem. My research provides an important first step in understanding the physiology of these animals that can help explain their role in the Antarctic ecosystem.

**References**

**Arnaud, F. and Bamber, R.N.** (1987) The biology of Pycnogonida. *Advances in Marine Biology* 24:1-96.

**Davenport, J., N. Blackstock, A. Davies, and M. Yarrington.** (1987). Observations on the physiology and integumentary structure of the Antarctic pycnogonid *Decolopoda australis*. *Journal of Zoology* 22: 451-465.

**Dell, R.K.** (1972). Antarctic benthos. In *Advances in Marine Biology*, Vol. 10 (ed. F. S. Russell 464 and M. Yonge), pp. 102-172. London: Academic Press.

TABLE OF CONTENTS

**Chapter 1:** Cuticular gas exchange by Antarctic sea spiders

Steven J. Lane[a], Amy L. Moran[b], Caitlin M. Shishido[b], Bret W. Tobalske[a], H. Arthur Woods[a]

[a]Division of Biological Sciences, University of Montana, Missoula, Montana 59812

[b]Department of Biology, University of Hawai'i at Mānoa, Honolulu, Hawai'i 96822

**Abstract**

Many marine organisms and life stages lack specialized respiratory structures, like gills, and rely instead on cutaneous respiration, which they facilitate by having thin integuments. This respiratory mode may limit body size, especially if the integument also functions in support or locomotion. Pycnogonids, or sea spiders, are marine arthropods that lack gills and rely on cutaneous respiration but still grow to large sizes. Their cuticle contains pores, which may play a role in gas exchange. Here, we examined alternative paths of gas exchange in sea spiders: 1) oxygen diffuses across pores in the cuticle, a common mechanism in terrestrial eggshells, 2) oxygen diffuses directly across the cuticle, a common mechanism in small aquatic insects, or 3) oxygen diffuses across both pores and cuticle. We examined these possibilities by modeling diffusive oxygen fluxes across all pores in the body of sea spiders and asking whether those fluxes differed from measured metabolic rates. We estimated fluxes across pores using Fick's law parameterized with measurements of pore morphology and oxygen gradients. Modeled oxygen fluxes through pores closely matched oxygen consumption across a range of body sizes, which means the pores facilitate oxygen diffusion. Furthermore, pore volume scaled hypermetrically with body size, which helps larger species facilitate greater diffusive oxygen fluxes across their cuticle. This likely presents a functional trade-off between gas exchange and structural support, in which cuticle must be thick enough to prevent buckling due to external forces but porous enough to allow sufficient gas exchange.

**Introduction**

Many animals exchange some or all of their respiratory gases across their outer integument (*i.e.*, skin or cuticle), a process known as cutaneous respiration (Graham, 1988; Feder and Burggren, 1985). The proportion of total gas exchanged across the outer integument varies across animals, especially among those that live in marine habitats (Feder and Burggren, 1985). Small animals, with relatively thin integuments and relatively low metabolic rates (e.g., flatworms and most marine larvae), rely on diffusion alone (Graham, 1988). By contrast, many larger marine organisms (e.g., many adult vertebrates and arthropods) have relatively thick integuments (skin or cuticle) such that oxygen diffusion alone cannot supply their relatively higher metabolic rates, which are distributed throughout larger volumes. Instead, these groups often have specialized and highly-ramified structures (e.g., gills) where most gas exchange occurs. Nevertheless, cutaneous respiration plays a role in all of these groups (Graham, 1988). For example, even in many adult fish, ~ 30% of oxygen uptake occurs across the integument (Weibel et al., 1998). Therefore, understanding the mechanisms of cutaneous respiration is important to understanding the physiology of marine animals.

We studied cutaneous respiration in sea spiders (phylum Arthropoda, class Chelicerata). Sea spiders are a basal group in the Arthropoda (Arango and Wheeler, 2007) that lack specialized respiratory structures such as gills, but nevertheless can grow to substantial sizes (Moran and Woods, 2012; Child, 1995; Arnaud and Bamber, 1987; Dell, 1972). Sea spiders have reduced thoraces and abdomens and many of their metabolically active tissues, like guts and gonads, are distributed into their legs (Davenport et al., 1987), which reduces the distance oxygen must travel through the body by diffusion. Although sea spiders have been studied for over 150 years (see reviews by Arnaud and Bamber, 1987; King, 1973), we still lack an understanding of the functional morphology of the cuticle as it relates to gas exchange. An obvious possibility is that oxygen diffuses via the pores that appear to cross the cuticles of most species (Fahrenbach, 1994; Davenport et al., 1987; King, 1973), but this idea has never been tested. Here, we test the role of cuticular pores in oxygen diffusion across the cuticle of sea spiders using a combination of empirical measurements and mathematical modeling.

There are several different avenues by which oxygen may cross the cuticle. First, as hypothesized by Davenport et al. (1987), oxygen may diffuse in through pores that cross the cuticle. In insects, the diffusion coefficient of oxygen through chitin is ~ 4 % that of the diffusion

coefficient through water (Krogh, 1919), which is too low for adequate diffusive supply of oxygen unless the cuticle is extremely thin (e.g., ~ 0.2-1.2 µm in the order Plecoptera, Resh et al. 2008). If the diffusion coefficient of oxygen through sea spider cuticle is similar to that of insect cuticle, then pores may permit much higher oxygen fluxes by reducing the amount of solid cuticle through which oxygen must diffuse. Pores in other cutaneous-respiring organisms appear to support almost all of the flux, especially when the integument is also used for support. For example, the pores in sea spiders are morphologically similar to those described from vertebrate and invertebrate eggshells (Rokitka and Rahn, 1987; Kern and Fergusen, 1997; Woods et al., 2005). These pores have been studied relatively extensively, and they do support almost all of the oxygen flux to the embryo (Wangensteen et al., 1971; Paganelli, 1980; Hinton, 1981; Tøien et al., 1988; Rahn and Paganelli, 1990).

Alternatively, cuticular pores may not facilitate oxygen flux; they may be incidental or have some other function (e.g., secretion). Cuticular pores have long been considered to have a secretory function (Fahrenbach 1994), and it is possible they serve a dual function (secretion and gas exchange). Sea spiders are chelicerates, and the structure of chelicerate cuticle is, in general, morphologically and chemically similar to the cuticles of insects and other arthropods (Davenport et al., 1987; Nentwig, 1987). The thickness of sea spider cuticle ranges from 20 to 150 µm, depending on body size (Lane et al. 2017), which is similar to observed thicknesses of insect cuticle (1 to more than 200 µm) (Vincent and Wegst, 2003) and slightly thicker than *Limulus* gill cuticle (3-10 µm) (Henry et al., 1996). Sea spiders, however, have unsclerotized and non-calcified cuticle and a microstructure that resembles the thin cuticle of the gills of *Limulus* and Malacostraca (Fahrenbach, 1994). These observations suggest that even non-porous sea spider cuticle may support high rates of oxygen diffusion. Therefore, sea spider cuticle may support relatively high diffusion coefficients of oxygen, or, at least in small sea spider species, it may be thin enough to permit adequate direct diffusion of oxygen even through chitin, as has been observed in many aquatic insects (Weis-Fogh, 1964; Eriksen, 1986; Kehl and Dettner, 2009; Seymour and Matthews, 2013).

Finally, there is an intermediate scenario: each of the two pathways, pores and cuticle, supports some flux. If so, then a third hypothesis is that their relative importance changes in a size-dependent way, where smaller species with relatively thin cuticle take up oxygen directly across the cuticle and through pores while larger species take up oxygen only through pores.

To determine whether pores permit most or all of the inward flux across a range of taxa and body sizes, we measured the density and size of pores and estimated the diffusive fluxes of oxygen across sea spider cuticle. Diffusive fluxes were estimated using a mathematical model based on Fick's law (Fick 1855; Tøien et al., 1988) that incorporated the shape of the pores and the oxygen gradient between the external and internal environments. This model allowed us to quantitatively estimate the rates of flux across individual pores, which, along with estimates of pore density, we scaled up to whole-animal fluxes of oxygen. We then compared the scaling of oxygen flux to the scaling of metabolic rate, to test the following three hypotheses (Fig. 1). H1: if pores facilitate most of the oxygen movement, then the total flux attributable to pores should closely match metabolic demand across a range of taxa and body sizes. H2: if the pores do not facilitate oxygen diffusion, then the total flux through pores should be lower than that of metabolic demand across a range of taxa and body sizes. H3: if the relative importance of pores varies in a size dependent way, then small individuals with thin cuticles may obtain sufficient oxygen directly across the cuticle, but large individuals with relatively thick cuticles obtain larger fractions through their pores.

**Materials and Methods**

We collected sea spiders while SCUBA diving at sites in McMurdo Sound, Antarctica in 2015 and 2016. Animals were brought to Crary Lab, McMurdo Station and kept in sea water tables at -1 to 0 °C (ambient seawater temperature ~ -1.8 °C). Individuals were used within two weeks of collection. We collected data from 10 different species of sea spiders in five different families (Ammotheidae: *Ammothea glacialis* (Hodgson, 1907), *A. longispina* (Gordon, 1932), *A. sp.*; Colossendeidae: *Colossendeis hoeki* (Gordon, 1944), *C. megalonyx* (Hoek, 1881), *C. Scotti* (Calman, 1915); Nymphonidae: *Nymphon australe* (Hodgson, 1902)*, Pentanymphon antarcticum* (Hodgson, 1904); Pallenopsidae: *Pallenopsis patagonica* (Hoek, 1881); Pycnogonidae: *Pycnogonum gaini*(Bouvier, 1910)). Because we do not know the age of the animals or time since last molt, the animals used in this study were chosen without bias to cuticle condition to try and minimize any variation in cuticle condition based on age or time since last molt.

*Morphological measurements*

We weighed and photographed each individual. Each individual was blotted dry, to remove excess water weight, and then weighed on a microbalance ($\pm$ 0.001 g). Photographs were taken of the dorsal side, the animal placed flat with its legs fully extended, using a Nikon D7100 digital camera (Nikon Inc, Melville, NY, USA) attached to a tripod. Surface areas were estimated in imageJ (v1.49, Rasband 2014) by tracing around the individual and multiplying by two. To account for the three-dimensional shape of the animal, we treated the body of a sea spider as an open cylinder with a calculated surface area as $S_3 = 2\pi rL$, where $r$ and L are the radius and length of a leg segment, versus the surface area of a two-dimensional rectangle ($S_2$) of the same diameter and length ($S_2 = 2 \times 2rL$). These two estimates of surface area are related by the expression, $\frac{S_3}{S_2} = \frac{\pi}{2}$, and so $S_3 = 1.57 \times S_2$, where $S_2$ was the surface area found using imageJ.

To measure cuticle thickness, or pore length ($x$, cm), we prepared multiple thin sections (< 1 mm each) of a single femur per individual using a razor blade. The thin sections were then mounted under a compound microscope and imaged (Zeiss Axioscope, Zeiss International, Germany). From those images, we extracted cuticle thickness, which closely approximates pore length. Values were averaged per individual and then per species. Images of each cross-section (e.g., Fig. 2A,C,E,G,I) were taken using a camera mounted on a compound microscope and then analyzed in imageJ.

We estimated pore density by taking multiple longitudinal sections of a single femur from each animal using a razor blade. Longitudinal images (e.g., Fig 2B,D,F,H,G) were taken using a camera mounted on a compound microscope (Zeiss Axioscope). In imageJ, pore density ($P$, pores cm$^{-2}$) was calculated as the total number of pores in a measured area, which were counted and averaged per individual and then per species. To calculate pore volume ($PV$, cm$^3$), the total volume of the cuticle that is porous, we calculated the average volume of a single pore and then multiplied it by the total number of pores for each animal. Total number of pores was estimated by taking pore density ($P$) and multiplying it by the surface area ($S_3$). As with pore density above, these values were averaged per species.

The above traits were measured in the femur of 10 different species. To determine whether cuticle and pore structure varied by leg segment, however, we also used the same methods to measure these traits on the 1$^{st}$ and 2$^{nd}$ tibias of three of those species: *Ammothea glacialis* (N = 8), *Colossendeis megalonyx* (N = 8), and *Nymphon australe* (N = 8).

*Oxygen gradient*

Internal oxygen levels were measured within a single femur from each individual sea spider (n = 46, 2 to 8 of each species) using a 100 µm tip Clark-style oxygen electrode (Unisense, Aarhus, Denmark) positioned using a micromanipulator. The leg was removed underwater at the proximal end of the third coxa, and the electrode tip was immediately advanced into the center of the femur. Each measurement took place within a water-jacketed glass platform. Seawater temperature was maintained at -1 °C using a recirculating water bath. We also measured external oxygen levels 1 cm away from the leg segment. The electrode was connected to a picoammeter (PA2000, Unisense), and data were recorded onto a computer running Expedata (v1.8.4, Sable Systems, North Las Vegas, NV, USA). Prior to each measurement, the electrode was calibrated in $N_2$ and air-saturated seawater at the measurement temperature (~ -1 °C). Internal $PO_2$ was then subtracted from external $PO_2$ to estimate the transcuticular oxygen gradient for each animal.

*Oxygen consumption*

We used data on oxygen consumption from Lane et al. 2017, which was obtained using closed-system respirometry. See Lane et al. 2017 for methods and data values.

*Model of oxygen flux through pores*

We estimated resistance to oxygen across the cuticular pores following the approach of Tøien et al. (1988), who analyzed diffusive resistance of bird eggshells using Fick's first law (Fick, 1855). We made 20 cross-sectional measurements across a single pore from each individual (Fig. 3). These measurements were made in at least three pores from each individual and then the estimated resistances were averaged together. We used ImageJ to perform a segment analysis of pore morphology. Pore shape can vary substantially within an individual (e.g. see Fig. 2C,I). For this analysis, however, we measured only pores that had the most common pore shape (shape shared by at least 65 % of total pores per species) for each given species (e.g. identified with "p" in Fig. 2A, C, E, G, I). We calculated resistance for a given cross-sectional segment using Fick's law:

$$R_{seg} = k * \frac{l\mathrm{p}}{A_n} \qquad (1)$$

where $R_{seg}$ is the resistance of each segment within the pore in kPa s µmol$^{-1}$ (Fig. 3), $\ell_p$ is the thickness of each cross-sectional segment in cm, and $A_n$ is the cross-sectional area of each segment in cm$^2$. $k$ is equal to $R*T/D$ in cm kPa s µmol$^{-1}$, where $R$ is the gas constant in cm$^3$ kPa µmol$^{-1}$ K$^{-1}$, $T$ is temperature in K, and $D$ is the diffusion coefficient of the body fluid within the pores in cm$^2$ s$^{-1}$. Because we did not know the diffusion coefficient of the fluid within the pores, we bracketed our results by running two separate models with different estimates of the diffusion coefficient. One model was run by calculating $k$ using the diffusion coefficient of seawater (9.86 $\times$ 10$^{-6}$ cm$^2$ s$^{-1}$) at the experimental temperature ($\sim$ 0 °C). This model used $k_w$ in place of $k$ to calculate each cross-sectional segment ($R_{seg}$, Eqn 1). The second model assumed that pores are filled with muscle tissue. Although pores likely do not contain muscle, the diffusion coefficients of oxygen in muscle are relatively well known and provide a lower limit for possible diffusion coefficients in our system. For this model, we set $k$ as $k_t$ for calculating resistance at each cross-sectional segment ($R_{seg}$, Eqn 1), $k_t$ was calculated using the diffusion coefficient of muscle tissue (3.95 $\times$ 10$^{-6}$ cm$^2$ s$^{-1}$). We estimated the diffusion coefficient of oxygen through muscle tissue based on Krogh (1919) and Davenport et al. (1987), who estimated that the diffusion coefficient of muscle tissue is approximately 40 % that of seawater.

All studied species had a small layer of cuticle separating the top of the pore from the external environment. We estimated the resistance of this thin piece of cuticle as:

$$R_{cuticle} = k_c * \frac{lc}{A_c} \tag{2}$$

Where $k_c$ is the constant $k$ described above calculated using the diffusion coefficient of oxygen in chitin. This diffusion coefficient was also estimated based on Krogh (1919), where he calculated that the diffusion coefficient through chitin is approximately 4 % that of seawater (3.95 $\times$ 10$^{-7}$ cm$^2$ s$^{-1}$). $\ell_c$ is the thickness of the cuticle layer (measured in imageJ), and $A_c$ is the cross-sectional area of the cuticle directly above the pore.

Like Tøien et al. (1988), we also included boundary layer resistances at the top and bottom of the pore ($R_{top}$ and $R_{bot}$, fig 2, respectively) using Stefan's law (Meidner and Mansfield, 1968):

$$R_{top} = k_w * \frac{1}{2*d_c} \tag{3}$$

Where, in $R_{top}$, $d_c$ is the diameter of the top of the pore (top cross-sectional measurement, Fig. 3) and $k_w$, which was calculated using the diffusion coefficient of seawater. $R_{bot}$ was calculated similarly, except it used the constant $k_w$ or $k_t$ (depending on the model), and $d_{20}$, in place of $d_c$, which was the diameter of the bottom of the pore. We estimated total resistance by summing the resistances for all the middle segments ($R_{cuticle}$ and $R_{seg}$) and the boundary layer resistances ($R_{top}$ and $R_{bot}$) ($R_{tot}$, Fig. 3). And from $R_{tot}$, we calculated conductance through a single pore ($G_p$, µmol $s^{-1}$ $kPa^{-1}$):

$$G_p = \frac{1}{R_{tot}} \tag{4}$$

where conductance is a measure of how fast oxygen moves across a material given a difference in partial pressures (Dejours, 1981).

The diffusive oxygen flux through a single pore ($J_p$, µmol $s^{-1}$) was then calculated using Fick's first law (Dejours, 1981):

$$J_p = G_p * \Delta PO_2 \tag{5}$$

where $\Delta PO_2$ is the oxygen gradient in kPa, and $J_p$ is the number of moles moving across a single pore per unit time. We then scaled this up to the whole body ($J_a$) by multiplying the diffusive flux across a single pore by the density of pores ($P$, pores $cm^{-2}$) and then the total calculated surface area of the animal ($S_3$, $cm^2$):

$$J_a = J_p * (P * S_3). \tag{6}$$

We then compared whole body flux for a given species to the species oxygen consumption (Lane et al., 2017) to determine how well the total diffusive oxygen flux through the pores matches the whole animal's oxygen uptake.

8

Because most oxygen uptake occurs across the sea spider's legs (Davenport et al., 1987), we focused our analyses on the pore morphology and physiology of the major leg segments. To determine if there was any variation among segments within individuals and species, we estimated oxygen conductance through an average pore on the femur, $1^{st}$ tibia, and $2^{nd}$ tibia of three species (*Ammothea glacialis* (n = 8), *Colossendeis megalonyx* (n = 8), and *Nymphon austral* (n=3-4)) following the methods described above. Using a linear mixed effects model, with individual as a random factor, we did not find any differences between leg segments for any of the three species for any of the measured variables (Table S1, S3). We therefore used pore characteristics from just the femur of each species, which were extrapolated to the whole animal using equation 6.

*Statistical analyses*

For all scaling analyses, we measured body mass, pore diameter, pore length, pore density, oxygen flux, and oxygen consumption in 10 different species (from five different families) of sea spiders (Tables S4-5). To compare how those traits changed with body size, we $log_{10}$-transformed the data and fitted ordinary least squares regressions (OLS). For each trait, we took the average measurements from 2 to 8 individuals, which varied depending on the trait. However, for several species (*Ammothea* sp., *Colossendeis hoeki*, *Pallenopsis patagonica*, *Pentanymphon antarcticum*, and *Pycnogonum gaini*), we collected data on pore density from only one individual.

To account for potential phylogenetic effects on traits, we also conducted phylogenetic least square regressions (PGLS) on the data following the procedures of Lane et al. (2017). We constructed trees using mitochondrial cytochrome c oxidase (CO1) sequences collected from our samples and then conducted PGLS analyses using: (1) an unconstrained phylogeny built from our CO1 data (PGLS-mtCO1), and (2) a constrained phylogeny following the tree topology of Arango and Wheeler (2007) in which branch lengths were free to vary based on our CO1 data (PGLS-var. brlens). The tree from Arango and Wheeler (2007) was constructed using three nuclear and three mitochondrial genes from 63 different species, representing all 9 sea spider families. We also created a third tree using the constrained topology in (2) but with equal branch lengths (PGLS-equal brlens). As in the OLS models described above, we used species averages and $log_{10}$-transformed the data prior to running each PGLS model.

We then used Pagel's Lambda (Pagel, 1999) to test for phylogenetic signal. Only two variables showed a significant phylogenetic signal (pore diameter and pore density, Table S2). In the two cases where we detected a phylogenetic signal, the PGLS model results are reported in text and figures (only PGLS-equal brlens are reported, for brevity), otherwise, the OLS results were reported (see Table 1 and Table S2 for full results).

All statistical analyses were conducted in R (v3.3.0) (R Core Team 2016) and the PGLS models were conducted using the R package 'ape' (v3.5) (Pagel, 1992). Data are reported as means ± standard error.

## Results

*Interspecific variation in pore morphology*

A phylogenetic signal was detected for pore diameter ($d$, µm), pore density (*PD*, pores cm$^{-2}$), and pore volume (*PV*, cm$^3$) with the PGLS-equal brlens model (Table S2), so the PGLS results are presented here, while no signal was detected for pore length ($x$, µm) (Table S2), so the OLS results are presented here (see Table 1 for regression summary of all models). Pore length and pore diameter both increased with body size (Fig. 4A,B, respectively, Table 1). The relationship between pore length ($x$, µm) and body size ($M$, g) is $x = -2.30 \times M^{0.37}$. For pore diameter ($d$, µm) the relationship with body size is $d = 1.17 \times M^{0.30}$. Pore density decreased slightly with increasing body size as $PD = 4.32 \times M^{-0.23}$ (Fig. 4C). *Pycnogonum gaini*, which had substantially fewer pores per square centimeter than expected for its body size (over one order of magnitude lower), was treated as an outlier and was not included in the pore density analysis. Total pore volume of the entire cuticle (*PV*, cm$^3$) increased with increasing body size as $PV = -2.56 \times M^{1.35}$ (Fig. 4D).

*Oxygen flux and oxygen consumption*

We did not observe significant differences when diffusive oxygen flux was estimated using an assumed diffusion coefficient for water or tissue (Table 1). Therefore, for brevity, only the tissue model is described here.

Diffusive oxygen flux across the cuticular pores and oxygen consumption both increased with body size (Fig. 5, Table 1). The relationship between oxygen flux ($J_a$, µmol s$^{-1}$), using the tissue model, and body size is $J_a = -4.13 \times M^{1.01}$. The relationship between oxygen consumption

($OC$, µmol s$^{-1}$) and body size is $OC = -3.96 \times M^{0.80}$. Furthermore, the regression coefficient for slope and intercept did not vary between oxygen flux and oxygen consumption based on overlapping confidence intervals (Table 1).

**Discussion**

Although we cannot formally disprove hypothesis 2, that gas exchange occurs across solid cuticle, our data supports hypothesis 1, that sea spiders take up oxygen primarily via cuticular pores. Broadly speaking, there was a close match between the scaling of known rates of oxygen uptake (based on our measurements of metabolic rate; Lane et al., 2017) and the scaling of calculated rates of oxygen flux via pores. Those fluxes match closely over two orders of magnitude in body size. Nevertheless, our data also suggest some size-dependence of the relative contribution of pore-based fluxes (H3, Fig 1). In large-bodied species, estimated pore-based fluxes were higher than measured metabolic rates, whereas in small-bodied species they were lower (Figure 4). This pattern suggests that large-bodied species rely more exclusively on pore-based fluxes of oxygen. The broad confidence intervals in our data (Table 1) preclude distinguishing hypotheses 1 and 3 more quantitatively.

The size dependence of oxygen uptake via pores emerges from the scaling of pore morphology. Larger species have thicker cuticle (as described by pore length), which decreases flux by increasing the distance that oxygen must move. Cuticle thickness and pore diameter scaled approximately as expected for geometric similarity (b = 0.37 and b = 0.30, respectively). Pore density decreased slightly with increasing body size (b = -0.23). Pore volume, however, scaled with a larger coefficient (b = 1.35) than expected for geometric similarity (b = 1.00, Schmidt-Nielsen, 1984). This means, that to offset the decrease in flux associated with thicker cuticle, larger species have wider pores which results in greater total pore volume.

Rather than possess high pore density, one of the species in our study—*Pycnogonum gaini*—maintains adequate diffusive oxygen flux with relatively few but large pores. For its body size, *Pycnogonum gaini* (Fig. 2E) has substantially fewer pores per square area than expected, which would convey relatively low oxygen flux. Nevertheless, it meets its required diffusive fluxes of oxygen by also having much wider pores than expected for its body size.

The boundary layer resistances above and below the pores conferred little resistance to oxygen movement (Table S6). Therefore, flow conditions across the outer cuticle or within the

11

hemolymph likely have little effect on total oxygen flux. Conversely, in most species, the cuticular cap conferred the greatest resistance to oxygen diffusion. For example, in the three *Colossendeis* species, resistance across the cuticular cap accounted for over 80 % of the total resistance. The thickness of this cap can play a large role in restricting oxygen flux. Colonizing organisms, such as bryozoans, could increase the functional thickness of the cuticle and greatly decrease oxygen flux. We are currently testing the effects of different colonizing organisms on sea spider gas exchange.

To calculate resistances at the top and bottom of each pore, we used Stefan's law. This is appropriate when the diffusing molecule enters or leaves the pore from a concentration gradient distributed hemispherically around the pore opening. This is possible only if the pore openings are spaced far enough apart—otherwise, the hemispherical concentration gradients interfere with one another, which has the effect of raising the total resistance (Brown and Escombe, 1900; Ting and Loomis, 1963). In general, Stefan's law is thought to hold if pore openings are spaced more than 10 diameters apart. In our study, pore openings on the external cuticle met this assumption (data not shown). Conversely, pore openings on the internal side of the cuticle generally were closer than 10 diameters from one another, thus violating the Stefan assumption. Theoretically, this raises the total resistance provided by the internal layers of hemolymph. We decided, however, to ignore this problem—both because the calculated internal resistances are on the order of 1% of the total resistance, and because agitation of the hemolymph by gut peristalsis (Woods et al. 2017) probably reduces this resistance anyway.

The presence of pores in the cuticle likely presents a functional trade-off between gas exchange and structural support: more total pore volume supports greater fluxes of oxygen but likely also weakens the cuticle. Alternatively, thicker cuticle provides greater strength, but it reduces the rate of diffusive oxygen flux by lengthening the pores. While many studies have discussed the relationship between shell thickness, shell material composition, and structural support in eggshells (Ar et al., 1979; Board and Scott, 1982; Board, 1980), few have tested the relationship between structural support and porosity. Tyler (1955) discussed that the distribution of pores in avian egg shells, ~ 2 pores per square millimeter, may help reduce the number of weak areas in an egg shell as areas of greater pore density would be weaker and act as sites for crack propagation. The relationship between structural support and pore shape has also been studied in vertebrate bones and engineered materials. In vertebrate bones, increasing porosity

lowers fracture strength, the ability of a material to withstand breaking, because pores reduce the load bearing area of the bone (Yeni et al., 1997). In metallic glass, an amorphous metal used in electronics and medical devices, and ceramic microsieves, material used in microfiltration, the diameter of the pore affects material strength; wider pores yield weaker material strength because the edge of the pore is the weakest point, so pores with larger diameters will be weaker than those with smaller diameters (Gao et al., 2016; Kuiper et al., 2002).

The structure of sea spider cuticle may therefore present an evolutionary compromise to minimize strength reduction while maintaining sufficient oxygen flux, as we have hypothesized recently (Lane et al., 2017). In an absolute sense, large sea spiders have thicker cuticle, which provides greater strength but also long distances over which oxygen must diffuse. Large species, therefore, must have larger average diameter pores to offset the resistance to oxygen flux arising from these long distances, which may weaken the cuticle. The species of *Colossendeis* and *Ammothea* are the largest-bodied individuals in our analyses, and they have many conical pores, with the small aperture near the surface of the cuticle. This pore design may allow these species to grow to relatively large sizes by minimizing the structural weakness associated with pores, because conical pores concentrate chitinous material away from the central axis and therefore offer greater polar moments of area (Vogel, 2013) relative to the same pore areas distributed by cylinder pores. We are presently testing the structural integrity of sea spider cuticles with different pore shapes and densities.

In conclusion, sea spider cuticle is not solid but rather contains many pores (Fahrenbach, 1994; Davenport et al., 1987). The volume and density of pores both scale with body size to allow sufficient oxygen into the body to meet the sea spider's metabolic demands, especially for larger-bodied species. Future studies should examine sea spiders from different environments, such as those living in temperate or tropical locations or those living in the intertidal zone, to see if pore structure changes with temperature or likelihood of strong external forces. For instance, because higher temperatures stimulate metabolic rates more than they do rates of diffusive flux (Woods, 1999; Verberk, 2011), we predict that, for their small body sizes, tropical species will have higher conductance cuticles, which could be achieved by thinner or more porous cuticle. The trade-off discussed above may be more acute for warm-water species, as those living in the intertidal zone and other areas with higher current may be more at risk from external forces (e.g.,

tide cycles, current surges) and may need proportionately thicker cuticle with fewer pores to prevent structural damage.

## Competing Interests

No competing interests declared.

## Data availability

Data are available from the supplementary information associated with this manuscript.

**List of abbreviations and symbols used**

|  | Definition | Units |
|---|---|---|
| $\Delta PO_2$ | oxygen gradient | kPa |
| $A_c$ | cross-sectional area of cuticle segment at top of pore | $cm^2$ |
| $A_n$ | cross-sectional area of segment within pore | $cm^2$ |
| $D_c$ | diffusion coefficient of oxygen in cuticle | $cm^2\ s^{-1}$ |
| $D_t$ | diffusion coefficient of oxygen in tissue | $cm^2\ s^{-1}$ |
| $D_w$ | diffusion coefficient of oxygen in water | $cm^2\ s^{-1}$ |
| $d$ | diameter of segment within model | cm |
| $G_p$ | conductance through single pore | $\mu mol\ s^{-1}\ kPa^{-1}$ |
| $J_a$ | oxygen flux through pores across whole body | $\mu mol\ s^{-1}$ |
| $J_p$ | oxygen flux through a single pore | $\mu mol\ s^{-1}$ |

| | | |
|---|---|---|
| $k_c$ | $RT/D_c$ | cm kPa s $\mu$mol$^{-1}$ |
| $k_t$ | $RT/D_t$ | cm kPa s $\mu$mol$^{-1}$ |
| $k_w$ | $RT/D_w$ | cm kPa s $\mu$mol$^{-1}$ |
| $\ell_c$ | thickness of segment of cuticle above pore | cm |
| $\ell_p$ | thickness of segment within pore | cm |
| P | density of pores | cm$^{-2}$ |
| PV | pore volume across whole animal | cm$^3$ |
| R | gas constant | cm$^3$ kPa $\mu$mol$^{-1}$ K$^{-1}$ |
| $R_{bot}$ | boundary layer resistance at bottom of pore | kPa s $\mu$mol$^{-1}$ |
| $R_{cuticle}$ | resistance of thin piece of cuticle at top of pore | kPa s $\mu$mol$^{-1}$ |
| $R_{seg}$ | resistance of each segment within pore | kPa s $\mu$mol$^{-1}$ |
| $R_{top}$ | boundary layer resistance at top of pore | kPa s $\mu$mol$^{-1}$ |
| $R_{tot}$ | total summed resistances | kPa s $\mu$mol$^{-1}$ |
| $S_3$ | surface area of whole animal based on 3-d shape | cm$^2$ |
| T | temperature | K |
| x | Cuticle thickness or pore length | cm |

## References

**Ar, A., Rahn, H., and Paganelli, C.V.** (1979) The avian egg: mass and strength. *The Condor* 81: 331-337.

**Arango, C.P. and Wheeler, W.C.** (2007) Phylogeny of the sea spiders (Arthropoda, Pycnogonida) based on the direct optimization of six loci and morphology. *Cladistics* 23: 255-293.

**Arnaud, F. and Bamber, R.N.** (1987) The biology of Pycnogonida. *Adv Mar Biol* 24:1-96.

**Board, R.G.** (1980) Properties of avian egg shells and their adaptive value. *Biol Rev* 57: 1-28.

**Board, R.G. and Scott, C.D.** (1980) Porosity of the avian eggshelf. *Am Zoo* 20: 339-349.

**Blomberg, S.P., Garland Jr, T., and Ives, A.R.** (2003) Testing for phylogenetic signal in comparative data: behavioral traits are more labile. *Evolution* 57: 717-745.

**Brown, H.T. and Escombre, F.** (1900) Static diffusion of gases and liquids in relation to the assimilation of carbon and translocation in plants. *Phil Trans Roy Soc London* 193B: 223-291.

**Child, C.A.** (1995). Antarctic and subantarctic pycnogonids. Nymphonidae, Colossendeidae, Rhynchothoracidae, Pycnogonidae, Endeidae and Callipallenidae. In Biology of Antarctic Seas XXIV, Antarctic Research Series, Vol. 69 (ed. S. D. Cairns), pp. 1-165. Washington, DC: American Geophysical Union

**Davenport, J., Blackstock, N., Davies, D.A., and Yarrington, M.** (1987) Observations on the physiology and integumentary structure of the Antarctic pycnogonid *Decolopoda australis*. *J Zool* 211: 451–465.

**Dejours, P.** (1981) *Principles of comparative respiratory physiology*. Amsterdam: Elsevier/North-Holland Biomedical Press. pp. 265.

**Dell, R.K.** (1972). Antarctic benthos. In *Advances in Marine Biology*, Vol. 10 (ed. F. S. Russell and M. Yonge), pp. 102-172. London: Academic Press.

**Eriksen, C.H.** (1986) Respiratory roles of caudal lamellae (gills) in a Lestid damselfly (Odonata:Zygoptera). *Journal of the North American Benthological Society* 5: 16–27.

**Fahrenbach, W.H.** (1994) Microscopic anatomy of Pycnogonida: I. cuticle, epidermis, and muscle. *J Morph* 222: 33-48.

**Feder M.E. and Burggren, W.W.** (1985) Skin Breathing in Vertebrates. *Sci Am* 253:126-142.

**Fick, A.** (1855) Ueber diffusion. *Ann Phys* 170(1):59–86

**Gao, M., Dong, J., Huan, Y., Wang, Y.T., and Wang, W.H.** (2016) Macroscopic tensile plasticity by scalarizating stress distribution in bulk metallic glass. *Sci. Rep.* 6: 21929.

**Graham, J.B.** (1988) Ecological and evolutionary aspects of integumentary respiration: body size, diffusion, and the invertebrata. *Amer Zool* 28: 1031-1045.

**Henry R.P., Jackson, S.A., and Mangum, C.P.** (1996) Ultrastructure and transport-related enzymes of the gills and coxal gland of the horseshoe crab *Limulus Polyphemus*. *Biol Bull* 191: 241-250.

**Hinton, H.E.** (1981) *Biology of insect eggs. Volume 1*. Pergammon Press. Elmsford, NY 473 p.

**Kehl, S. and Dettner, K.** (2009) Surviving submerged-setal tracheal gills for gas exchange in adult rheophilic diving beetles. *J Morph* 270: 1348-1355.

**Kern, M.D. and Ferguson, M.W.J.** (1997) Gas permeability of American alligator eggs and its anatomical basis. *Physiol Zool* 70:530–546.

**King, P.E.** (1973) *Pycnogonids*. Hutchinson, London. 144 p.

**Krogh, A.** (1919) The rate of diffusion of gases through animal tissues, with some remarks on the coefficient of invasion. *J Phys* 52: 391-408.

**Kuiper, S., Brink, R., Nijdam, W., Krijnen, G.J.M., and Elwenspoek, M.C.** (2002) Ceramic microsieves: influence of perforation shape and distribution on flow resistance and membrane strength

**Lane, S.J., Shishido, C.M., Moran, A.L., Tobalske, B.W., Arango, C.P., and Woods, H.A.** (2017) Upper limits to body size imposed by respiratory-structural trade-offs in Antarctic pycnogonids. *Proc R Soc B* 284: 20171779. http://dx.doi.org/10.1098/rspb.2017.1779.

**Meidner, H. and Mansfield, T.A.** (1968) *Physiology of stomata*. New York, McGraw Hill.

**Moran, A.L. and Woods, H.A.** (2012) Why might they be giants? Towards an understanding of polar gigantism. *J Exp Biol* 215: 1995-2002.

**Nentwig, W.** (1987) *Ecophysiology of spiders*. Springer-Verlag, Berlin. 447 p.

**Paganelli, C.V.** (1980) The physics of gas exchange across the avian eggshell. *American Zoologist* 20: 329-338.

**Pagel, M.D.** (1999) Inferring the historical patterns of biological evolution. *Nature* 401: 877-884.

**Pagel, M.D.** (1992) A method for the analysis of comparative data. *J theor Biol* 156: 431-442

**R Core Team** (2016). R: A language and environment for statistical computing (R Foundation for Statistical Computing, Vienna, Austria).

**Rahn, H. and Paganelli, C.V.** (1990) Gas fluxes in avian eggs: driving forces and the pathway for exchange. *Comp Biochem Physiol* 95A: 1-15.

**Rasband, W.S.** (2014) ImageJ [Online]. U. S. National Institutes of Health, Bethesda, MD. Available: http://imagej.nih.gov/ij/ [2015, June 1].

**Resh, V.H., Buchwater, D.B., Lamberti, and Eriksen, C.H.** (2008) Aquatic insect respiration. Pp 39-54 in Merritt, R.W., Cummins, K.L., and Berg, M.B. eds. *An Introduction to the Aquatic Insects of North America* 4th ed. Dubuque, IA: Kendall/Hunt Pub Co.

**Rokitka, M.A. and Rahn, H.** (1987) Regional differences in shell conductance and pore density of avian egg eggs. *Resp Phys* 68: 371-376.

**Schmidt-Nielsen, K.** (1984) *Scaling: why is animal size so important?* Cambridge: Cambridge University Press. pp 241.

**Seymour, R.S. and Matthews, P.G.D.** (2013) Physical gills in diving insects and spiders: theory and experiment. *J Exp Biol* 216: 164-170.

**Simkiss, K.** (1986) Eggshell conductance – Fick's or Stefan's law? *Resp Phys* 65: 213-222.

**Ting, I.P. and Loomis, W.E.** (1963) Diffusion through stomates. *Am J Bot* 50:866-872.

**Tøien, Ø., Paganelli, C.V., Rahn, H., and Johnson, R.R.** (1988) Diffusive resistance of avian eggshell pores. *Resp Phys* 74: 345-354

**Tyler, C.** (1955) Studies on eggshells. IV. The distribution of pores in eggshells. *J Sci Food Agric* 6: 170-176.

**Verberk, W.C.E.P., Bilton, D.T., Calosi, P., and Spicer, J.I.** (2011) Oxygen supply in aquatic ectotherms: partial pressure and solubility together explain biodiversity and size patterns. *Ecology* 92: 1565-1572.

**Vincent, J.F.V. and Wegst, U.G.K.** (2004) Design and mechanical properties of insect cuticle. *Arthropod Struct Dev* 33: 187-199.

**Vogel, S.** (2013) *Comparative biomechanics: life's physical world*. Princeton University Press.

**Wangensteen, O.D., Wilson, D., and Rahn, H.** (1971) Diffusion of gases across the shell of the hen's egg. *Resp Phys* 11: 16-30.

**Weis-fogh, T.** (1964) Diffusion in insect wing muscle, the most active tissue known. *J Exp Biol* 41: 229-256.

**Woods, H.A.** (1999) Egg-mass size and cell size: Effects of temperature on oxygen distribution. *Am Zool* 39: 244-252.

**Woods, H.A., Bonnecaze, R.T., and Zrubek, B.** (2005) Oxygen and water flux across eggshells of *Manduca sexta*. *J Exp Biol* 208:1297–1308.

**Woods, H.A., Lane, S.J., Shishido, C., Tobalske, B.W., Arango, C.P., and Moran, A.L.** (2017). Respiratory gut peristalsis by sea spiders. *Current Biology* 27: R638-R639.

**Yeni, Y.N., Brown, C.U., Wang, Z., and Norman, T.L.** (1997) The influence of bone morphology on fracture toughness of the human femur and tibia. *Bone* 21: 453-459.
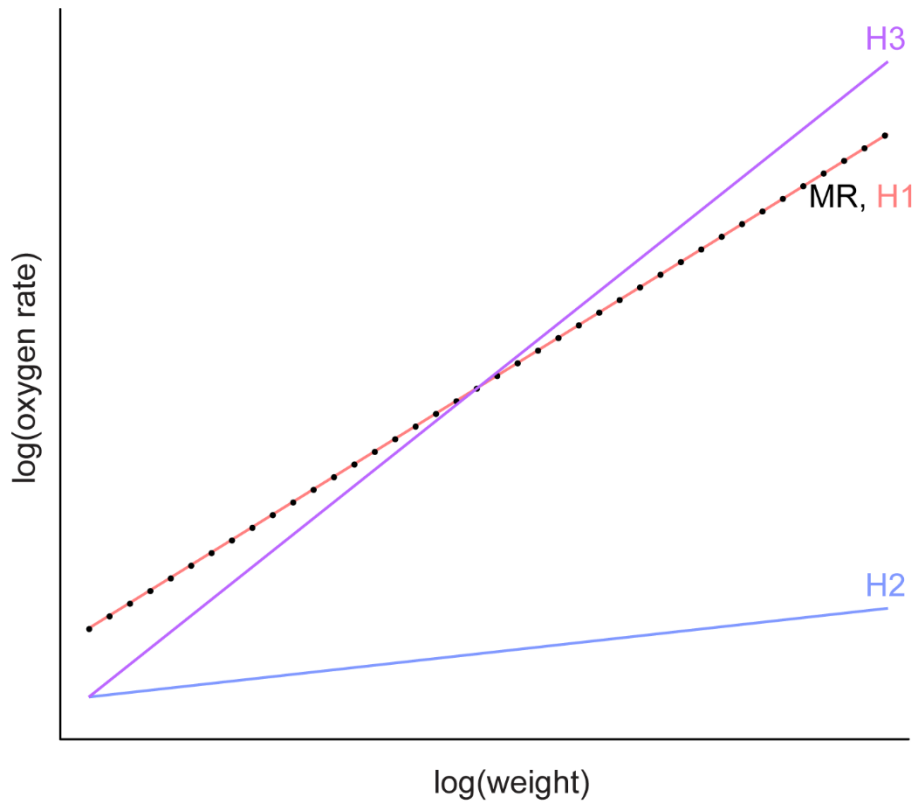
**Figure 1. Hypothesized scaling of measured metabolic rates and modeled rates of oxygen flux across pores.** Metabolic rates (MR; dotted line) were taken from Lane et al., 2017. Hypothesis 1 (H1; red line): if pores facilitate most of the oxygen movement, then the total flux attributable to pores should closely match metabolic demand across a range of taxa and body sizes. Hypothesis 2 (H2; blue line): if the pores do not facilitate oxygen diffusion, then the total flux through pores should be lower than that of metabolic demand across a range of taxa and body sizes. Hypothesis 3 (H3; purple line): if the relative importance of pores varies in a size dependent way, then small individuals with thin cuticles may obtain sufficient oxygen directly across the cuticle, but large individuals with relatively thick cuticles obtain larger fractions through their pores.
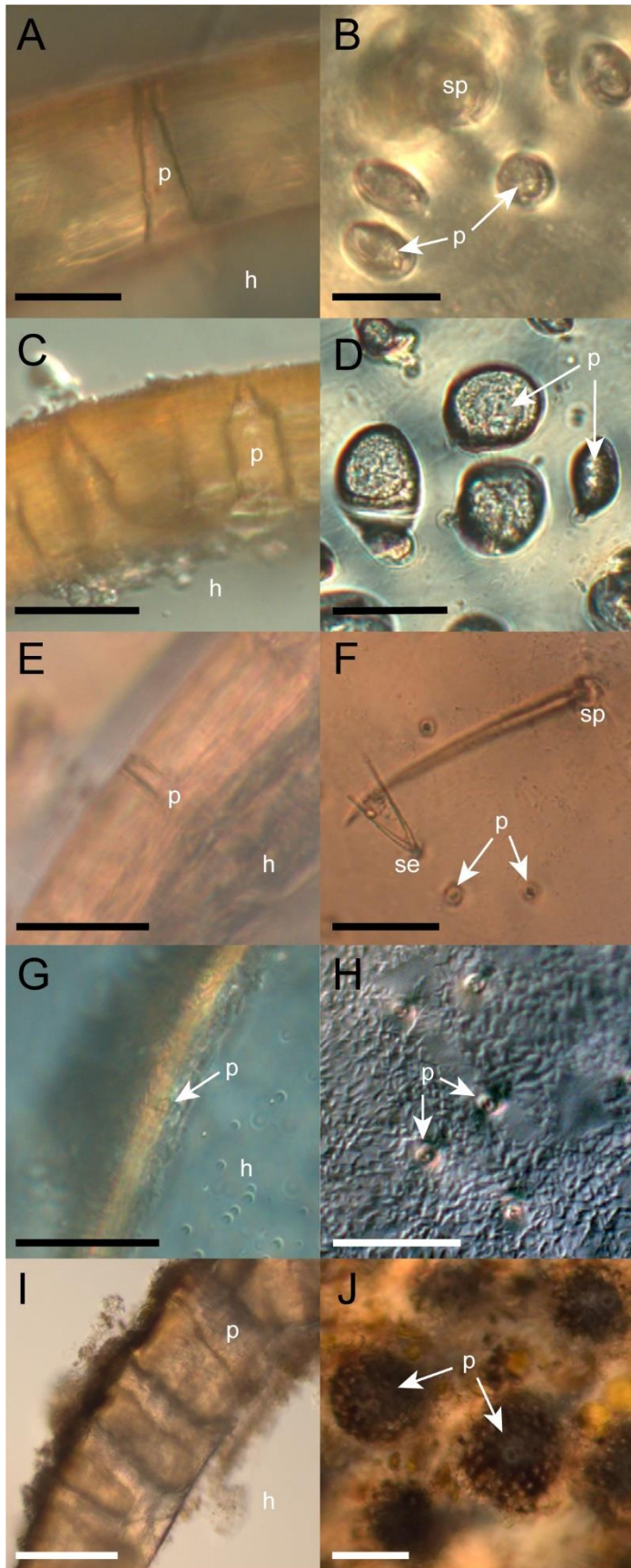
**Figure 2. Pore structure for one representative of each sea spider family in study.** Images on left side are from cross-sectional sections and those on the right side are from longitudinal sections. A-B) Ammotheidae, C-D) Colossendeidae, E-F) Nymphonidae, G-H) Pallenopsidae, I-J) Pycnogonidae. p, pore; h, hemocoel; sp, cuticular spines; and se, cuticular setae. Scale bar is 50 µm long in A-F, H, and J. Scale bar is 25 µm in G. Scale bar is 100 µm in I.



$$R_{top} = k_w * \frac{1}{2d_c}$$
$$+$$
$$R_{cuticle} = k_c * \frac{\ell_c}{A_c}$$
$$+$$
$$R_{seg} = k * \frac{\ell_p}{A_n}$$
$$+$$
$$\vdots$$
$$+$$
$$R_{bot} = k * \frac{1}{2d_{20}}$$
$$\overline{R_{tot}}$$
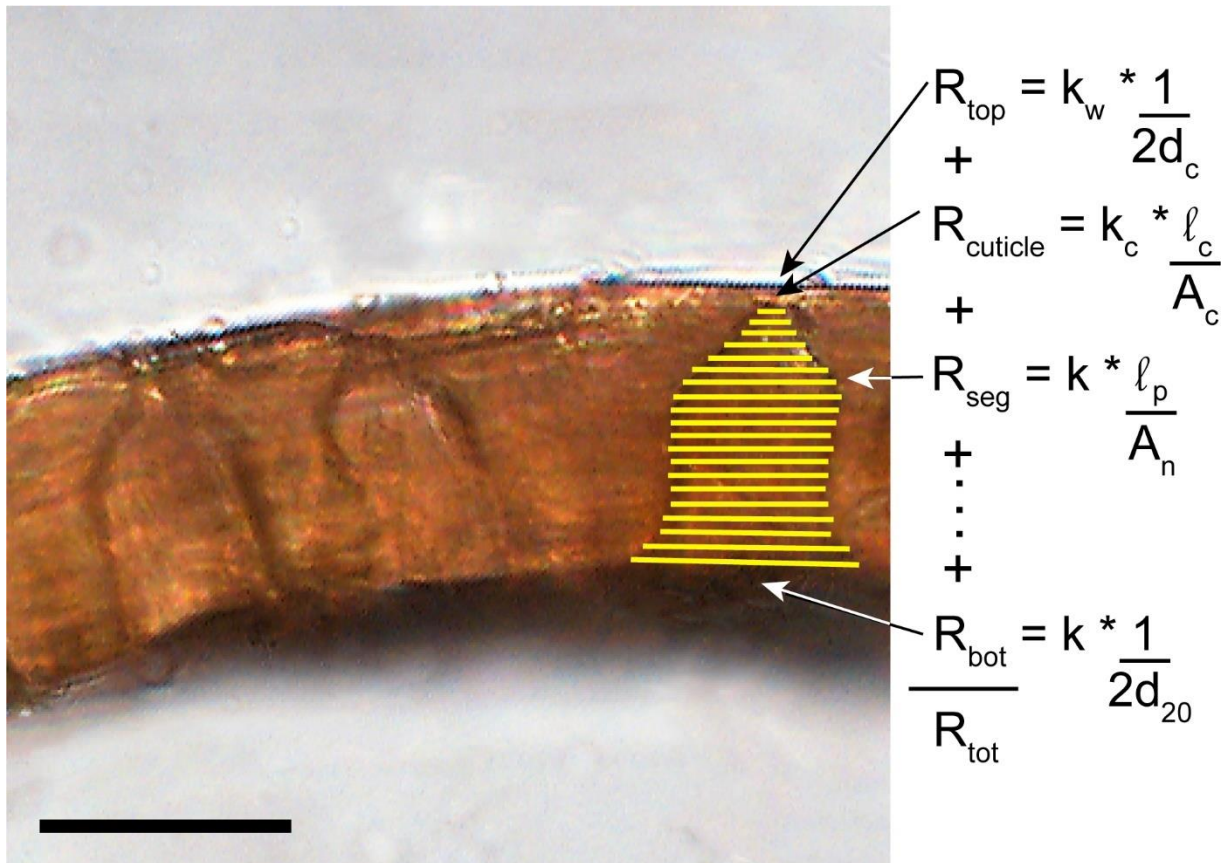
**Figure 3. Diagram of pore divided into 20 equally separated segments (yellow lines).**
Resistance was calculated as the sum of the resistances for all 20 segments and the layer of cuticle immediately above the pore (Tøien et al. 1988). $R_{top}$ (kPa s µmol$^{-1}$), which represents boundary layer resistance at the top of the pore is inversely proportional to two times the segment diameter immediately below the layer of cuticle ($d_c$, cm). Constant $k_w$ (cm kPa s µmol$^{-1}$) was calculated based on the diffusion coefficient through water. $R_{bot}$, conversely, represents the boundary layer resistance at the bottom of the pore and is inversely proportional to two times the segment diameter ($d_{20}$) times $k$, which was calculated based on the diffusion coefficient through water or tissue. $R_{cuticle}$ represents the resistance through the portion of cuticle above the pore. $\ell_c$

(cm) is the thickness of the cuticular cap above the pore and was divided by the cross-sectional area ($A_c$, cm$^2$) of the first segment, assuming the segment is circular. The following middle segment resistances ($R_{seg}$) were calculated using the thickness of each segment through the pore ($\ell_p$), which was the same for each segment, divided by the cross-sectional area ($A_n$). $A_n$ was calculated by measuring the segmental pore diameter ($d_n$) and assuming each segment is circular. The constant $k = RT/D$ (cm kPa s µmol$^{-1}$), where $R$ is the gas constant, $T$ is temperature, and $D$ is the diffusion coefficient of the material (water, cuticle, or tissue). See text for more details. Scale bar equals 50 µm.
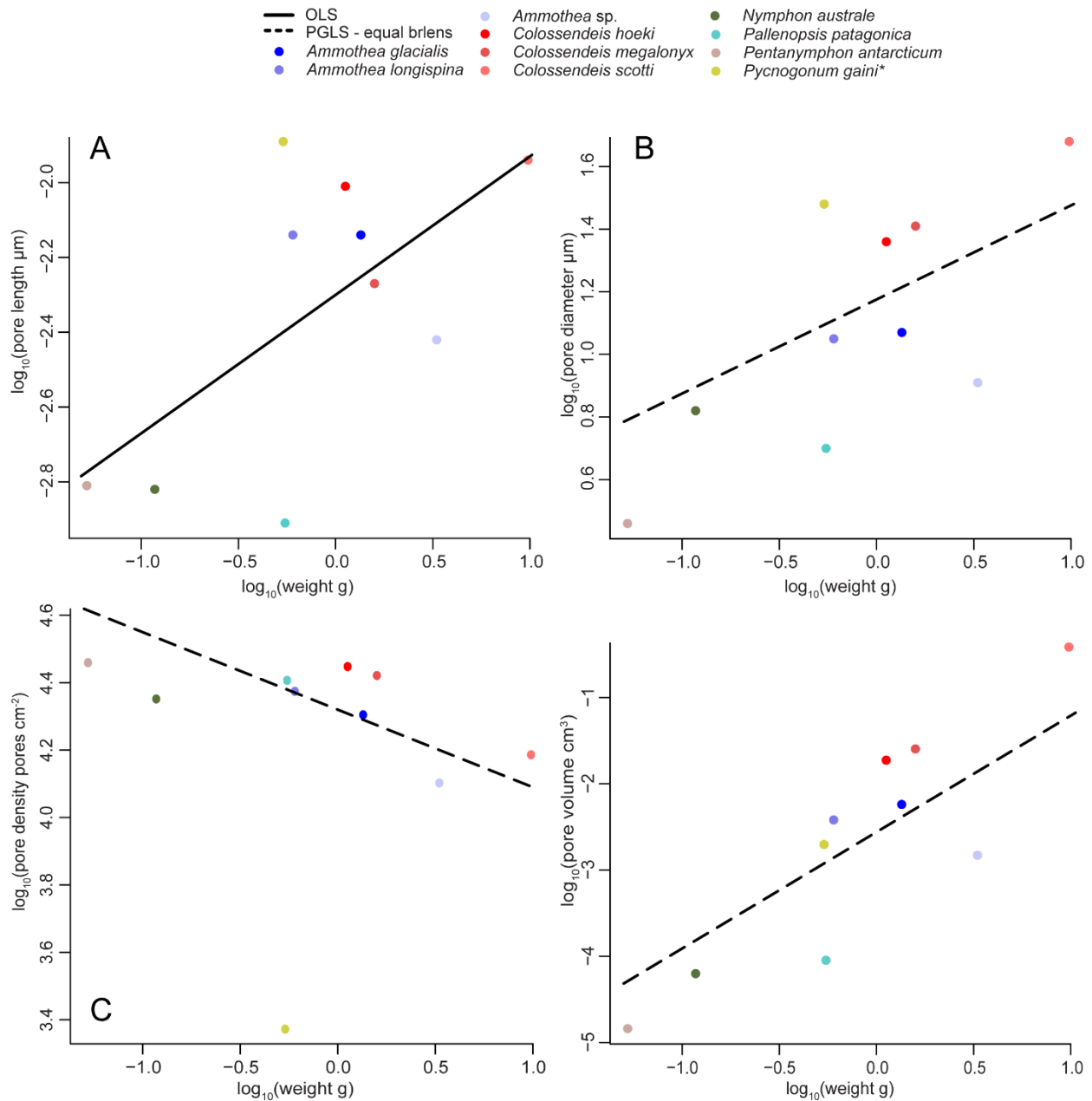
**Figure 4. Regression lines for scaling relationships between cuticle thickness (A) (n = 10), pore diameter (B) (n = 10), pore density (C) (n = 9), and pore volume across the entire cuticle (D) (n = 10) to body mass.** In A, line indicates fit using OLS and in B, C, and D lines indicate fit using PGLS-equal brlens regressions. See text for details. See table 1 for regression coefficients. *Pycnogonum gaini* appears to be an outlier and was not used in the pore density regression.
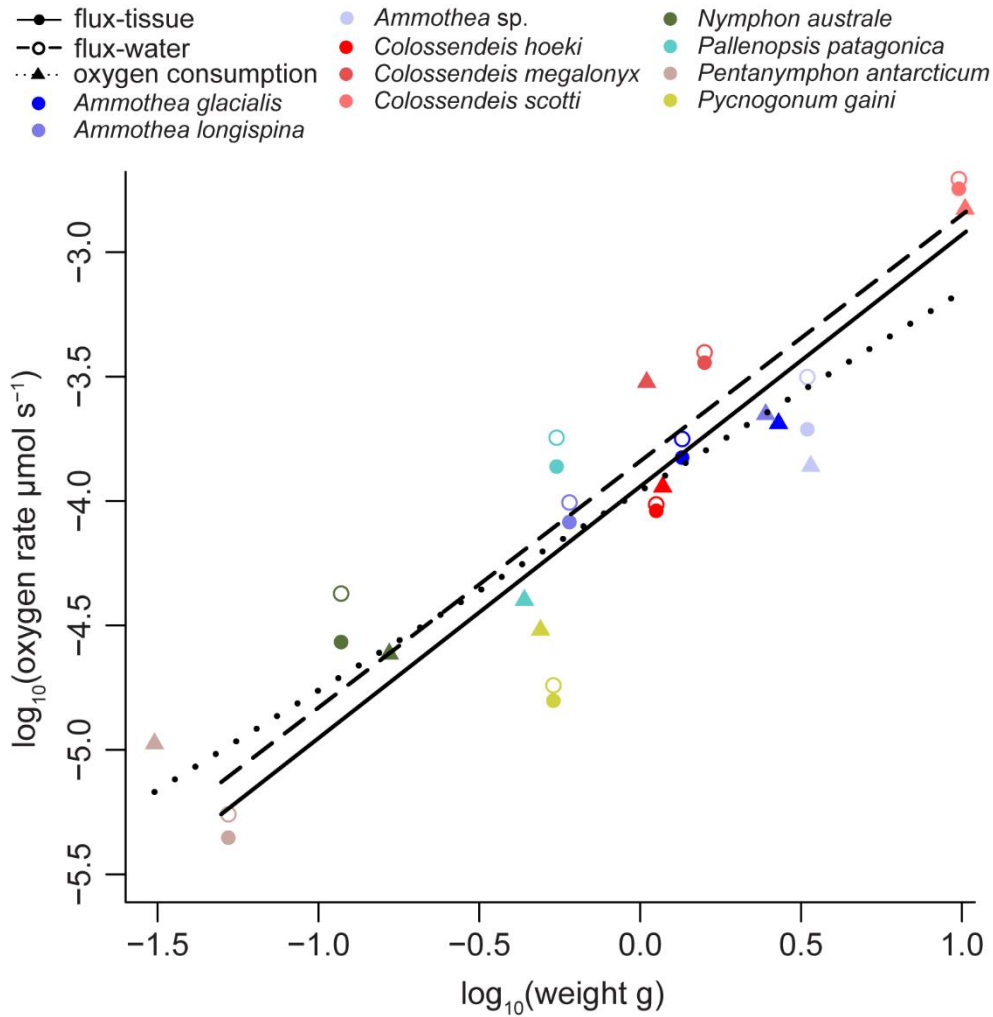
**Figure 5. Regression lines comparing total diffusive oxygen flux through pores using the tissue-diffusion model (solid line and solid circles), the water-diffusion model (dashed line and open circles, and oxygen consumption (dotted line and triangles) to body mass.** Regression lines were calculated based on OLS models. N = 10. Oxygen consumption rates were taken from Lane et al., 2017. See table 1 for regression coefficients.

**Table 1**. Summary of OLS and PGLS regression analyses.

| Models | *N* | a | 95 % CI | P | b | 95 % CI | P | R² |
|---|---|---|---|---|---|---|---|---|
| *Pore length* (cm) *vs weight* (g) | | | | | | | | |
| OLS | 10 | -2.30 | (-2.53,-2.06) | < 0.001 | 0.37 | (0.00,0.74) | 0.049 | 0.33 |
| PGLS-mtCO1 | 10 | -2.44 | (-2.93,-1.94) | < 0.001 | 0.18 | (-0.19,0.56) | 0.286 | |
| PGLS-var. brlens | 10 | -2.35 | (-2.74,-1.96) | < 0.001 | 0.20 | (-0.20,0.59) | 0.281 | |
| PGLS-equal brlens | 10 | -2.28 | (-2.74,-1.82) | < 0.001 | 0.23 | (-0.15,0.60) | 0.196 | |
| *Pore diameter* (cm) *vs weight* (g) | | | | | | | | |
| OLS | 10 | 1.14 | (0.93,1.35) | < 0.001 | 0.42 | (0.08,0.76) | 0.020 | 0.45 |
| PGLS-mtCO1 | 10 | 1.06 | (0.63,1.49) | < 0.001 | 0.29 | (-0.03,0.61) | 0.069 | |
| PGLS-var. brlens | 10 | 1.12 | (0.80,1.44) | < 0.001 | 0.30 | (-0.02,0.63) | 0.064 | |
| PGLS-equal brlens | 10 | 1.17 | (0.82,1.52) | < 0.001 | 0.30 | (0.02,0.58) | 0.038 | |
| *Pore density* (pores cm⁻²) *vs weight* (g) | | | | | | | | |
| OLS | 9 | 4.33 | (4.25,4.41) | < 0.001 | -0.12 | (-0.23,0.00) | 0.053 | 0.35 |
| PGLS-mtCO1 | 9 | 4.31 | (4.14,4.48) | < 0.001 | -0.23 | (-0.35,-0.11) | 0.003 | |
| PGLS-var. brlens | 9 | 4.31 | (4.18,4.44) | < 0.001 | -0.23 | (-0.35,-0.11) | 0.003 | |
| PGLS-equal brlens | 9 | 4.32 | (4.17,4.48) | < 0.001 | -0.23 | (-0.35,-0.11) | 0.003 | |
| *Pore volume* (cm³) *vs weight* (g) | | | | | | | | |
| OLS | 10 | -2.51 | (-3.03,-1.99) | < 0.001 | 1.79 | (0.97,2.61) | 0.001 | 0.73 |
| PGLS-mtCO1 | 10 | -2.89 | (-4.04,-1.75) | < 0.001 | 1.25 | (0.40,2.11) | 0.010 | |
| PGLS-var. brlens | 10 | -2.72 | (-3.60,-1.84) | < 0.001 | 1.28 | (0.39,2.17) | 0.010 | |
| PGLS-equal brlens | 10 | -2.56 | (-3.54,-1.57) | < 0.001 | 1.35 | (0.55,2.14) | 0.005 | |
| *Whole animal flux* (µmol s⁻¹) *vs weight* (g) (D = water) | | | | | | | | |
| OLS | 10 | -3.84 | (-4.09,-3.60) | < 0.001 | 0.99 | (0.60,1.37) | < 0.001 | 0.79 |
| PGLS-mtCO1 | 10 | -3.80 | (-4.38,-3.22) | < 0.001 | 1.04 | (0.60,1.48) | < 0.001 | |
| PGLS-var. brlens | 10 | -3.86 | (-4.31,-3.41) | < 0.001 | 1.04 | (0.59,1.48) | < 0.001 | |
| PGLS-equal brlens | 10 | -3.89 | (-4.46,-3.32) | < 0.001 | 1.03 | (0.56,1.49) | < 0.001 | |
| *Whole animal flux* (µmol s⁻¹) *vs weight* (g) (D = tissue) | | | | | | | | |
| OLS | 10 | -3.94 | (-4.17,-3.70) | < 0.001 | 1.01 | (0.64,1.39) | < 0.001 | 0.81 |
| PGLS-mtCO1 | 10 | -3.91 | (-4.48,-3.34) | < 0.001 | 1.01 | (0.59,1.44) | < 0.001 | |
| PGLS-var. brlens | 10 | -3.96 | (-4.40,-3.53) | < 0.001 | 1.01 | (0.57,1.44) | < 0.001 | |
| PGLS-equal brlens | 10 | -3.99 | (-4.55,-3.43) | < 0.001 | 1.00 | (0.55,1.45) | 0.001 | |
| *Oxygen consumption* (µmol s⁻¹) *vs weight* (g) | | | | | | | | |
| OLS | 10 | -3.96 | (-4.15,-3.77) | < 0.001 | 0.80 | (0.52,1.08) | < 0.001 | 0.83 |
| PGLS-mtCO1 | 10 | -4.03 | (-4.47,3.59) | < 0.001 | 0.77 | (0.46,1.07) | < 0.001 | |
| PGLS-var. brlens | 10 | -4.01 | (-4.34,-3.69) | < 0.001 | 0.77 | (0.46,1.07) | < 0.001 | |
| PGLS-equal brlens | 10 | -3.99 | (-4.39,-3.60) | < 0.001 | 0.75 | (0.47,1.04) | < 0.001 | |

"N": Number of species used in each analysis. Regression coefficients: intercept ("a") and scaling exponent ("b"). Variables with "(D = water/tissue)" differentiate between which model was conducted to calculate flux. Different PGLS models: "mtCO1" tree built with unconstrained topology, "var. brlens" tree with variable branch lengths, and "equal brlens"same tree topology but with all branch lengths set to 1. *Individual oxygen consumption rates were taken from Lane et al., 2017.

**Supplementary Information for *Cuticular gas exchange by Antarctic sea spiders***

Lane, SJ, AL Moran, CM Shishido, BW Tobalske, and HA Woods

Journal of Experimental Biology

**Table S1.** Intravariation of cuticle morphology and physiology between leg segments in three species of sea spiders: pore length (µm), pore diameter (µm), pore density (pores cm$^{-2}$), conductance_water (µmol s$^{-1}$ kPa$^{-1}$ pore$^{-1}$), and conductance_tissue (µmol s$^{-1}$ kPa$^{-1}$ pore$^{-1}$).

| Variable | Species | leg segment | *N* | mean | s.e.m. | *F* | *P* |
|---|---|---|---|---|---|---|---|
| Pore length | | | | | | | |
| | *Ammothea glacialis* | femur | 8 | 72.96 | ± 2.06 | 0.712 | 0.507 |
| | | 1st tibia | 8 | 67.20 | ± 2.59 | | |
| | | 2nd tibia | 8 | 68.72 | ± 5.19 | | |
| | *Colossendeis megalonyx* | femur | 8 | 53.12 | ± 2.10 | 1.883 | 0.189 |
| | | 1st tibia | 8 | 51.31 | ± 1.73 | | |
| | | 2nd tibia | 8 | 54.69 | ± 1.41 | | |
| | *Nymphon australe* | femur | 3 | 15.31 | ± 3.09 | 0.638 | 0.575 |
| | | 1st tibia | 3 | 20.00 | ± 10.00 | | |
| | | 2nd tibia | 4 | 21.25 | ± 4.27 | | |
| Pore diameter | | | | | | | |
| | *Ammothea glacialis* | femur | 8 | 12.91 | ± 0.40 | 2.192 | 0.149 |
| | | 1st tibia | 8 | 14.14 | ± 0.64 | | |
| | | 2nd tibia | 8 | 13.92 | ± 0.53 | | |
| | *Colossendeis megalonyx* | femur | 8 | 25.66 | ± 1.23 | 0.576 | 0.575 |
| | | 1st tibia | 8 | 24.04 | ± 1.80 | | |
| | | 2nd tibia | 8 | 25.06 | ± 1.10 | | |
| | *Nymphon australe* | femur | 3 | 6.56 | ± 1.13 | 1.201 | 0.391 |
| | | 1st tibia | 3 | 6.72 | ± 0.45 | | |
| | | 2nd tibia | 4 | 5.67 | ± 0.33 | | |
| Pore density | | | | | | | |
| | *Ammothea glacialis* | femur | 8 | 22062 | ± 944 | 2.241 | 0.143 |
| | | 1st tibia | 8 | 22553 | ± 924 | | |
| | | 2nd tibia | 8 | 24274 | ± 745 | | |
| | *Colossendeis megalonyx* | femur | 8 | 26384 | ± 1830 | 0.860 | 0.445 |
| | | 1st tibia | 8 | 26207 | ± 1131 | | |
| | | 2nd tibia | 8 | 27509 | ± 1372 | | |
| | *Nymphon australe* | femur | 8 | 16993 | ± 2175 | 1.168 | 0.340 |

| | | | | | | | |
|---|---|---|---|---|---|---|---|
| | | 1st tibia | 8 | 17032 | ± 1833 | | |
| | | 2nd tibia | 8 | 20086 | ± 1038 | | |
| Conductance_water | | | | | | | |
| | *Ammothea glacialis* | femur | 8 | $6.14 \times 10^{-11}$ | $\pm 8.87 \times 10^{-12}$ | 3.654 | 0.053 |
| | | 1st tibia | 8 | $4.64 \times 10^{-11}$ | $\pm 5.19 \times 10^{-12}$ | | |
| | | 2nd tibia | 8 | $3.75 \times 10^{-11}$ | $\pm 3.66 \times 10^{-12}$ | | |
| | *Colossendeis megalonyx* | femur | 8 | $8.46 \times 10^{-11}$ | $\pm 9.97 \times 10^{-12}$ | 2.110 | 0.158 |
| | | 1st tibia | 8 | $7.09 \times 10^{-11}$ | $\pm 1.76 \times 10^{-11}$ | | |
| | | 2nd tibia | 8 | $5.01 \times 10^{-11}$ | $\pm 4.07 \times 10^{-12}$ | | |
| | *Nymphon australe* | femur | 3 | $2.62 \times 10^{-10}$ | $\pm 4.60 \times 10^{-11}$ | 4.264 | 0.102 |
| | | 1st tibia | 3 | $1.74 \times 10^{-10}$ | $\pm 3.81 \times 10^{-11}$ | | |
| | | 2nd tibia | 4 | $1.35 \times 10^{-10}$ | $\pm 1.21 \times 10^{-11}$ | | |
| Conductance_tissue | | | | | | | |
| | *Ammothea glacialis* | femur | 8 | $4.99 \times 10^{-11}$ | $\pm 1.73 \times 10^{-11}$ | 3.596 | 0.055 |
| | | 1st tibia | 8 | $4.02 \times 10^{-11}$ | $\pm 1.10 \times 10^{-11}$ | | |
| | | 2nd tibia | 8 | $3.28 \times 10^{-11}$ | $\pm 8.52 \times 10^{-12}$ | | |
| | *Colossendeis megalonyx* | femur | 8 | $7.66 \times 10^{-11}$ | $\pm 8.85 \times 10^{-12}$ | 1.988 | 0.174 |
| | | 1st tibia | 8 | $6.35 \times 10^{-11}$ | $\pm 1.57 \times 10^{-11}$ | | |
| | | 2nd tibia | 8 | $4.68 \times 10^{-11}$ | $\pm 3.65 \times 10^{-12}$ | | |
| | *Nymphon australe* | femur | 3 | $1.71 \times 10^{-10}$ | $\pm 3.26 \times 10^{-11}$ | 3.455 | 0.134 |
| | | 1st tibia | 3 | $1.23 \times 10^{-10}$ | $\pm 2.63 \times 10^{-11}$ | | |
| | | 2nd tibia | 4 | $9.21 \times 10^{-11}$ | $\pm 3.90 \times 10^{-12}$ | | |

**Table S2**. Pagel's lambda and log likelihood scores for PGLS regression analyses.

| Models | $N$ | Pagel's Lambda | logL | logL0 | logL P-value |
|---|---|---|---|---|---|
| *Pore length* (cm) *vs weight* (g) | | | | | |
| PGLS-mtCO1 | 10 | 1.00 | -1.96 | -3.60 | 0.070 |
| PGLS-var. brlens | 10 | 1.00 | -1.89 | -2.40 | 0.310 |
| PGLS-equal brlens | 10 | 1.00 | -1.91 | -3.50 | 0.075 |
| *Pore diameter* (cm) *vs weight* (g) | | | | | |
| PGLS-mtCO1 | 10 | 1.00 | 0.10 | -1.58 | 0.067 |
| PGLS-var. brlens | 10 | 1.00 | 0.34 | -1.24 | 0.075 |
| PGLS-equal brlens | 10 | 1.00 | 0.67 | -2.29 | 0.015 |
| *Pore density* (pores cm$^{-2}$) *vs weight* (g) | | | | | |
| PGLS-mtCO1 | 9 | 1.00 | 10.21 | 8.21 | 0.045 |
| PGLS-var. brlens | 9 | 1.00 | 10.38 | 7.96 | 0.028 |
| PGLS-equal brlens | 9 | 1.00 | 9.98 | 6.68 | 0.010 |
| *Pore volume* (cm$^{3}$) *vs weight* (g) | | | | | |
| PGLS-mtCO1 | 10 | 0.89 | -10.66 | -11.83 | 0.126 |

|  |  |  |  |  |  |
| --- | --- | --- | --- | --- | --- |
| PGLS-var. brlens | 10 | 0.68 | -10.54 | -11.05 | 0.315 |
| PGLS-equal brlens | 10 | 1.00 | -8.43 | -10.54 | 0.040 |
| *Whole animal flux* (µmol s⁻¹) *vs weight* (g) (D = water) | | | | | |
| PGLS-mtCO1 | 10 | 1.00 | -1.96 | -2.13 | 0.562 |
| PGLS-var. brlens | 10 | 0.00 | -1.58 | -1.58 | 1.000 |
| PGLS-equal brlens | 10 | 1.00 | -3.77 | -3.78 | 0.869 |
| *Whole animal flux* (µmol s⁻¹) *vs weight* (g) (D = tissue) | | | | | |
| PGLS-mtCO1 | 10 | 0.00 | -1.99 | -1.99 | 1.000 |
| PGLS-var. brlens | 10 | 0.00 | -1.59 | -1.59 | 1.000 |
| PGLS-equal brlens | 10 | 0.00 | -3.33 | -3.33 | 1.000 |
| *Oxygen consumption* (µmol s⁻¹) *vs weight* (g) | | | | | |
| PGLS-mtCO1 | 10 | 0.55 | 0.69 | 0.50 | 0.548 |
| PGLS-var. brlens | 10 | 0.65 | 0.68 | 0.25 | 0.352 |
| PGLS-equal brlens | 10 | 1.00 | 0.97 | 0.03 | 0.169 |

**Table S3**. Summary of data used in intra-variation calculations for *Ammothea glacialis*, *Colossendeis megalonyx*, and *Nymphon australe*: pore length (µm), pore diameter (µm), and conductance (µmol s⁻¹ kPa⁻¹ pore⁻¹)

| species | individual | leg segment | pore length | pore diameter | total # pores | Conductance* | |
| --- | --- | --- | --- | --- | --- | --- | --- |
| | | | | | | water model | tissue model |
| *Ammothea glacialis* | ind1 | femur | 85.83 | 11.75 | 19778 | 1.09E-10 | 8.02E-11 |
| | | 1 tibia | 69.05 | 13.20 | 25510 | 3.30E-11 | 3.00E-11 |
| | | 2 tibia | 79.40 | 14.47 | 28420 | 4.69E-11 | 4.08E-11 |
| *Ammothea glacialis* | ind2 | femur | 68.19 | 12.62 | 22817 | 5.73E-11 | 4.86E-11 |
| | | 1 tibia | 68.64 | 14.31 | 24032 | 4.27E-11 | 3.86E-11 |
| | | 2 tibia | 69.95 | 11.44 | 22551 | 2.88E-11 | 2.48E-11 |
| *Ammothea glacialis* | ind3 | femur | 72.65 | 13.45 | 18741 | 7.54E-11 | 6.00E-11 |
| | | 1 tibia | 68.90 | 15.24 | 20736 | 3.54E-11 | 3.17E-11 |
| | | 2 tibia | 70.24 | 15.45 | 21324 | 2.64E-11 | 2.43E-11 |
| *Ammothea glacialis* | ind4 | femur | 68.29 | 12.86 | 25130 | 3.81E-11 | 3.33E-11 |
| | | 1 tibia | 63.71 | 14.27 | 20795 | 6.04E-11 | 5.04E-11 |
| | | 2 tibia | 65.52 | 12.68 | 25245 | 4.31E-11 | 3.86E-11 |
| *Ammothea glacialis* | ind5 | femur | 70.34 | 11.09 | 19412 | 5.39E-11 | 4.45E-11 |
| | | 1 tibia | 64.13 | 10.72 | 18619 | 6.80E-11 | 5.60E-11 |
| | | 2 tibia | 55.53 | 14.01 | 24368 | 2.89E-11 | 2.56E-11 |
| *Ammothea glacialis* | ind6 | femur | 73.60 | 14.16 | 25357 | 7.83E-11 | 6.49E-11 |
| | | 1 tibia | 72.01 | 17.11 | 22792 | 3.22E-11 | 2.96E-11 |
| | | 2 tibia | 88.43 | 14.84 | 24903 | 5.10E-11 | 4.21E-11 |
| *Ammothea glacialis* | ind7 | femur | 75.48 | 14.38 | 24235 | 4.58E-11 | 3.84E-11 |

| | | | | | | | |
|---|---|---|---|---|---|---|---|
| | | 1 tibia | 53.01 | 14.47 | 26309 | 3.72E-11 | 3.28E-11 |
| | | 2 tibia | 78.77 | 12.75 | 23390 | 2.82E-11 | 2.48E-11 |
| *Ammothea glacialis* | ind8 | femur | 69.32 | 12.98 | 21027 | 3.31E-11 | 2.96E-11 |
| | | 1 tibia | 78.16 | 13.81 | 21633 | 6.21E-11 | 5.23E-11 |
| | | 2 tibia | 41.90 | 15.69 | 23993 | 4.70E-11 | 4.13E-11 |
| *Colossendeis megalonyx* | ind1 | femur | 55.34 | 20.25 | 20893 | 4.68E-11 | 4.20E-11 |
| | | 1 tibia | 51.87 | 25.59 | 22300 | 1.32E-10 | 1.16E-10 |
| | | 2 tibia | 59.21 | 23.93 | 23057 | 6.72E-11 | 6.22E-11 |
| *Colossendeis megalonyx* | ind2 | femur | 55.01 | 29.23 | 27162 | 6.31E-11 | 5.87E-11 |
| | | 1 tibia | 49.60 | 26.32 | 25879 | 6.63E-11 | 6.24E-11 |
| | | 2 tibia | 53.13 | 23.92 | 25573 | 4.59E-11 | 4.26E-11 |
| *Colossendeis megalonyx* | ind3 | femur | 50.22 | 27.81 | 20289 | 1.09E-10 | 9.97E-11 |
| | | 1 tibia | 49.47 | 19.09 | 22287 | 4.98E-11 | 4.65E-11 |
| | | 2 tibia | 54.95 | 28.23 | 22166 | 4.81E-11 | 4.53E-11 |
| *Colossendeis megalonyx* | ind4 | femur | 61.29 | 26.93 | 22466 | 9.34E-11 | 8.50E-11 |
| | | 1 tibia | 59.82 | 26.42 | 23379 | 3.93E-11 | 2.95E-11 |
| | | 2 tibia | 55.48 | 26.39 | 27076 | 5.77E-11 | 5.42E-11 |
| *Colossendeis megalonyx* | ind5 | femur | 45.29 | 30.09 | 32158 | 1.01E-10 | 9.31E-11 |
| | | 1 tibia | 52.87 | 33.57 | 29447 | 1.59E-10 | 1.42E-10 |
| | | 2 tibia | 47.26 | 28.21 | 31030 | 4.93E-11 | 4.67E-11 |
| *Colossendeis megalonyx* | ind6 | femur | 46.63 | 22.00 | 31638 | 1.16E-10 | 1.03E-10 |
| | | 1 tibia | 43.12 | 21.51 | 29432 | 2.48E-11 | 2.36E-11 |
| | | 2 tibia | 52.62 | 26.26 | 32783 | 4.50E-11 | 4.24E-11 |
| *Colossendeis megalonyx* | ind7 | femur | 60.47 | 24.82 | 23968 | 1.01E-10 | 8.85E-11 |
| | | 1 tibia | 54.99 | 22.46 | 29425 | 2.30E-11 | 2.18E-11 |
| | | 2 tibia | 59.96 | 24.95 | 31096 | 2.89E-11 | 2.75E-11 |
| *Colossendeis megalonyx* | ind8 | femur | 50.69 | 24.12 | 32500 | 4.62E-11 | 4.29E-11 |
| | | 1 tibia | 48.78 | 17.35 | 27507 | 7.26E-11 | 6.56E-11 |
| | | 2 tibia | 54.94 | 18.60 | 27290 | 5.90E-11 | 5.33E-11 |
| *Nymphon australe* | ind1 | femur | 16.44 | 5.49 | 26780 | 1.71E-10 | 1.06E-10 |
| | | 1 tibia | 10.00 | 7.27 | 18196 | 2.35E-10 | 1.72E-10 |
| | | 2 tibia | 25.00 | 6.12 | 23748 | 1.60E-10 | 9.97E-11 |
| *Nymphon australe* | ind2 | femur | 9.49 | 5.37 | 10623 | 3.19E-10 | 1.99E-10 |
| | | 1 tibia | 10.00 | 5.82 | 10503 | 1.04E-10 | 8.28E-11 |
| | | 2 tibia | 10.00 | 4.73 | 22427 | 1.15E-10 | 8.84E-11 |
| *Nymphon australe* | ind3 | femur | 20.00 | 8.81 | 23216 | 2.96E-10 | 2.08E-10 |

| | | | | | | | |
|---|---|---|---|---|---|---|---|
| | | 1 tibia | 40.00 | 7.06 | 16932 | 1.84E-10 | 1.13E-10 |
| | | 2 tibia | 30.00 | 6.13 | 22188 | 1.51E-10 | 9.75E-11 |
| *Nymphon australe* | ind4 | femur | NA | NA | 17692 | NA | NA |
| | | 1 tibia | NA | NA | 9194 | NA | NA |
| | | 2 tibia | 20.00 | 5.68 | 18223 | 1.13E-10 | 8.30E-11 |
| *Nymphon australe* | ind5 | femur | NA | NA | 11261 | NA | NA |
| | | 1 tibia | NA | NA | 23664 | NA | NA |
| | | 2 tibia | NA | NA | 19630 | NA | NA |
| *Nymphon australe* | ind6 | femur | NA | NA | 19057 | NA | NA |
| | | 1 tibia | NA | NA | 15866 | NA | NA |
| | | 2 tibia | NA | NA | 16609 | NA | NA |
| *Nymphon australe* | ind7 | femur | NA | NA | 9793 | NA | NA |
| | | 1 tibia | NA | NA | 19133 | NA | NA |
| | | 2 tibia | NA | NA | 15884 | NA | NA |
| *Nymphon australe* | ind8 | femur | NA | NA | 17525 | NA | NA |
| | | 1 tibia | NA | NA | 22765 | NA | NA |
| | | 2 tibia | NA | NA | 21978 | NA | NA |

*Conductance was calculated based on the 2 different models used to calculate resistance. One with the diffusion coefficient of water and one with the diffusion coefficient of tissue. See text for more details

**Table S4.** Summary of data used in scaling analyses and calculating flux: pore length (x, µm), pore diameter (d, µm), resistance (R, kPa s µmol$^{-1}$), and pore density (P, pores cm$^{-2}$)

| Species | x | d | water model R | tissue model R | P |
|---|---|---|---|---|---|
| Ammotheidae | | | | | |
| *Ammothea glacialis* | 85.83 | 12.98 | 9.17E+09 | 1.25E+10 | 19778 |
| | 68.19 | 14.38 | 1.75E+10 | 2.06E+10 | 22817 |
| | 72.65 | 11.54 | 1.33E+10 | 1.67E+10 | 18741 |
| | 68.29 | 10.32 | 2.62E+10 | 3.00E+10 | 25130 |
| | 70.34 | 11.63 | 1.85E+10 | 2.24E+10 | 19412 |
| | 73.60 | 13.45 | 1.28E+10 | 1.54E+10 | 25357 |
| | 75.48 | 9.44 | 2.18E+10 | 2.60E+10 | 24235 |
| | 69.32 | 10.74 | 3.02E+10 | 3.38E+10 | 21027 |
| *Ammothea longispina* | 73.14 | 9.79 | 9.02E+09 | 1.33E+10 | 32038 |
| | 71.36 | 12.60 | 3.10E+10 | 3.46E+10 | 23689 |
| *Ammothea sp* | 33.31 | 6.83 | 4.84E+09 | 7.21E+09 | 12662 |
| | 43.36 | 9.34 | 7.78E+09 | 1.32E+10 | NA |
| Colossendeidae | | | | | |
| *Colossendeis hoeki* | 89.13 | 21.98 | 2.05E+10 | 2.20E+10 | 28047 |
| | 108.38 | 23.38 | 4.92E+10 | 5.20E+10 | NA |
| *Colossendeis megalonyx* | 55.34 | 24.12 | 2.14E+10 | 2.38E+10 | 20893 |

|  |  |  |  |  |
|---|---|---|---|---|
|  | 55.01 | 24.82 | 1.58E+10 | 1.70E+10 | 27162 |
|  | 50.22 | 22.00 | 9.15E+09 | 1.00E+10 | 20289 |
|  | 61.29 | 30.09 | 1.07E+10 | 1.18E+10 | 22466 |
|  | 45.29 | 26.93 | 9.89E+09 | 1.07E+10 | 32158 |
|  | 46.63 | 27.81 | 8.60E+09 | 9.70E+09 | 31638 |
|  | 60.47 | 29.23 | 9.86E+09 | 1.13E+10 | 23968 |
|  | 50.69 | 20.25 | 2.17E+10 | 2.33E+10 | 32500 |
| *Colossendeis scotti* | 99.68 | 43.62 | 8.61E+09 | 9.13E+09 | 14842 |
|  | 130.33 | 51.27 | 7.03E+09 | 8.03E+09 | 15854 |
| Nymphonidae |  |  |  |  |  |
| *Nymphon australe* | 16.44 | 5.49 | 5.83E+09 | 9.47E+09 | 26780 |
|  | 9.49 | 5.37 | 3.14E+09 | 5.03E+09 | 10623 |
|  | 20.00 | 8.81 | 3.37E+09 | 4.82E+09 | 23216 |
|  | NA | NA | NA | NA | 17692 |
|  | NA | NA | NA | NA | 11261 |
|  | NA | NA | NA | NA | 19057 |
|  | NA | NA | NA | NA | 9793 |
|  | NA | NA | NA | NA | 17525 |
| *Pentanymphon antarcticum* | 9.81 | 2.48 | 4.49E+10 | 5.88E+10 | 28811 |
|  | 21.46 | 3.30 | 9.84E+10 | 1.19E+11 | NA |
| Pallenopsidae |  |  |  |  |  |
| *Pallenopsis patagonica* | 10.95 | 4.32 | 1.29E+10 | 1.61E+10 | 25529 |
|  | 13.76 | 5.77 | 4.38E+09 | 6.51E+09 | NA |
| Pycnogonidae |  |  |  |  |  |
| *Pycnogonum gaini* | 122.71 | 31.24 | 4.21E+09 | 4.99E+09 | 2355 |
|  | 135.44 | 32.35 | 9.23E+09 | 1.05E+10 | NA |

**Table S5**. Summary of mass (M, g), surface area (A, cm$^2$), and oxygen gradient ($\Delta PO_2$) data for individuals used in scaling analyses and calculating flux and total pore number.

| Species | *M* | *A* | *$\Delta PO_2$* |
|---|---|---|---|
| Ammotheidae |  |  |  |
| *Ammothea glacialis* | 1.60 | 28.480 | 5.16 |
|  | 1.07 | 20.457 | 8.9 |
|  | 1.32 | 25.352 | 6.86 |
|  | 1.36 | 27.594 | 4.15 |
| *Ammothea longispina* | 0.510 | 14.837 | 7.55 |
|  | 0.647 | 16.893 | 6.16 |
|  | 0.664 | 16.783 | 6.68 |
| *Ammothea* sp. | 3.54 | 47.219 | 3.16 |
|  | 3.11 | 45.310 | 3.61 |
| Colossendeidae |  |  |  |
| *Colossendeis hoeki* | 1.22 | 29.076 | 2.04 |
|  | 0.982 | 23.299 | 7.47 |
|  | 1.13 | 20.740 | 7.94 |
| *Colossendeis megalonyx* | 2.20 | 49.675 | 8.88 |

|  |  |  |  |
|---|---|---|---|
|  | 2.54 | 62.831 | 6.61 |
|  | 0.470 | 17.458 | 3.29 |
|  | 1.10 | 31.745 | NA |
| *Colossendeis scotti* | 12.60 | 118.692 | 5.5 |
|  | 8.39 | 109.837 | 10.4 |
|  | 8.40 | 96.304 | 9 |
| Nymphonidae |  |  |  |
| *Nymphon australe* | 0.140 | 7.819 | NA |
|  | 0.160 | 4.898 | 0.82 |
|  | 0.100 | 5.338 | 1.43 |
|  | 0.070 | 3.674 | 0.27 |
|  | 0.190 | 6.245 | 2.73 |
|  | 0.090 | 5.307 | NA |
|  | 0.070 | 4.553 | NA |
| *Pentanymphon antarcticum* | 0.035 | 3.799 | 2.13 |
|  | 0.068 | 5.495 | 3.94 |
|  | 0.069 | 6.390 | 5.13 |
|  | 0.036 | 3.941 | 1.26 |
| Pallenopsidae |  |  |  |
| *Pallenopsis patagonica* | 0.776 | 19.295 | 4.51 |
|  | 0.395 | 10.582 | 5.17 |
|  | 0.469 | 12.733 | 3.18 |
| Pycnogonidae |  |  |  |
| *Pycnogonum gaini* | 0.618 | 10.833 | NA |
|  | 0.440 | 8.368 | 6.26 |
|  | 0.543 | 8.161 | 5.11 |

**Table S6.** Summary of average component resistances (kpa s μmol$^{-1}$) for each layer of model for each species.

| Species | Rtop | Rcut | water model Rseg | tissue model Rseg | water model Rbot | tissue model Rbot | water model Rtot | tissue model Rtot |
|---|---|---|---|---|---|---|---|---|
| *Ammothea glacialis* | 2.04E+08 | 1.61E+10 | 2.29E+09 | 5.72E+09 | 4.88E+07 | 1.22E+08 | 1.87E+10 | 2.22E+10 |
| *Ammothea longispina* | 2.27E+08 | 1.71E+10 | 2.58E+09 | 6.45E+09 | 5.06E+07 | 1.26E+08 | 2.00E+10 | 2.39E+10 |
| *Ammothea sp* | 1.40E+08 | 3.55E+09 | 2.54E+09 | 6.35E+09 | 7.52E+07 | 1.88E+08 | 6.31E+09 | 1.02E+10 |
| *Colossendeis hoeki* | 2.33E+08 | 3.32E+10 | 1.40E+09 | 3.50E+09 | 3.71E+07 | 9.27E+07 | 3.48E+10 | 3.70E+10 |
| *Colossendeis megalonyx* | 2.22E+08 | 1.23E+10 | 8.60E+08 | 2.15E+09 | 2.90E+07 | 7.24E+07 | 1.34E+10 | 1.47E+10 |
| *Colossendeis scotti* | 9.82E+07 | 7.22E+09 | 4.88E+08 | 1.22E+09 | 1.36E+07 | 3.40E+07 | 7.82E+09 | 8.58E+09 |
| *Nymphon australe* | 1.81E+08 | 2.38E+09 | 1.40E+09 | 3.50E+09 | 1.52E+08 | 3.79E+08 | 4.11E+09 | 6.44E+09 |
| *Pentanymphon antarcticum* | 8.36E+08 | 5.94E+10 | 1.12E+10 | 2.80E+10 | 2.08E+08 | 5.19E+08 | 7.16E+10 | 8.87E+10 |
| *Pallenopsis patagonica* | 2.70E+08 | 6.61E+09 | 1.59E+09 | 3.98E+09 | 1.75E+08 | 4.37E+08 | 8.65E+09 | 1.13E+10 |
| *Pycnogonum gaini* | 1.01E+08 | 5.94E+09 | 6.59E+08 | 1.64E+09 | 2.30E+07 | 5.73E+07 | 6.72E+09 | 7.74E+09 |

# PROCEEDINGS B

## Research

**Author for correspondence:**
Steven J. Lane
e-mail: steven.lane@umontana.edu

## THE ROYAL SOCIETY
PUBLISHING

# Upper limits to body size imposed by respiratory–structural trade-offs in Antarctic pycnogonids

Steven J. Lane[1], Caitlin M. Shishido[2], Amy L. Moran[2], Bret W. Tobalske[1], Claudia P. Arango[3] and H. Arthur Woods[1]

[1]Division of Biological Sciences, University of Montana, Missoula, MT 59812, USA
[2]Department of Biology, University of Hawai'i at Mānoa, Honolulu, HI 96822, USA
[3]Biodiversity Program, Queensland Museum, South Brisbane, Queensland 4101, Australia

SJL, 0000-0002-3361-2244; BWT, 0000-0002-5739-6099; CPA, 0000-0003-1098-830X

Across metazoa, surfaces for respiratory gas exchange are diverse, and the size of those surfaces scales with body size. In vertebrates with lungs and gills, surface area and thickness of the respiratory barrier set upper limits to rates of metabolism. Conversely, some organisms and life stages rely on cutaneous respiration, where the respiratory surface (skin, cuticle, eggshell) serves two primary functions: gas exchange and structural support. The surface must be thin and porous enough to transport gases but strong enough to withstand external forces. Here, we measured the scaling of surface area and cuticle thickness in Antarctic pycnogonids, a group that relies on cutaneous respiration. Surface area and cuticle thickness scaled isometrically, which may reflect the dual roles of cuticle in gas exchange and structural support. Unlike in vertebrates, the combined scaling of these variables did not match the scaling of metabolism. To resolve this mismatch, larger pycnogonids maintain steeper oxygen gradients and higher effective diffusion coefficients of oxygen in the cuticle. Interactions among scaling components lead to hard upper limits in body size, which pycnogonids could evade only with some other evolutionary innovation in how they exchange gases.

## 1. Background

Understanding how and why rates of oxygen consumption scale with body size is a critical question in integrative biology [1,2]—because body size and metabolic rate play such central roles in physiology, ecology and evolution. One approach to understanding the scaling of organismal traits is to examine how they emerge from the scaling of, and interactions among, lower-level traits [3]. Here we do so for a form of respiratory exchange widely used by aquatic and marine organisms (cnidarians, nemerteans, poriferans, plethodontid salamanders, etc.)—cutaneous gas exchange. This mode is readily modelled using the Fick equation [4], which describes the flux of oxygen across a barrier and, as we describe below, provides a simple, powerful framework for integrating the lower-level traits that influence rates of gas exchange. We examine this problem using sea spiders (Pycnogonida), a diverse and basal clade of arthropods. Our results indicate that respiratory–structural trade-offs play critical roles in the evolution of gas exchange across body sizes. In addition, the scaling of the underlying Fick components suggests physiological limits to upper body size in sea spiders. While most marine arthropods possess specialized respiratory structures, which help them minimize or negate respiratory constraints on their cuticle, sea spiders rely exclusively on cutaneous gas exchange [5], yet still span a wide range of body sizes. Large-bodied individuals may face particularly difficult trade-offs, as their cuticle must withstand external forces while permitting sufficient gas exchange.

In all animals, oxygen moves across respiratory barriers by diffusion, which can be modelled using Fick's law [4,6]. Fick's law states that the flux of oxygen ($J$, $\mu mol\ s^{-1}$) across a barrier depends on the barrier's conductance ($G$, $\mu mol\ s^{-1}\ kPa^{-1}$) and the driving gradient for oxygen transport across it

**2**

(specifically, the gradient in partial pressure, $\Delta PO_2$, kPa) [7]:

$$J = G \times \Delta PO_2. \tag{1.1}$$

Conductance is thus a measure of how rapidly oxygen moves across a material given a difference in partial pressures. Whole-animal conductance is proportional to the surface area of the respiratory barrier ($A$, cm$^2$), the diffusion coefficient of oxygen in the material ($D_c$, cm$^2$ s$^{-1}$), the capacitance coefficient of the medium ($\beta$, $\mu$mol cm$^{-3}$ kPa$^{-1}$) and it is inversely proportional to the barrier's thickness ($x$, cm) [7]:

$$G = \frac{A}{x} \times D_c \times \beta. \tag{1.2}$$

The capacitance coefficient describes the increase in oxygen concentration per unit increase in partial pressure [7]. The capacitance coefficient is governed by physical properties and varies based on type of medium (i.e. air, freshwater, saltwater) and temperature of the medium. Substituting equation (1.2) into equation (1.1) gives the flux of oxygen as:

$$J = \frac{A}{x} \times D_c \times \beta \times \Delta PO_2. \tag{1.3}$$

To sustain aerobic metabolism, the flux of oxygen must on average match its consumption by metabolism. If the metabolic rate rises transiently higher than the flux, then internal $PO_2$ will decline. When internal $PO_2$ declines too severely, metabolic rate will subsequently decline or the animal must switch over to anaerobic processes. Alternatively, if the metabolic rate falls below the flux, then internal $PO_2$ will increase. The $\Delta PO_2$ between organism and environment will then decrease, until the flux once again balances the metabolic rate.

The relationship between oxygen flux and metabolic rate in vertebrates, including both endotherms and ectotherms, was recently analysed by Gillooly et al. [8]. They examined the size-scaling of both oxygen consumption and oxygen flux, which they defined as diffusive transport of oxygen across respiratory barriers (gills and lungs). Relationships between body mass and respiratory variables are typically described by the power law $Y = aM^b$, where $Y$ is a respiratory variable, $M$ is body mass, $a$ is the normalization constant and $b$ is the scaling exponent [9,10]. The scaling of oxygen consumption in endotherms and ectotherms ($b = 0.75$ and $0.84$, respectively) was closely matched by the scaling of diffusive oxygen flux ($b = 0.79$ and $0.82$, respectively) [8]. In addition, the 30-fold higher rates of oxygen consumption by endotherms were accommodated by 30-fold higher rates of flux, indicating differences in the normalization constant $a$ [8].

These findings allowed Gillooly et al. [8] to estimate how the scaling of oxygen flux emerges from the underlying Fick components. Gillooly et al. simplified this problem by leveraging prior results showing that $D_c$, $\beta$ and $\Delta PO_2$ are independent of body size ($b = 0$) [11,12], leaving just respiratory barrier thickness ($x$) and respiratory surface area ($A$) as potential controls on overall flux. In both endotherms and ectotherms, thickness scaled with a low coefficient ($b = 0.1$ and $b = -0.04$, respectively) and surface area with a high coefficient ($b = 0.89$ and $b = 0.78$, respectively), such that $A/x$ scaled as $b = 0.79$ and $b = 0.82$, respectively, very close to the observed scaling exponents of metabolic rate. Whether the conclusion, that respiratory surface area and barrier thickness entirely explain the scaling of flux, is broadly applicable across animals is unknown. In contrast to most vertebrates, which possess respiratory organs (gills and lungs) whose central function is gas exchange, many animals, particularly marine invertebrates, exchange gases directly across their cuticle or skin, a process called cutaneous gas exchange or 'skin-breathing', or across the eggshells in many egg-laying animals [13,14]. In cutaneous respiration, the cuticle or eggshell must allow adequate gas exchange while still providing structural support, and there is an apparent trade-off between these demands. The surface must be thin or porous enough to permit the diffusion of gases, and the cuticle or eggshell must protect the animal from predators and pathogens, and provide structural resistance to external forces [15–17]. This trade-off has also been hypothesized to exist in vertebrates, as the respiratory barrier must allow gas exchange but also be strong enough to prevent damage from different physical stresses (e.g. changes in gas pressure or surface tension) [6]. However, these internal barriers generally do not experience forces that are as large or as rapidly applied as those experienced by external structures (e.g. high current, grasping predators, crushing forces) and the trade-off may therefore not be as severe.

The conflicting demands of skin-breathing may fundamentally change how the components of Fick's law scale with body size. Perhaps the best-studied example of cutaneous respiration is that of vertebrate and invertebrate eggs. In eggs of most species, oxygen diffuses through air-filled pores in the eggshell [15,18,19]. Eggshell thickness and surface area scale ($b = 0.46$ and $0.66$, respectively) with mass [20,21]. These scaling coefficients differ from those found by Gillooly et al. [8] for the scaling of respiratory surface area and barrier thickness in vertebrates, probably reflecting that eggshells both exchange gases and provide structural support. In further contrast to adult vertebrates, the combined scaling of eggshell surface area and thickness is insufficient to explain the scaling of avian embryonic metabolism ($b = 0.73$) [22]. To meet this mismatch, pore area scales hypermetrically ($b = 1.24$) [20]. A high scaling coefficient of pore area is effectively similar to a high scaling coefficient of the effective diffusion coefficient ($D$, equation (1.3)), as a greater pore area allows for greater diffusion of oxygen by increasing the air-filled spaces in which oxygen can move easily. Therefore, an increase in pore surface area helps offset thicker shells and permits the higher oxygen conductance needed to meet the metabolic demands of larger embryos [9,20].

Here we use Antarctic sea spiders (class Pycnogonida) (figure 1), a group of arthropods that rely entirely on cutaneous respiration, to test whether the scaling of metabolic oxygen flux is controlled by just surface area and thickness (electronic supplementary material, figure S1a) or by simultaneous scaling of some or all the remaining Fick parameters. Sea spiders lack specialized respiratory structures such as gills, and rely instead on trans-cuticular diffusion of oxygen, probably via pores [5,23]. Like eggshells, the structure of pycnogonid cuticle reflects an evolutionary and functional compromise between gas exchange and structural support: the cuticle must be porous enough to allow in sufficient oxygen but strong enough to prevent buckling. Within the constraints of this trade-off, how do pycnogonids match flux capacity to metabolic rate across body sizes? Body sizes of Antarctic pycnogonids range from approximately 1 cm to approximately 70 cm across all lineages [5]. We envision multiple alternatives that could achieve this matching (electronic supplementary material, figure S1). We limit the full range of possibilities by first characterizing the size-dependence of the two parameters, $A$ and $x$, that are most likely to be constrained. Because the shape of sea spiders does not change radically with size, we
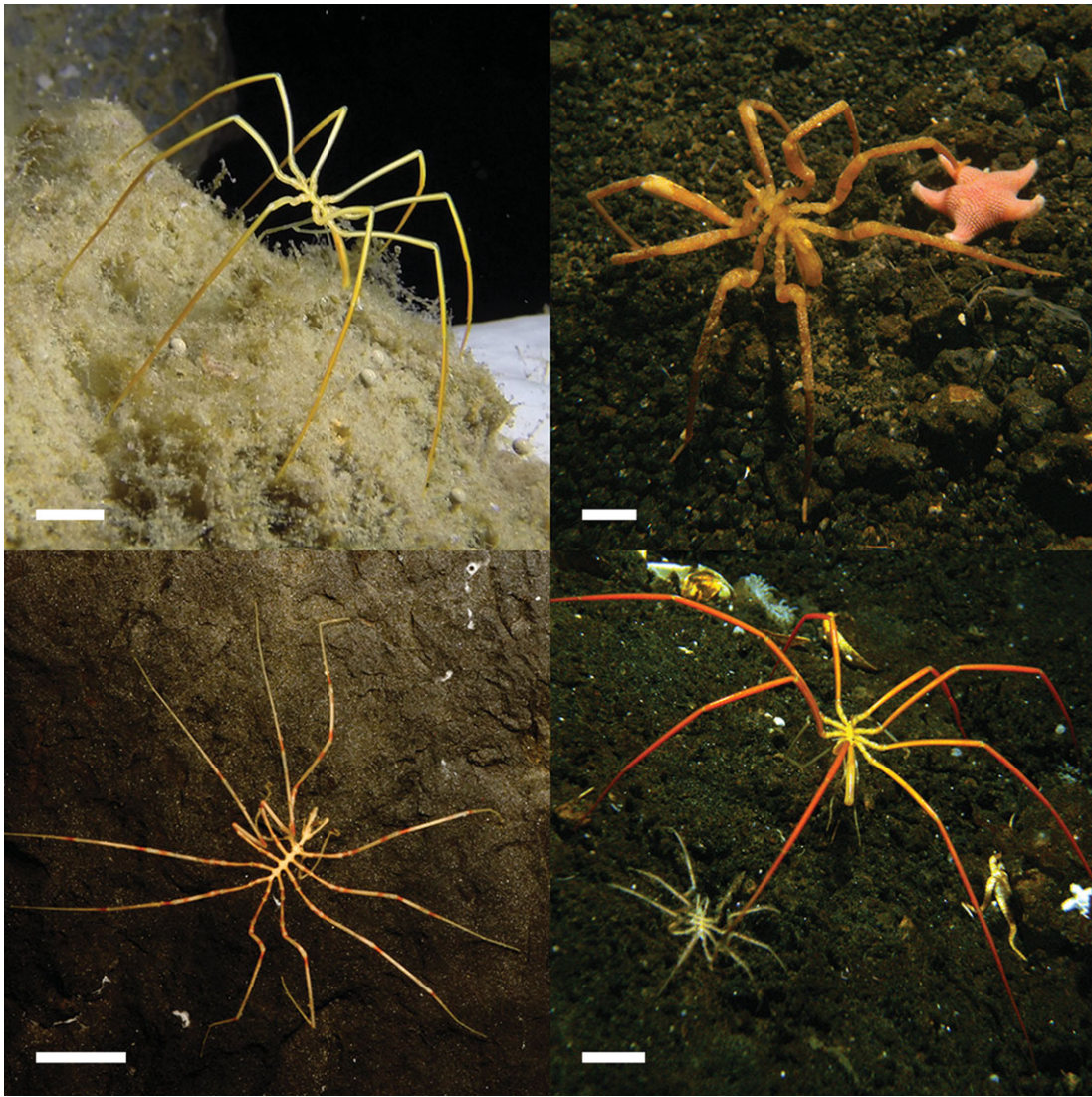
**Figure 1.** Various sea spiders (Arthropoda, Pycnogonida) collected in McMurdo Sound, Antarctica. Scale bars are approximately 1 cm in each panel. Top left: *Colossendeis megalonyx*, top right: *Ammothea glacialis*, bottom left: *Pentanymphon antarcticum*, bottom right: *Nymphon australe* (smaller animal) and *Colossendeis hoeki* (larger animal). Photo credit to H.A.W. and B.W.T.

expect that $A$ scales with geometric isometry ($b = 0.66$). This prediction is supported by an earlier study of Antarctic sea spiders [24]. We also predict that cuticle thickness, $x$, scales with geometric isometry ($b = 0.33$), because larger-bodied individuals will need more reinforced legs to handle larger forces. (Note that this is the key point of divergence from thickness of vertebrate respiratory surface, $b = 0.1$ [8].) If the structural variables scale this way, then $A/x$ scales as $b = 0.66 - 0.33 = 0.33$, which is far lower than any expected scaling of metabolic rate. Electronic supplementary material, figure S1$b-d$ lays out alternative ways that sea spiders could make up the difference.

In addition to measuring the scaling of oxygen consumption, we also measured the scaling of surface area, cuticle thickness, oxygen gradient across the cuticle and the functional diffusion coefficient of oxygen through sea spider cuticle, which allowed us to estimate the total flux of oxygen across cuticle (using a derivative of Fick's law, equation (1.3)). These factors were measured in 12 species of Pycnogonida from five families.

## 2. Methods

Sea spiders were collected by diving using SCUBA in McMurdo Sound, Antarctica ($77°85'$ S, $166°84'$ E) in October and November 2015 and 2016. Seawater temperatures averaged $-1.8°C$. Animals were kept in seawater tables $1-2°C$ above ambient seawater temperatures and used within two weeks of collection.

Scaling analyses were conducted on 12 Antarctic species (electronic supplementary material, tables S1–S3). Species representatives were identified on the basis of morphology and confirmed using DNA barcoding and published sequences. We used the DNeasy kit (Qiagen, Inc., Valencia, CA, USA) to extract DNA from an approximately 1 mm$^3$ piece of the dactyl of one leg of each individual pycnogonid. Samples were incubated overnight with 5 μl of proteinase K in a heated ($56°C$) shaking block (900 r.p.m.). Seven hundred and twelve base pairs of the mitochondrial cytochrome oxidase-1 (*CO1*) gene were PCR-amplified from the extracted DNA using the jgHCO2198 and jgLCO1490 primers of [25]. Reactions were composed of 9.5 μl dH$_2$O, 12.5 μl *Taq* 2X Ready Mix (Bioline, Taunton, MA, USA), 1 μl of each 10 μM primer and 1 μl of genomic DNA. The amplification cycle consisted of an initial denaturing step at $94°C$ for 1 m, followed by 30 cycles of $94°C$ for 1 m, $48°C$ for 1 m and $72°C$ for 1 m. PCR products were cleaned by incubating with exonuclease I and shrimp alkaline phosphatase (New England BioLabs, Ipswich, MA, USA) at $37°C$ for 30 m. Approximately 600–650 bp were then sequenced from each primer by Sanger sequencing at the Advanced Studies in Genomics, Proteomics, and Bioinformatics core facility, University of Hawai'i at Mānoa. Complementary sequences were aligned in Geneious 9.1.5 (Biomatters Ltd., Auckland, NZ). Each consensus sequence was

compared with available GenBank sequences using the BLASTN search routine implemented with default parameters in GenBank.

## (a) Oxygen consumption

Rates of oxygen consumption were measured using an oxygen optode system (2-channel FireSting, PyroScience) with temperature-compensation and closed-system respirometry. Chambers were custom-milled from blocks of nylon. Chambers were built in pairs whose volumes were matched to the size of each sea spider measured (9, 17, 70, 292 and 3650 ml; all volumes measured gravimetrically as the difference between mass with and without freshwater), and each chamber had a Teflon-covered magnetic stir bar, shielded with a small housing made of PVC and Nitex mesh to protect the sea spider. During runs, the chambers were held in 5-l baths of water set on top of magnetic stir plates. Initial dye tests showed that water in the chambers was fully mixed in 20–30 s. The sensor spot of the optode system was fixed with silicone glue to thin (less than 2 mm) glass discs, which were sealed to the tops of the chambers with rubber gaskets and held in place with screw-down Plexiglas tops.

Metabolic measurements were made in a cold room with mean temperature $-1.1°C$ (range $-1.7$ to $-0.6°C$). In most runs (35 of 38), the chambers were run in pairs, with one blank and the other containing a sea spider. To set up a run, fresh seawater was bubbled with air in the cold room for 6–12 h. Optodes were calibrated at the beginning of every run by immersing them for 5–10 min in the bubbled water and recording the air saturated raw values from both sensors. The bubbles were then turned off and the chambers loaded entirely underwater with its stir bar, housing, and a sea spider (for one of the pair; the other of the pair was identical but contained no sea spider). The chamber was then sealed with the glass disc and Plexiglas top, connected to the fibre optic cable from the optode electronics, and immersed into a water bath on one of the stir plates. The room was dark during respirometry runs. Oxygen levels in the chambers were recorded onto a computer at 1 Hz for 8–24 h using FireSting recording software. Oxygen traces were analysed using scripts written in R (v. 3.0.2) [26]. Using the calibration values, raw sensor values were converted to oxygen concentrations, and the rates of oxygen consumption were estimated by multiplying the volume of the chamber by the difference between the slopes of the traces in the experimental and blank chambers, giving metabolic rate in $\mu mol\ O_2\ h^{-1}$. Blank chambers had slopes near zero, indicating little exchange of oxygen between the water and the nylon of the chambers and little consumption of oxygen by microorganisms in the seawater.

## (b) Morphological parameters

We measured sea spider body size by weighing and photographing each individual. Individuals were blotted dry and weighed using a microbalance ($\pm 0.001$ g, AE163 Mettler-Toledo). Sea spiders were photographed (dorsal side) using a stereomicroscope fitted with a Nikon D7100 digital camera and microscope adapter. Individuals too large to be adequately viewed under a stereomicroscope were imaged with the Nikon camera attached to a tripod. Surface area measurements were made in imageJ (v1.49) [27]. Projected surface area for one side was multiplied by two to account for the dorsal and ventral sides. Leg span was also measured in imageJ from these images. Leg span was measured between the tips of the first pair of walking legs as described previously [28]. If one of the legs was damaged or missing, leg span was measured between the second pair of walking legs.

Cuticle thickness was measured on the femur of the second left leg of each individual or, if it was damaged or missing, on the second right leg. The leg was removed from the body and multiple thin sections (less than 1 mm, each) were made of the femur using a single-edge razor blade. Thin sections were cut after measuring

diffusion through the leg (see *Diffusion coefficients* below), cross-sectional images were then taken using a compound microscope and cuticle thickness was measured in imageJ.

## (c) Oxygen microelectrodes

In the following sections (*Diffusion coefficients* and *Internal oxygen levels*), oxygen levels were measured using Clark-style microelectrodes (50 or 100 µm glass tips; Unisense, Denmark) mounted on a micromanipulator. The electrode was connected to a picoammeter (PA2000; Unisense) and data were recorded once per second by a UI-2 interface (Sable Systems, Las Vegas, NV, USA) controlled by Expedata (v1.8.4; Sable Systems). At the beginning of a set of measurements, an electrode was calibrated at the measurement temperature (between $-1.5$ and $2°C$) using air-bubbled and $N_2$-bubbled seawater held in a small, water-jacketed glass platform whose temperature was controlled by a recirculating water bath. Between each sea spider the electrode was re-calibrated in air-bubbled seawater.

## (d) Diffusion coefficients

The functional diffusion coefficient of oxygen through cuticle reflects two separate diffusion processes: the movement of oxygen directly through the cuticle and the movement of oxygen through tissue-filled pores in the cuticle. Owing to the chitinous exoskeleton of sea spiders, the diffusion of oxygen through cuticle is probably very low, while the diffusion of oxygen through pores is probably very high, close to that of seawater. Therefore, the measured *functional* diffusion coefficients presented here reflect both processes and probably are dominated by diffusion via pores.

We estimated functional diffusion coefficients of oxygen in cuticle using step-change experiments in which oxygen levels inside legs were monitored as external $PO_2$ was altered [29]. Each measurement was conducted on a single femur from each individual and the step-change took place within the water-jacketed glass platform described above. First, an oxygen electrode was inserted into the centre of a sea spider femur. Once the oxygen electrode within the femur had stabilized, the air-saturated water around the femur was rapidly replaced by deoxygenated ($N_2$-bubbled) water (generally within 5 s). The container was covered and $N_2$ gas was bubbled into the container after the step-change to prevent invasion of external $O_2$. During the step-change, we measured how long it took the internal oxygen pressure to reach zero. This change in oxygen pressure over time was modelled by an analytic equation to estimate the diffusion coefficient of the cuticle [29,30]. We included two layers in the model, the thickness of the cuticle and the radius of the haemocoel. Assumptions of the model included that the electrode was in the centre of the femur and not against the internal cuticle and there was no metabolic consumption of oxygen. The model also assumed that the fluid within the haemocoel was unmixed and that oxygen moved only by diffusion (with a diffusion coefficient identical to that in seawater). Individual runs often took less than 45 min.

To prevent oxygen consumption by leg sections, internal tissues were removed with forceps (in individuals $>1$ g) or killed using a brief ethanol treatment (in individuals $<1$ g); additional tests showed that there was no difference in diffusion coefficients in sea spider legs before and after a 2-min treatment with 95% ethanol ($t_7 = 0.689$, $p = 0.513$). In either method, the interior space of the femur was fully filled with seawater before the step-change assay. In large sea spiders (more than 5 g), the femur was sealed from the open environment with Loctite marine epoxy (Henkel Corp., Düsseldorf, Germany) on each end. In small sea spiders (less than 5 g), the oxygen electrode was inserted through the coxa and into the femur, creating a natural seal that prevented the free movement of seawater into the femur. In each case, the femur was held in place in a glass container containing seawater that was bubbled continuously with air.

5

rspb.royalsocietypublishing.org    Proc. R. Soc. B 284: 20171779

**Table 1.** Summary of OLS and PGLS regression analyses for $A$ (surface area), $x$ (cuticle thickness), $D_c$ (diffusion coefficient), $\Delta PO_2$ (oxygen gradient), $J$ (flux), $MR$ (metabolic rate) and $LS$ (leg span) versus body mass in sea spiders. '$N$' represents number of species used in each analysis. '$a$' represents the intercept and '$b$' represents the scaling exponent. 'mtCO1' indicates PGLS using tree built with unconstrained topology, 'var. brlens' indicates PGLS using tree with variable branch lengths and 'equal brlens' indicates PGLS using same tree topology but with all branch lengths set to 1. Data are listed in electronic supplementary material, tables S1–S3.

| models | $N$ | $a$ | 95% CI | $p$ | $b$ | 95% CI | $p$ | $R^2$ |
|---|---|---|---|---|---|---|---|---|
| $A$ (cm$^2$); figure 2a | | | | | | | | |
| OLS | 12 | 1.15 | (1.08,1.21) | <0.001 | 0.63 | (0.54,0.71) | <0.001 | 0.96 |
| PGLS-mtCO1 | 12 | 1.12 | (0.95,1.29) | <0.001 | 0.59 | (0.48,0.69) | <0.001 | |
| PGLS-var. brlens | 12 | 1.12 | (0.99,1.24) | <0.001 | 0.58 | (0.48,0.69) | <0.001 | |
| PGLS-equal brlens | 12 | 1.13 | (0.97,1.28) | <0.001 | 0.61 | (0.50,0.71) | <0.001 | |
| $x$ (cm); figure 2b | | | | | | | | |
| OLS | 12 | −2.22 | (−2.37,−2.05) | <0.001 | 0.27 | (0.06,0.49) | 0.019 | 0.38 |
| PGLS-mtCO1 | 12 | −2.32 | (−2.70,−1.94) | <0.001 | 0.15 | (−0.09,0.38) | 0.196 | |
| PGLS-var. brlens | 12 | −2.24 | (−2.53,−1.95) | <0.001 | 0.16 | (−0.09,0.40) | 0.188 | |
| PGLS-equal brlens | 12 | −2.19 | (−2.51,−1.87) | <0.001 | 0.14 | (−0.07,0.36) | 0.174 | |
| $D_c$ (cm$^2$ s$^{-1}$); figure 2c | | | | | | | | |
| OLS | 11 | −5.93 | (−6.05,−5.80) | <0.001 | 0.20 | (0.04,0.37) | 0.021 | 0.40 |
| PGLS-mtCO1 | 11 | −5.96 | (−6.27,−5.65) | <0.001 | 0.12 | (−0.12,0.36) | 0.300 | |
| PGLS-var. brlens | 11 | −5.96 | (−6.27,−5.65) | <0.001 | 0.10 | (−0.15,0.35) | 0.400 | |
| PGLS-equal brlens | 11 | −5.94 | (−6.27,−5.62) | <0.001 | 0.13 | (−0.08,0.35) | 0.200 | |
| $\Delta PO_2$ (kPa); figure 2d | | | | | | | | |
| OLS | 11 | 0.66 | (0.55,0.77) | <0.001 | 0.27 | (0.12,0.42) | 0.003 | 0.60 |
| PGLS-mtCO1 | 11 | 0.66 | (0.31,1.00) | 0.002 | 0.22 | (0.01,0.44) | 0.044 | |
| PGLS-var. brlens | 11 | 0.66 | (0.41,0.91) | <0.001 | 0.21 | (−0.01,0.44) | 0.055 | |
| PGLS-equal brlens | 11 | 0.67 | (0.36,0.98) | <0.001 | 0.19 | (−0.02,0.40) | 0.069 | |
| $J$ (μmol s$^{-1}$); figure 3 | | | | | | | | |
| OLS | 11 | −3.71 | (−4.06,−3.36) | <0.001 | 0.83 | (0.34,1.31) | 0.004 | 0.58 |
| PGLS-mtCO1 | 11 | −4.01 | (−4.83,−3.19) | <0.001 | 0.64 | (0.13,1.15) | 0.019 | |
| PGLS-var. brlens | 11 | −3.89 | (−4.53,−3.25) | <0.001 | 0.65 | (0.10,1.20) | 0.025 | |
| PGLS-equal brlens | 11 | −3.77 | (−4.65,−2.90) | <0.001 | 0.74 | (0.15,1.34) | 0.020 | |
| $MR$ (μmol s$^{-1}$); figure 3 | | | | | | | | |
| OLS | 10 | −3.96 | (−4.15,−3.77) | <0.001 | 0.80 | (0.52,1.08) | 0.002 | 0.83 |
| PGLS-mtCO1 | 10 | −4.03 | (−4.47,−3.59) | <0.001 | 0.77 | (0.47,1.08) | <0.001 | |
| PGLS-var. brlens | 10 | −4.01 | (−4.34,−3.69) | <0.001 | 0.77 | (0.47,1.07) | <0.001 | |
| PGLS-equal brlens | 10 | −3.99 | (−4.39,−3.60) | <0.001 | 0.75 | (0.47,1.04) | <0.001 | |
| $LS$ (cm); electronic supplementary material, figure S1 | | | | | | | | |
| OLS | 12 | 1.05 | (0.97,1.13) | <0.001 | 0.32 | (0.22,0.42) | <0.001 | 0.81 |
| PGLS-mtCO1 | 12 | 1.03 | (0.84,1.23) | <0.001 | 0.27 | (0.15,0.39) | <0.001 | |
| PGLS-var. brlens | 12 | 1.02 | (0.87,1.16) | <0.001 | 0.27 | (0.15,0.39) | <0.001 | |
| PGLS-equal brlens | 12 | 1.02 | (0.83,1.21) | <0.001 | 0.30 | (0.17,0.42) | <0.001 | |

## (e) Internal oxygen levels

On each sea spider, oxygen levels were measured in the femur and in the ambient seawater in which it was contained. A single leg was cut off (underwater) across the second coxa of a living sea spider and the electrode tip was advanced through the third coxa and well into the femur. This process was done as quickly as possible (usually less than 1 min) to minimize changes in internal $PO_2$ occurring from tissue dead or changes in circulation; this time course is reasonable because metabolic rates are very low. During these measurements, which took several minutes to stabilize for each individual, the temperature of the water in the plastic container generally rose by 1–2°C. The effects of these temperature changes on the electrode readings were offset by noting the local change (rise) in the measured oxygen level in the ambient seawater. Raw electrode readings were converted to oxygen concentrations using the calibration measurements.

## (f) Oxygen flux

After estimating the diffusion coefficient of the cuticle ($D_c$) and measuring the cuticle thickness ($x$), surface area ($S$) and oxygen
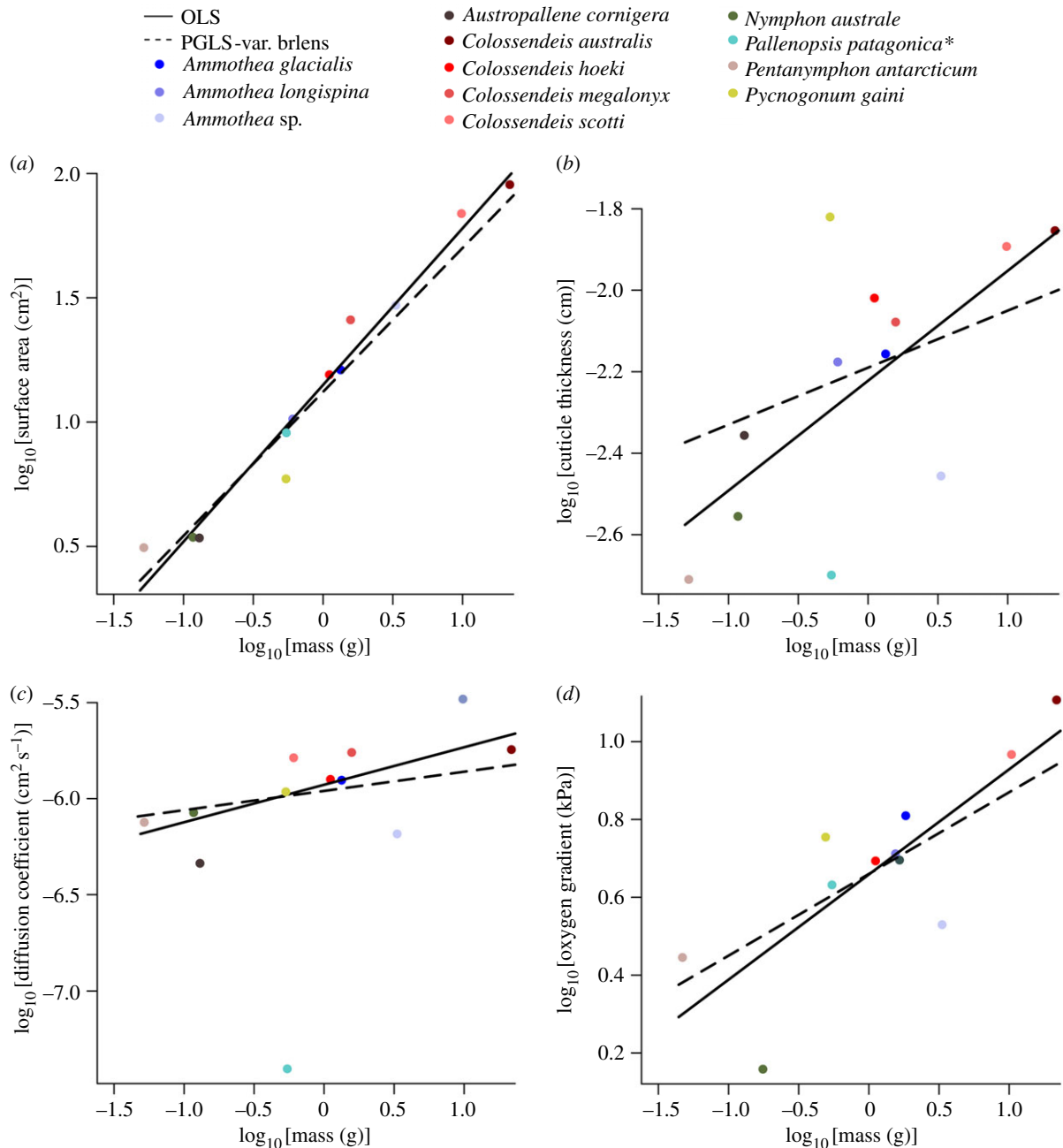
**Figure 2.** Scaling relationships for surface area ($N = 12$) ($a$), cuticle thickness ($N = 12$) ($b$), cuticle diffusion coefficient ($N = 11$) ($c$) and oxygen gradient ($N = 11$) ($d$) to body mass in Antarctic sea spiders. Lines indicate fits using OLS and PGLS-var. brlens regression. See table 1 for scaling coefficients, and the data used are listed in electronic supplementary material, tables S1–S3. *Pallenopsis patagonica* appears to be an outlier and was not used in calculating the diffusion coefficient scaling relationship.

gradient ($\Delta PO_2$), we calculated flux ($J$) with equation (1.3). The capacitance coefficient of seawater ($\beta$) was taken from Dejours [7] based on ambient water temperatures (approximately $-1°C$).

## (g) Statistical analysis

To analyse scaling relationships, we $\log_{10}$-transformed the data and then fitted ordinary least square models (OLS) to each respiratory variable (surface area, cuticle thickness, diffusion coefficient, oxygen gradient, flux, oxygen consumption and leg span) versus body mass. For most species, we took the average measurements from 2 to 11 individuals, which varied within each species and measurement (electronic supplementary material, tables S1–S3). However, we had only one individual of *Austropallene cornigera* and *Colossendeis australis*. All statistical analyses were carried out in R (v. 3.3.0) [26].

In comparative studies, closely related species tend to be similar because they share relatively recent common ancestry [31]. To

account for this possibility, we conducted multiple phylogenetic general least square (PGLS) models using a tree built with mitochondrial cytochrome $c$ oxidase (CO1) sequences collected from the samples used in this study. The tree was constructed using a maximum-likelihood approach in PAUP* (v4.0) [32]. The tree was constructed using the best model of molecular evolution selected by ModelTest (v3.7) [33] using Akaike information criteria. The best fit model was GTR + I + G. The tree was estimated using a heuristic search with the tree bisection reconnection algorithm for five replicate starting trees constructed by random sequence addition, and node robustness was estimated after 100 bootstrap replicates (electronic supplementary material, figure S2a). The topology of this tree was different from other published pycnogonid phylogenies [34]. Therefore, owing to limited taxonomic sampling in our dataset, we also created a second tree by constraining the topology at the family level to match the family topology of Arango & Wheeler [34] (electronic supplementary material, figure S2b). Their tree was built using six different

nuclear or mitochondria genes and included 63 species of Pycnogonida from all extant families. After constraining the topology of the tree in this manner, the branch lengths were left to vary based on our CO1 data. Because of our low taxon sampling and the associated uncertainty in branch lengths of a single gene tree, we bracketed our hypotheses by comparing our data based on a star phylogeny (OLS), an unconstrained phylogeny built with our CO1 data (PGLS-mtCO1), a constrained phylogeny where branch lengths were free to vary based on our CO1 data (PGLS-var. brlens) and a constrained phylogeny using equal branch lengths (i.e. setting branch lengths to one) (PGLS-equal brlens) which accounts for branching patterns among taxa but not branch lengths [32].

Phylogenetic generalized least-squares models were conducted using all three types of phylogenetic trees using the R package 'ape' (v3.5) [35,36]. In each case, we assumed a Brownian motion model of trait evolution [31], which was the same model Gilooly *et al.* used on similar trait data [8]. As in the OLS model described above, we used $log_{10}$-transformed data and took species averages to fit each PGLS model.

We tested for phylogenetic signal using Pagel's lambda [37,38]. Estimates of lambda for the respiratory variables spanned from 0 (no phylogenetic signal) to 1 (strong phylogenetic signal). Log-likelihood tests showed that the lambdas for only two of the variables, cuticle thickness and flux, were significantly different from 0, but these two variables were not significant across all types of PGLS analyses (electronic supplementary material, table S4). After applying a Bonferroni correction to account for multiple comparisons within each variable ($\alpha = 0.05/3 = 0.017$), however, no value of lambda differed significantly from 0. Clearly, these analyses for phylogenetic signal are limited by taxonomic sampling, which may prevent us from identifying a signal even if it is present. In general, studies with more than 20 sampled taxa can detect phylogenetic signals if they are present, whereas those with fewer than 20 sampled taxa have substantially less power [39]. On the basis of the lack of almost any detectable phylogenetic signal, only the OLS results were discussed.

## 3. Results and discussion

In vertebrates, surface area and barrier thickness alone constrain oxygen flux (electronic supplementary material, figure S1*a*) [8]. Here, our results (table 1, figure 2*a*–*d*) indicate that surface area did not scale as high in Antarctic sea spiders as it does in vertebrates (0.63, figure 2*a*, and 0.89, respectively), but barrier thickness scaled higher in Antarctic sea spiders than in vertebrates (0.27, figure 2*b*, and 0.1, respectively) [8]. These differences probably result from the dual roles of the cuticle in both gas exchange and structural support. Furthermore, the combined scaling of surface area and cuticle thickness (i.e. $0.63 - 0.27 = 0.36$) does not scale high enough to meet the metabolic demands of sea spiders (0.8). To offset this disparity, both the effective cuticular diffusion coefficient and the oxygen gradient scaled positively with body size (0.2, figure 2*c*, and 0.27, figure 2*d*, respectively). The combined scaling of the diffusion coefficient, oxygen gradient, surface area, and barrier thickness give an estimate of flux scaling (i.e. $0.63 - 0.27 + 0.2 + 0.27 = 0.83$) that matches metabolic scaling very closely (0.8, figure 3). In contrast to vertebrates, therefore, in sea spiders, which rely on cutaneous respiration, all components of Fick's Law (except for $\beta$, because it is governed by physical properties) increase with body size (electronic supplementary material, figure S1*d*).

Like the scaling coefficients, the intercepts of estimated fluxes (from the Fick analysis) and of metabolic rate were quite similar (−3.71 and −3.96, respectively, with overlapping
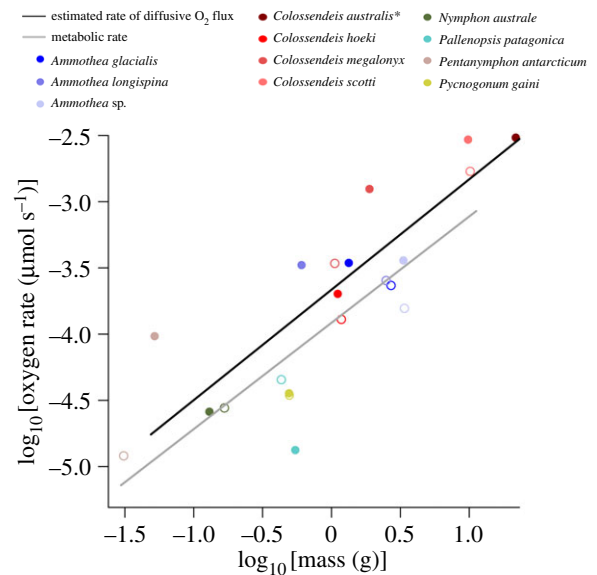


**Figure 3.** Scaling relationship for estimated rate of diffusive oxygen flux and metabolic rate to body mass in Antarctic sea spiders. The estimated rates of diffusive oxygen flux for each species are indicated by solid circles ($N = 11$) while the metabolic rate values are indicated by open circles ($N = 10$). Lines were fitted using OLS regression. See table 1 for scaling coefficients, and the data used are in electronic supplementary material, tables S1–S3. *We did not get metabolic data on *Colossendeis australis*.

confidence intervals). This close match means that our measurements and analyses account for all of the major processes contributing to metabolic fluxes of oxygen.

Two of the four tunable variables of Fick's law (equation (1.3)) cannot continue increasing indefinitely and so impose upper limits on body size: the cuticular diffusion coefficient ($D_c$) and the oxygen gradient across the cuticle ($\Delta PO_2$). The cuticular diffusion coefficient rises with cuticular porosity, but it obviously cannot rise above some upper limit (e.g. 100% porosity would mean that the cuticle did not exist). Davenport *et al.* [23] calculated the porosity of one large Antarctic species (*Decalopoda australis*) to be about 35%. Here, as a conservative estimate, we estimated maximum porosity as 50%, which would give an effective diffusion coefficient of approximately half the diffusion coefficient of oxygen in seawater ($5 \times 10^{-6}$ cm$^2$ s$^{-1}$), assuming that the material within the pores does not significantly slow rates of diffusion. Together with the remaining scaling coefficients (table 1), this value indicates that sea spiders would approach this limit at approximately 1400 g (figure 4*a*). The scaling of the oxygen gradient also imposes limits. Physically, internal $PO_2$ cannot go below 0 kPa (gradient of approx. 21 kPa). Projecting out to larger body sizes (table 1) shows that sea spiders hit this limit at approximately 300 g (figure 4*b*), which means that the oxygen gradient should limit large size substantially sooner than should cuticle porosity. The largest sea spider (*Colossendeis colossea*) ever reported had a leg span somewhat larger than 70 cm but no body mass was given [5]. Using our scaling coefficients for leg span (table 1), a 70 cm sea spider has a projected body size of approximately 300 g (electronic supplementary material, figure S3), right at the size limit predicted by the scaling of the oxygen gradient. This analysis suggests that evolving larger size would require evolutionary innovations in the mechanisms for obtaining and distributing oxygen. For example, other groups of large-bodied marine invertebrates, such as
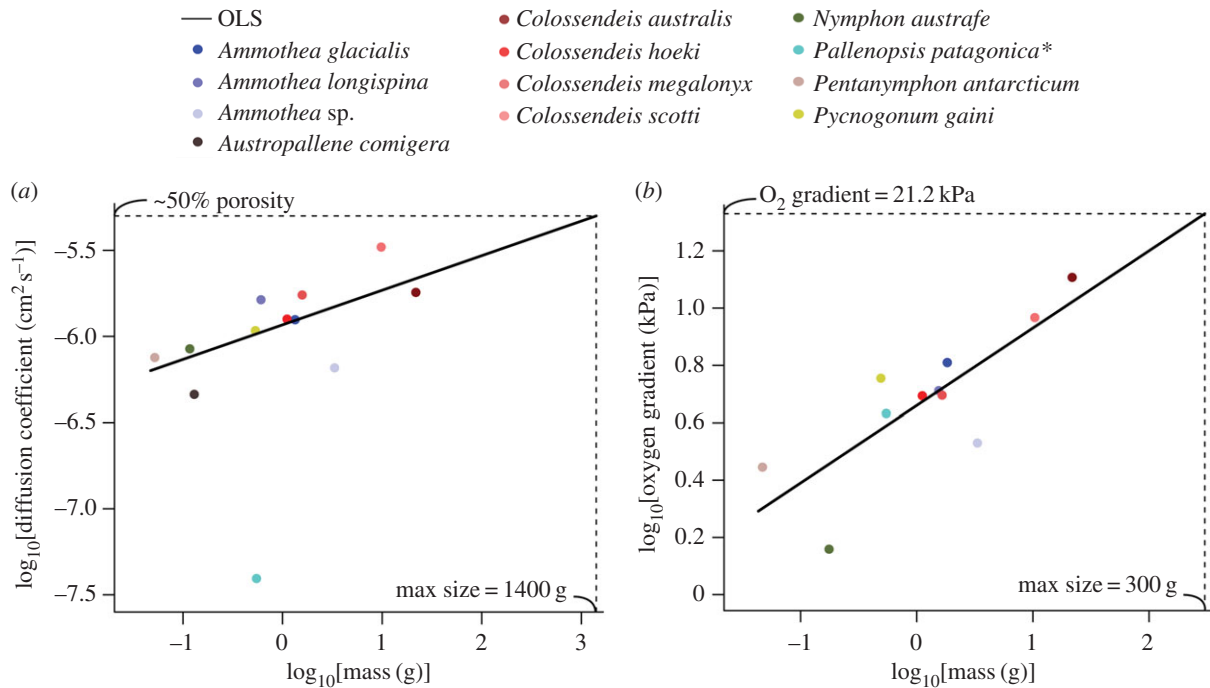
**Figure 4.** Upper limits to body size estimated from the diffusion coefficient ($N = 11$) (a) and oxygen gradient ($N = 11$) (b). Upper limits were found by extrapolating OLS regression line out to the point where the line intersected the estimated y-values. See table 1 for scaling coefficients. See text for details. *Pallenopsis patagonica* appears to be an outlier and was not used in calculating the upper limits to body size using the diffusion coefficient scaling relationship.

other groups of large arthropods (e.g. crustaceans), evade respiratory constraints by using both respiratory pigments and strong heart-driven flows of haemolymph [9]. Sea spiders drive circulatory flows with both their hearts and guts [40]. In addition, they are known to transcribe the genes for respiratory pigments (i.e. haemocyanin) [41], but no proteins have yet been detected in the haemolymph [42].

An obvious alternative path to balancing the oxygen budget would be to have thinner or more porous cuticle. One outlier in our data suggests that one species has done so. *Pallenopsis patagonica* has very low porosity (figure 2c) but also very thin cuticle for its body size (figure 2b). Perhaps its ecology protects it from strong external forces. We often found this species clinging to hydroids rather than walking freely on the benthos. We hypothesize that there is a trade-off between the ability of sea spiders to get oxygen and their ability to resist external forces. Extremely thin cuticle may buckle as the animal walks around, while cuticle constructed of more than half pores may collapse due to external forces. Alternatively, *Colossendeis* spp. have proportionally thick and porous cuticle for their body sizes (figure 2b,c). Individuals of these species were often found freely moving along the benthos, actively foraging. To quantify this trade-off, future studies should measure the mechanical strength of the cuticle with different levels of porosity. For example, some deep-sea species also grow to large sizes [5] but live in an environment with proportionately less oxygen. These species may also experience lower external forces (such as strong currents), which may allow them to evolve relatively thin, porous cuticles without risking breakage.

Body size profoundly alters both the demand of organisms for oxygen and the challenges and possible evolutionary solutions to obtaining it. Gillooly *et al.* [8] showed, in vertebrates, that changes in respiratory surface area and thickness alone are sufficient to balance the oxygen budget across body sizes. Our study, of sea spiders, provides a strikingly different picture: changes in body size lead to the simultaneous co-adjustment of four of the underlying Fick variables, not just surface area and cuticular thickness. Our result suggests that the evolutionary opportunities available to, and constraints operating on, respiratory systems across body sizes change in important ways among groups with different fundamental body plans. Moreover, alternative evolutionary trajectories among different high-level taxonomic groups (classes, phyla) probably play important roles in generating different upper limits to body size among groups.

# References

1.  West GB, Brown JH, Enquist BJ. 1997 A general model for the origin of allometric scaling laws in biology. *Science* **276**, 122–126. (doi:10.1126/science.276.5309.122)

2.  West GB, Brown JH. 2005 The origin of allometric scaling laws in biology from genomes to

9

rspb.royalsocietypublishing.org    Proc. R. Soc. B 284: 20171779

ecosystems: towards a quantitative unifying theory of biological structure and organization. *J. Exp. Biol.* **208**, 1575–1592. (doi:10.1242/jeb.01589)

3. Banavar JR, Damuth J, Maritan A, Rinaldo A. 2002 Supply-demand balance and metabolic scaling. *Proc. Natl Acad. Sci. USA* **99**, 10 506–10 509. (doi:10.1073/pnas.162216899)

4. Fick A. 1855 Ueber diffusion. *Ann. Phys.* **170**, 59–86. (doi:10.1002/andp.18551700105)

5. Arnaud F, Bamber RN. 1987 The biology of Pycnogonida. *Adv. Mar. Biol.* **24**, 1–96.

6. Maina JN, West JB. 2005 Thin and strong! The bioengineering dilemma in the structural and functional design of the blood-gas barrier. *Physiol. Rev.* **85**, 811–844. (doi:10.1152/physrev.00022.2004)

7. Dejours P. 1981 *Principles of comparative respiratory physiology*, p. 265. Amsterdam, The Netherlands: Elsevier/North-Holland Biomedical Press.

8. Gillooly JF, Gomez JP, Mavrodiev EV, Rong Y, McLamore ES. 2016 Body mass scaling of passive oxygen diffusion in endotherms and ectotherms. *Proc. Natl Acad. Sci USA* **113**, 5340–5345. (doi:10.1073/pnas.1519617113)

9. Schmidt-Nielson K. 1984 *Scaling: why is animal size so important?* pp 241. Cambridge, UK: Cambridge University Press.

10. Mortola JP. 2015 Generalities of gas diffusion applied to the vertebrate blood–gas barrier. In *The vertebrate blood–gas barrier in health and disease*, (ed. AN Makanya), pp. 1–14. New York, NY: Springer.

11. Dawson TH. 2005 Modeling of vascular networks. *J. Exp. Biol.* **208**, 1687–1694. (doi:10.1242/jeb.01622)

12. Weibel ER, Taylor CR, Gehr P, Hoppeler H, Mathieu O, Maloiy GMO. 1981 Design of the mammalian respiratory system. IX. Functional and structural limits for oxygen flow. *Respir. Physiol.* **44**, 151–164. (doi:10.1016/0034-5687(81)90081-5)

13. Feder ME, Burggren WW. 1985 Skin breathing in vertebrates. *Sci. Am.* **253**, 126–142. (doi:10.1038/scientificamerican1185-126)

14. Graham JB. 1988 Ecological and evolutionary aspects of integumentary respiration: body size, diffusion, and the Invertebrata. *Am. Zool.* **28**, 1031–1045. (doi:10.1093/icb/28.3.1031)

15. Carey C. 1980 Introduction to the symposium: physiology of the avian egg. *Am. Zool.* **20**, 325–327. (doi:10.1093/icb/20.2.325)

16. Clarke BT. 1997 The natural history of amphibian skin secretions, their normal functioning and potential medical applications. *Biol. Rev. Camb. Philos. Soc.* **72**, 365–379. (doi:10.1017/S0006323197005045)

17. Rollins-Smith LA, Reinert LK, O'Leary CJ, Houston LE, Woodhams DC. 2005 Antimicrobial peptide defenses in amphibian skin. *Integr. Comp. Biol.* **45**, 137–142. (doi:10.1093/icb/45.1.137)

18. Kern MD, Ferguson MWJ. 1997 Gas permeability of American alligator eggs and its anatomical basis. *Physiol. Zool.* **70**, 530–546. (doi:10.1086/515860)

19. Woods HA, Bonnecaze RT, Zrubek B. 2005 Oxygen and water flux across eggshells of *Manduca sexta*. *J. Exp. Biol.* **208**, 1297–1308. (doi:10.1242/jeb.01525)

20. Ar A, Paganelli CV, Reeves RB, Greene DG, Rahn H. 1974 The avian egg: water vapor conductance, shell thickness, and functional pore area. *Condor* **76**, 153–158. (doi:10.2307/1366725)

21. Paganelli CV, Olzowka A, Ar A. 1974 The avian egg: surface area, volume, and density. *Condor* **76**, 319–325. (doi:10.2307/1366345)

22. Ar A, Rahn H. 1985 Pores in avian eggshells: gas conductance, gas exchange and embryonic growth rate. *Respir. Physiol.* **61**, 1–20. (doi:10.1016/0034-5687(85)90024-6)

23. Davenport J, Blackstock N, Davies A, Yarrington M. 1987 Observations on the physiology and integumentary structure of the Antarctic pycnogonid *Decolopoda australis*. *J. Zool.* **22**, 451–465. (doi:10.1111/j.1469-7998.1987.tb01545.x)

24. Woods HA, Moran AL, Arango CP, Mullen L, Shields C. 2009 Oxygen hypothesis of polar gigantism not supported by performance of Antarctic pycnogonids in hypoxia. *Proc. Biol. Sci.* **276**, 1069–1075. (doi:10.1098/rspb.2008.1489)

25. Geller J, Meyer C, Parker M, Hawk H.. 2013 Redesign of PCR primers for mitochondrial cytochrome c oxidase subunit I for marine invertebrates and application in all-taxa biotic surveys. *Mol. Ecol. Res.* **13**, 851–861. (doi:10.1111/1755-0998.12138)

26. R Core Team. 2016 *R: A language and environment for statistical computing*. Vienna, Austria: R Foundation for Statistical Computing.

27. Rasband WS. 2014 ImageJ [Online]. U.S. National Institutes of Health, Bethesda, MD. See http://imagej.nih.gov/ij/ [2015, June 1].

28. Key Jr MM, Knauff JB, Barnes DKA. 2013 Epizoic bryozoans on predatory pycnogonids from the South Orkney Islands, Antarctica: 'If you can't beat them, join them'. *Lect. Notes Earth Syst. Sci.* **143**, 137–153. (doi:10.1007/978-3-642-16411-8_10)

29. Woods HA, Moran AL. 2008 Oxygen profiles in egg masses predicted from a diffusion-reaction model. *J. Exp. Biol.* **211**, 790–797. (doi:10.1242/jeb.014613)

30. Crank J. 1975 *The mathematics of diffusion*, p. 414. 2nd edn. Oxford, UK: Oxford University Press.

31. Felsenstein J. 1985 Phylogenies and the comparative method. *Am. Nat.* **125**, 1–15. (doi:10.1086/284325)

32. Swofford DL. 2003 *PAUP\* phylogenetic analysis using parsimony (\* and other methods), version 4*. Sunderland, MA: Sinauer Associates.

33. Posada D, Crandall KA. 1998 ModelTest: testing the model of DNA substitution. *Bioinformatics* **14**, 817–818. (doi:10.1093/bioinformatics/14.9.817)

34. Arango CP, Wheeler WC. 2007 Phylogeny of the sea spiders (Arthropoda, Pycnogonida) based on the direct optimization of six loci and morphology. *Cladistics* **23**, 255–293. (doi:10.1111/j.1096-0031.2007.00143.x)

35. Pagel MD. 1992 A method for the analysis of comparative data. *J. Theor. Biol.* **156**, 431–442. (doi:10.1016/S0022-5193(05)80637-X)

36. Paradis E. 2012 *Analysis of phylogenetics and evolution with R*. New York, NY: Springer.

37. Pagel, MD. 1999 Inferring the historical patterns of biological evolution. *Nature* **401**, 877–884. (doi:10.1038/44766)

38. Revell, LJ. 2010 Phylogenetic signal and linear regression on species data. *Methods Ecol. Evol.* **1**, 319–329. (doi:10.1111/j.2041-210X.2010.00044.x)

39. Blomberg SP, Garland Jr T, Ives AR. 2003 Testing for phylogenetic signal in comparative data: behavioral traits are more labile. *Evolution* **57**, 717–745. (doi:10.1111/j.0014-3820.2003.tb00285.x)

40. Woods HA, Lane SJ, Shishido C, Tobalske BW, Arango CP, Moran AL. 2017 Respiratory gut peristalsis by sea spiders. *Curr. Biol.* **27**, R638–R639. (doi:10.1016/j.cub.2017.05.062)

41. Rehm P, Pick C, Borner J, Markl J, Burmester T. 2012 The diversity and evolution of chelicerate hemocyanins. *BMC Evol. Biol.* **12**, 19. (doi:10.1186/1471-2148-12-19)

42. Markl J. 1986 Evolution and function of structurally diverse subunits in the respiratory protein hemocyanin from arthropods. *Biol. Bull.* **171**, 90–115. (doi:10.2307/1541909)

# Upper limits to body size imposed by respiratory-structural trade-offs in Antarctic pycnogonids

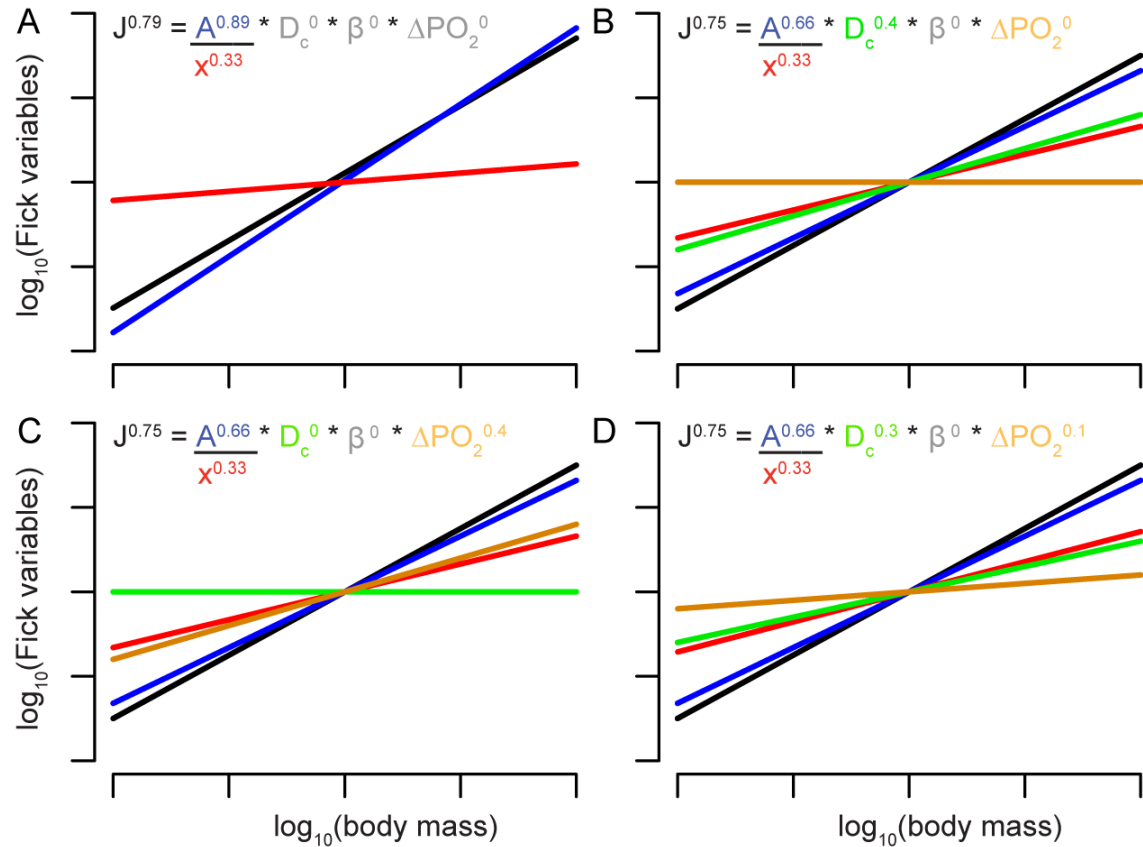Lane, SJ, CM Shishido, AL Moran, BW Tobalske, CP Arango, HA Woods

**Figure S1.** Scaling coefficients of flux ($J$), surface area ($A$), thickness ($x$), diffusion ($D_c$), capacitance ($\beta$), and the oxygen gradient ($\Delta PO_2$). Coloured lines correspond to coloured variables within Fick's law (eq. 3 and displayed on each graph). The exponents within the equation are equal to the scaling coefficient from the associated figure. **A)** Fick's law described in terms of scaling coefficients from Gillooly et al. (2016). In vertebrates, $D_c$, $\beta$, and $\Delta PO_2$ do not scale with body size and changes in $A$ and $x$ are sufficient to meet oxygen demands (*i.e.,* $0.89 - 0.1 = 0.79$). **B-D)** Hypothesized scaling coefficients of animals relying on cutaneous respiration. Slopes of all Fick variables, when added up following Fick's equation, should be equivalent to scaling of MR (null expectation, $b = 0.75$). $A$ and $x$ are hypothesized to scale with geometric isometry ($b = 0.66$ and $0.33$, respectively), because cuticle provides structural support. In contrast to vertebrates, either $D_c$ (**B**), $\Delta PO_2$ (**C**), or both (**D**) must scale positively to meet the increased oxygen demands of larger animals. Capacitance ($\beta$) is not expected to vary with body size as it is only dependent on the temperature and type of medium.
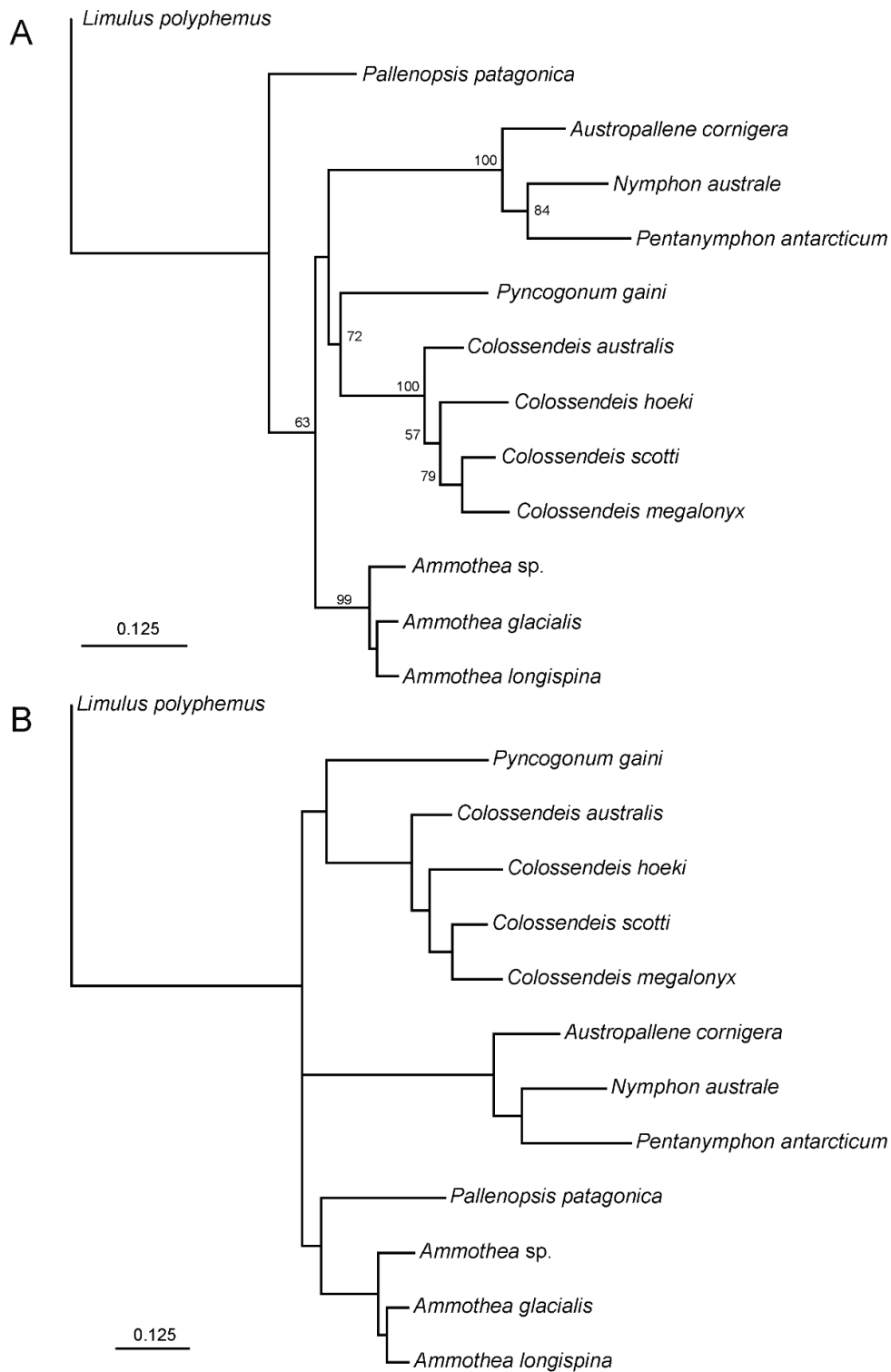
**Figure S2.** Maximum likelihood trees using CO1 sequence data. A) Unconstrained topology, values along branches indicate bootstrap values (in percent). Only values above 50% are shown. Bar represents 0.125 substitutions per site. B) Constrained tree following topology of Arango and Wheeler (32). See text for details.
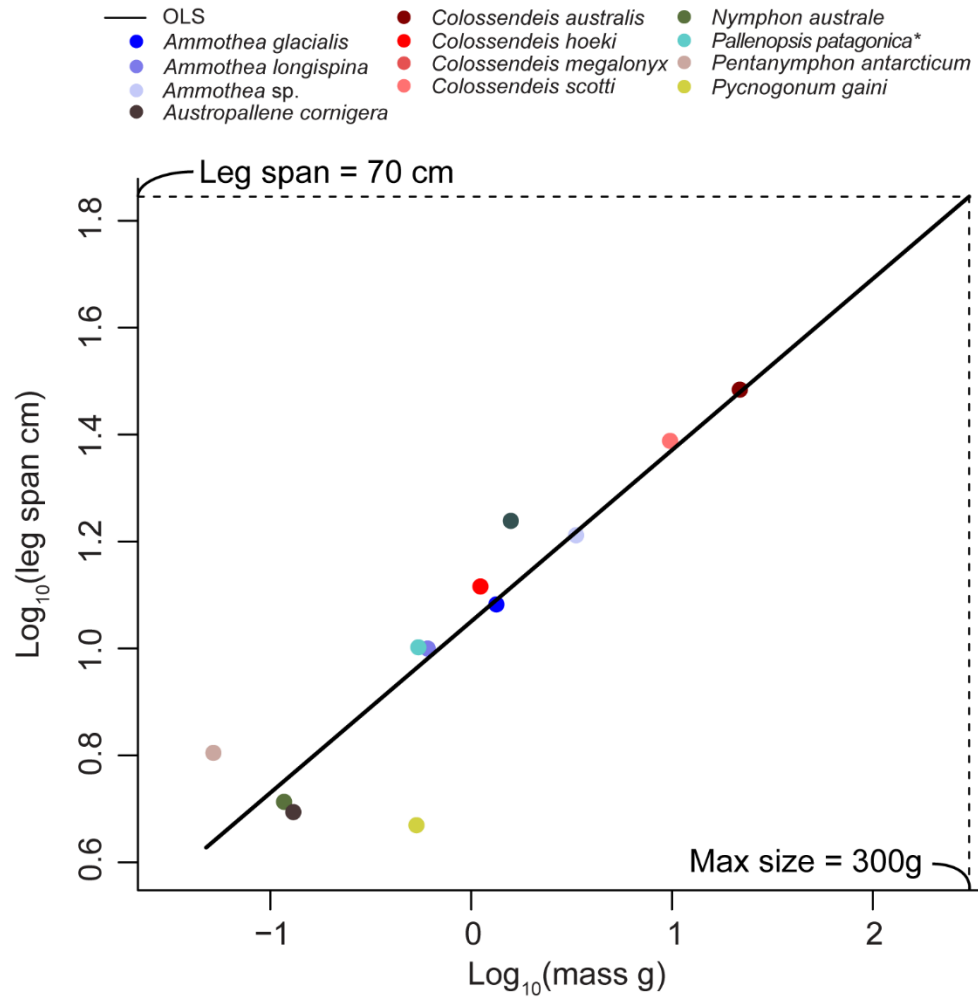
**Figure S3.** Body size estimated from the leg span of the largest sea spider reported. Leg span was reported in Arnaud and Bamber (1987). Estimated body size was found by extrapolating OLS regression line out to the point where the line intersected the estimated y-values. See Table 1 for scaling coefficients and Table S1 for data. See text for details.

**Table S1.** Summary of data for individuals used in scaling analyses. Body mass ($M$, g), cuticle thickness ($x$, cm), surface area ($A$, cm$^2$), the diffusion coefficient ($D_c$, cm$^2$ s$^{-1}$), leg span ($LS$, cm) for sea spiders.

| | $M$ | $x$ | $A$ | $D_c$ | $LS$ |
|---|---|---|---|---|---|
| Ammotheidae | | | | | |
| *Ammothea glacialis* | 1.60 | 0.0069 | 18.14 | 9.6E-07 | 14.0 |
| | 1.07 | 0.0070 | 13.03 | 9.3E-07 | 11.1 |
| | 1.32 | 0.0070 | 16.148 | 1.8E-06 | 10.8 |
| | 1.36 | 0.0070 | 17.576 | 1.3E-06 | 12.5 |
| *Ammothea longispina* | 0.510 | 0.0070 | 9.45 | 1.8E-06 | 9.3 |
| | 0.647 | 0.0070 | 10.76 | 1.5E-06 | 11.3 |
| | 0.664 | 0.0060 | 10.69 | 1.6E-06 | 9.5 |
| *Ammothea* sp. | 3.54 | 0.0030 | 30.076 | 4.8E-07 | 15.8 |
| | 3.11 | 0.0040 | 28.86 | 8.3E-07 | 16.8 |
| *Austropallene cornigera* | 0.130 | 0.0044 | 3.42 | 4.6E-07 | 4.9 |
| Colossendeidae | | | | | |
| *Colossendeis australis* | 21.80 | 0.0140 | 90.16 | 1.8E-06 | 30.5 |
| *Colossendeis hoeki* | 1.22 | 0.0087 | 18.52 | 1.7E-06 | 14.4 |
| | 0.982 | 0.0090 | 14.84 | 1.1E-06 | 12.4 |
| | 1.13 | 0.0110 | 13.21 | 9.8E-07 | 12.3 |
| *Colossendeis megalonyx* | 2.20 | 0.0080 | 31.64 | 4.8E-06 | 24.7 |
| | 2.54 | 0.0090 | 40.02 | 4.5E-07 | 18.9 |
| | 0.470 | 0.0068 | 11.12 | 1.1E-06 | 12.7 |
| | 1.10 | 0.0096 | 20.22 | 6.1E-07 | 12.9 |
| *Colossendeis scotti* | 12.60 | 0.0120 | 75.6 | 4.5E-06 | 25.4 |
| | 8.39 | 0.0134 | 69.96 | 1.7E-06 | 23.9 |
| | 8.40 | 0.0130 | 61.34 | 3.7E-06 | 24.0 |
| Nymphonidae | | | | | |
| *Nymphon australe* | 0.140 | 0.0021 | 4.98 | 1.6E-06 | 4.8 |
| | 0.160 | 0.0013 | 3.12 | 1.2E-06 | 5.2 |
| | 0.100 | 0.0034 | 3.4 | 4.7E-07 | 5.4 |
| | 0.070 | 0.0025 | 2.34 | 4.7E-07 | 4.8 |
| | 0.190 | 0.0049 | 3.978 | 9.1E-07 | 5.6 |
| | 0.090 | 0.0025 | 3.38 | 5.1E-07 | 5.8 |
| | 0.070 | 0.0028 | 2.9 | 7.6E-07 | 4.5 |
| *Pentanymphon antarcticum* | 0.035 | 0.0018 | 2.42 | 4.2E-07 | 5.7 |
| | 0.068 | 0.0020 | 3.5 | 5.8E-07 | 7.0 |
| | 0.069 | 0.0030 | 4.07 | 1.7E-06 | 7.3 |
| | 0.036 | 0.0010 | 2.51 | 3.1E-07 | 5.5 |
| Pallenopsidae | | | | | |
| *Pallenopsis patagonica* | 0.776 | 0.0030 | 12.29 | 3.6E-08 | 11.7 |
| | 0.395 | 0.0010 | 6.74 | 2.4E-08 | 8.8 |

| | | | | |
|---|---|---|---|---|
| 0.469 | 0.0020 | 8.11 | 5.8E-08 | 9.6 |

Pycnogonidae

| | | | | | |
|---|---|---|---|---|---|
| *Pycnogonum gaini* | 0.618 | 0.0159 | 6.9 | 1.5E-06 | 5.3 |
| | 0.440 | 0.0130 | 5.33 | 8.3E-07 | 4.1 |
| | 0.543 | 0.0165 | 5.198 | 9.1E-07 | 4.7 |

**Table S2.** Summary of data for individuals used in scaling analyses. Body mass ($M$, g), oxygen gradient ($\Delta PO_2$, kPa), and flux ($J$, µmol $O_2$ s$^{-1}$).

| | $M$ | $\Delta PO_2$ | $J$ |
|---|---|---|---|
| Ammotheidae | | | |
| *Ammothea glacialis* | 1.60 | 5.16 | 2.27E-04 |
| | 1.07 | 8.9 | 2.65E-04 |
| | 1.32 | 6.86 | 4.97E-04 |
| | 1.36 | 4.15 | 2.23E-04 |
| *Ammothea longispina* | 0.510 | 7.55 | 3.14E-04 |
| | 0.647 | 6.16 | 2.43E-04 |
| | 0.664 | 6.68 | 3.19E-04 |
| *Ammothea* sp. | 3.54 | 3.16 | 2.66E-04 |
| | 3.11 | 3.61 | 3.67E-04 |
| Colossendeidae | | | |
| *Colossendeis australis* | 21.80 | 12.8 | 2.68E-03 |
| *Colossendeis hoeki* | 1.22 | 2.04 | 1.29E-04 |
| | 0.982 | 7.47 | 2.34E-04 |
| | 1.13 | 7.94 | 1.68E-04 |
| *Colossendeis megalonyx* | 2.20 | 8.88 | 2.94E-03 |
| | 2.54 | 6.61 | 2.31E-04 |
| | 0.470 | 3.29 | 1.03E-04 |
| *Colossendeis scotti* | 12.60 | 5.5 | 3.36E-03 |
| | 8.39 | 10.4 | 1.61E-03 |
| | 8.40 | 9 | 2.77E-03 |
| Nymphonidae | | | |
| *Nymphon australe* | 0.160 | 0.82 | 4.19E-05 |
| | 0.100 | 1.43 | 1.18E-05 |
| | 0.070 | 0.27 | 2.08E-06 |
| | 0.190 | 2.73 | 3.53E-05 |
| *Pentanymphon antarcticum* | 0.035 | 2.13 | 2.10E-05 |
| | 0.068 | 3.94 | 6.97E-05 |
| | 0.069 | 5.13 | 2.33E-04 |
| | 0.036 | 1.26 | 1.54E-05 |
| Pallenopsidae | | | |
| *Pallenopsis patagonica* | 0.776 | 4.51 | 1.35E-05 |
| | 0.395 | 5.17 | 1.08E-05 |

| | | 0.469 | 3.18 | 1.08E-05 |
|---|---|---|---|---|

**Pycnogonidae**

| | | | | |
|---|---|---|---|---|
| *Pycnogonum gaini* | | 0.440 | 6.26 | 3.72E-05 |
| | | 0.543 | 5.11 | 2.56E-05 |

**Table S3.** Summary of data for individuals used in scaling analyses. Body mass ($M$, g) and metabolic rate ($MR$, $\mu$mol $O_2$ s$^{-1}$).

| | *M* | *MR* |
|---|---|---|
| Ammotheidae | | |
| *Ammothea glacialis* | 1.97 | 9.50E-05 |
| | 3.44 | 3.15E-04 |
| *Ammothea longispina* | 2.23 | 2.08E-04 |
| | 2.70 | 1.93E-04 |
| *Ammothea* sp. | 4.68 | 3.10E-04 |
| | 2.09 | 3.36E-04 |
| Colossendeidae | | |
| *Colossendeis hoeki* | 0.830 | 9.75E-05 |
| | 1.53 | 1.30E-04 |
| *Colossendeis megalonyx* | 0.43 | 9.53E-05 |
| | 0.022 | 4.03E-06 |
| | 0.23 | 1.11E-04 |
| | 2.66 | 1.22E-03 |
| | 0.46 | 6.86E-05 |
| | 2.98 | 6.17E-04 |
| | 0.38 | 5.89E-05 |
| | 1.29 | 2.24E-04 |
| *Colossendeis scotti* | 10.47 | 1.10E-03 |
| | 11.65 | 1.94E-03 |
| | 8.39 | 1.43E-03 |
| Nymphonidae | | |
| *Nymphon australe* | 0.240 | 4.11E-05 |
| | 0.041 | 8.06E-06 |
| | 0.035 | 7.06E-06 |
| | 0.102 | 1.82E-05 |
| | 0.340 | 6.95E-05 |
| | 0.210 | 4.44E-05 |
| | 0.016 | 2.47E-06 |
| | 0.440 | 2.70E-05 |
| | 0.150 | 1.31E-05 |
| | 0.049 | 6.64E-06 |
| | 0.210 | 3.02E-05 |
| *Pentanymphon antarcticum* | 0.029 | 9.89E-06 |
| | 0.033 | 1.13E-05 |

Pallenopsidae

| | | |
|---|---|---|
| *Pallenopsis patagonica* | 0.438 | 3.35E-05 |
| | 0.426 | 4.63E-05 |

Pycnogonidae

| | | |
|---|---|---|
| *Pycnogonum gaini* | 0.560 | 4.03E-05 |
| | 0.440 | 3.47E-05 |
| | 0.440 | 1.95E-05 |
| | 0.540 | 2.71E-05 |

**Table S4.** Pagel's lambda and log likelihood scores for PGLS regression analyses for *A* (surface area), *x* (cuticle thickness), $D_c$ (diffusion coefficient), $\Delta PO_2$ (oxygen gradient), *J* (flux), *MR* (metabolic rate), and *LS* (leg span) vs body mass in sea spiders.

| Models | N | Pagel's Lambda | logL | logL0 | logL P-value |
|---|---|---|---|---|---|
| *A* (cm$^2$); Fig. 3A | | | | | |
| PGLS-mtCO1 | 12 | 1.00 | 13.07 | 12.18 | 0.182 |
| PGLS-var. brlens | 12 | 1.00 | 13.24 | 11.89 | 0.100 |
| PGLS-equal brlens | 12 | 1.00 | 10.65 | 10.12 | 0.305 |
| *x* (cm); Fig. 3B | | | | | |
| PGLS-mtCO1 | 12 | 1.00 | 0.55 | -1.66 | 0.036 |
| PGLS-var. brlens | 12 | 1.00 | 0.71 | -0.50 | 0.119 |
| PGLS-equal brlens | 12 | 1.00 | 1.19 | -1.76 | 0.015 |
| $D_c$ (cm$^2$ s$^{-1}$); Fig. 3C | | | | | |
| PGLS-mtCO1 | 11 | 0.00 | 2.32 | 2.32 | 1.000 |
| PGLS-var. brlens | 11 | 0.08 | 2.41 | 2.39 | 0.839 |
| PGLS-equal brlens | 11 | 0.18 | 3.88 | 3.79 | 0.673 |
| $\Delta PO_2$ (µmol L$^{-1}$); Fig. 3D | | | | | |
| PGLS-mtCO1 | 11 | 0.00 | 5.96 | 5.96 | 1.000 |
| PGLS-var. brlens | 11 | 0.00 | 5.60 | 5.60 | 1.000 |
| PGLS-equal brlens | 11 | 0.14 | 4.59 | 4.54 | 0.735 |
| *J* (µmol s$^{-1}$); Fig. 4 | | | | | |
| PGLS-mtCO1 | 11 | 1.00 | -6.70 | -9.40 | 0.020 |
| PGLS-var. brlens | 11 | 1.00 | -6.75 | -7.71 | 0.166 |
| PGLS-equal brlens | 11 | 0.00 | -8.04 | -8.04 | 1.000 |
| *MR* (µmol O$_2$ s$^{-1}$); Fig. 4 | | | | | |
| PGLS-mtCO1 | 10 | 0.55 | 0.71 | 0.53 | 0.550 |
| PGLS-var. brlens | 10 | 0.65 | 0.70 | 0.26 | 0.347 |
| PGLS-equal brlens | 10 | 1.00 | 0.98 | 0.03 | 0.170 |
| LS (cm); Fig. S1 | | | | | |
| PGLS-mtCO1 | 12 | 1.00 | 11.12 | 10.01 | 0.136 |
| PGLS-var. brlens | 12 | 1.00 | 11.31 | 9.61 | 0.065 |
| PGLS-equal brlens | 12 | 1.00 | 7.65 | 7.15 | 0.318 |

# No Effects and No Control of Epibionts in Two Species of Temperate Pycnogonids

STEVEN J. LANE[1,*], CAITLIN M. SHISHIDO[2], AMY L. MORAN[2], BRET W. TOBALSKE[1], AND H. ARTHUR WOODS[1]

[1]*Division of Biological Sciences, University of Montana, Missoula, Montana 59812; and* [2]*Department of Biology, University of Hawai'i at Mānoa, Honolulu, Hawaii 96822*

**Abstract.** Essentially all surfaces of marine plants and animals host epibionts. These organisms may harm their hosts in a number of ways, including impeding gas exchange or increasing the costs of locomotion. Epibionts can also be beneficial. For example, they may camouflage their hosts, and photosynthetic epibionts can produce oxygen. In general, however, the costs of epibionts appear to outweigh their benefits. Many organisms, therefore, shed epibionts by grooming, molting, or preventing them from initially attaching, using surface waxes and cuticular structures. In this study, we examined how epibionts affect local oxygen supply to temperate species of pycnogonids (sea spiders). We also tested the effectiveness of different methods that pycnogonids may use to control epibionts (grooming, cuticle wettability, and cuticular waxes). In two temperate species: *Achelia chelata* and *Achelia gracilipes*, epibionts consisted primarily of algae and diatoms, formed layers approximately 0.25-mm thick, and they colonized at least 75% of available surface area. We used microelectrodes to measure oxygen levels in and under the layers of epibionts. In bright light, these organisms produced high levels of oxygen; in the dark, they had no negative effect on local oxygen supply. We tested mechanisms of control of epibionts by pycnogonids in three ways: disabling their ovigers to prevent grooming, extracting wax layers from the cuticle, and measuring the wettability of the cuticle; however, none of these experiments affected epibiont coverage. These findings indicate that in temperate environments, epibionts are not costly to pycnogonids and, in some circumstances, they may be beneficial.

\* To whom correspondence should be addressed. E-mail: steven.lane@umontana.edu

## Introduction

Virtually all marine plants and animals host communities of other organisms on their surfaces (Wahl, 1989; Wahl and Lafargue, 1990). These external organisms are known as epibionts, and they can be roughly classified into two groups: the microepibionts and the macroepibionts. Microepibionts include diatoms, protozoa, and biofilms, and communities of these components form biofilms (Davis *et al.*, 1989; Wahl, 1989). Macroepibionts include larger multicellular organisms, such as macroalgae, fungi, and sessile invertebrates (Richmond and Seed, 1991; Satuito *et al.*, 1997). Micro- and macroepibionts can occur together, and they influence one another (Richmond and Seed, 1991; Wahl *et al.,* 2012).

Epibionts can harm their hosts, for example, by limiting gas exchange in egg masses (Cohen and Strathmann, 1996) and across invertebrate gills (Burnett *et al.*, 2006; Scholnick *et al.*, 2006), which magnifies the effects of other environmental stressors. Epibionts can also increase the costs of locomotion by increasing drag and decreasing the flexibility of hosts, which may render them more susceptible to predators (Witman and Suchanek 1984; Shine *et al.*, 2010; Key *et al.*, 2013). In other cases, epibionts appear to help their hosts. Photosynthetic epibiotic algae can raise local levels of oxygen (Cohen and Strathmann, 1996; Larkum *et al.*, 2003; Roberts *et al.*, 2007; Woods and Podolsky, 2007). Some arthropods promote the growth of microepibionts that can reduce or prevent infection by toxic fungi (Gil-Turnes *et al.*, 1989; Armstrong *et al.*, 2000), and others use macroepibionts to conceal themselves from predators (Wicksten, 1980; Feifarek, 1987; Dougherty and Russell, 2005). Such camouflage is also used by decorator crabs (Wicksten, 1980).

Negative effects often appear to outweigh positive effects, and many host organisms have evolved ways to remove epibionts, or to prevent them from attaching in the first place. Most crustaceans and nematodes shed their external cuticles regularly (*i.e.,* molt), removing any existing epibionts (Dyrynda, 1986; Thomas *et al.*, 1999; Smirnov, 2014). Crustaceans and echinoderms also groom their gills and external surfaces (Bauer, 1981, 2013; Russell, 1984; Dyrynda, 1986). Crustaceans secrete waxes onto their cuticles, reducing cuticular wettability and possibly making it more difficult for epibionts to adhere (Becker *et al.*, 2000; Callow *et al.,* 2002). Slow-moving or sessile organisms, such as ascidians and gastropod molluscs, produce antifouling chemicals that prevent micro- and macroepibionts from attaching (Wahl and Banaigs, 1991; Wahl and Sönnichsen, 1992). Finally, the microtopography of the cuticle can prevent colonization or growth (Callow *et al.,* 2002; Bers and Wahl, 2004). For instance, surface ridges on the mussel *Mytilus galloprovincialis* prevented barnacle larvae from attaching, likely by decreasing the area available for attachment (Scardino *et al.*, 2003).

Although host organisms often appear to remove or control epibionts, the effects of epibionts on gas exchange have not been rigorously tested. Here we examine the effects of epibionts on gas exchange by pycnogonids (phylum Arthropoda), and test for the presence of active and passive mechanisms for epibiont control. Pycnogonids are ideal for this study because they are often found harboring epibionts (Pipe, 1982; Key *et al.*, 2013), and they lack a true respiratory system (Arnaud and Bamber, 1987), relying instead on the diffusion of oxygen directly across their thin cuticles or through pores piercing the cuticle (Davenport *et al.*, 1987; Lane *et al.,* unpublished data). Therefore, epibionts are likely to disrupt gas exchange by (i) increasing the thickness of the unstirred layers through which oxygen must diffuse, and (ii) directly consuming oxygen themselves. Both processes depress oxygen levels at the outer cuticular surface of the pycnogonids. We tested for these effects by measuring oxygen levels, using microelectrodes.

Pycnogonids, like crustaceans, have been observed grooming their legs with specialized appendages. These appendages are called ovigers, and they are also used by some species to carry egg masses (Arnaud and Bamber, 1987; Bamber, 2007). Previous work has reported that males carrying eggs have higher epibiont loads, suggesting a trade-off between egg-carrying and grooming (King, 1973). However, the role of ovigers in grooming has not been experimentally tested, and is suggested by only a few observations. We tested whether two species: *Achelia chelata* (Hilton, 1939) and *Achelia gracilipes* (Cole, 1904), use their ovigers to control epibionts. Additionally, we tested whether the structure and composition of the cuticle play a role in reducing colonization.

## Materials and Methods

We collected pycnogonids from hydroids (Family Haleciidae; 1–30 m deep) by scuba-diving in and around Friday Harbor, Washington (48° 32′ N, 123° 00′ W), in June, 2015. Seawater temperatures in this area averaged approximately 10 °C. Individuals were kept in seawater tables (12–15 °C) at the University of Washington's Friday Harbor Laboratories (FHL) until their use in experiments. No animal was held in the seawater tables for more than two weeks before being used in an experiment. We used only adult *Achelia chelata* and *Achelia gracilipes* with leg spans between 8–17 mm. Individuals were identified to species based on Kozloff and Price (1996) and Carlton (2007). The majority of individuals collected were *A. chelata* ($n = 27$ of 40 total); patterns of epibiont coverage and control, use of ovigers, and cuticular structure appeared similar between the two species. Both species were collected off of the same hydroids, and it was difficult to identify the individuals to species until after they were killed, after the experiments were finished. Merging the two datasets was justified, because epibiont coverage and species composition did not vary, and the individuals were similar in size, morphology, and habitat.

### Oxygen profiles through epibionts

Oxygen concentrations were measured using a Clark-style $O_2$ microelectrode (50-m tip; Unisense, Aarhus, Denmark) connected to a picoammeter (PA2000; Unisense). Measurements were made at 10.5 ± 0.2 °C (mean ± SEM), to approximate the average temperature of the pycnogonids' natural habitat, using a water-jacketed glass cell connected to a recirculating water bath. The electrode was calibrated at the experimental temperature in air- or $N_2$-bubbled seawater. The electrode was mounted in a micromanipulator. Data were recorded once per second by a Sable Systems (North Las Vegas, NV) UI-2 acquisition interface controlled by ExpeData (v1.8.4; Sable Systems).

We measured oxygen levels in the bulk seawater 1 cm from the pycnogonid, and at the surface of the cuticle of individuals with or without heavy epibiont coverage ($n = 8$ per group). Most of the individuals that we collected from the wild had low epibiont coverage (less than 10%); so the heavily fouled individuals (with greater than 75% epibiont coverage) from the Manipulation of Grooming Assay (see *Manipulation of Grooming* below) were used in this assay. We chose individuals with high epibiont loads to estimate how severely epibionts alter patterns of gas exchange. Pycnogonids were held between two glass coverslips connected at the corners by modeling clay. Air was bubbled gently into the chamber to maintain air-saturated conditions. In pycnogonids that were visually free of epibionts, oxygen

measurements were made at three randomly chosen locations along the legs and one on the trunk. On fouled individuals, or on those that were visually hosting epibionts, the same number of measurements were taken, but sampling locations that had thick epibiont layers were chosen.

Pycnogonids that were free of visible macroepibionts were illuminated, using a Fiber-Lite 180 illuminator (Dolan-Jenner Industries, Inc., Boxborough, MA) equipped with light guides featuring an EKE 21 Volt, 150-watt lamp (Ushio America, Cypress, CA) with a nominal color temperature of 3250 K, which is slightly redder than sunlight (5800 K). To standardize light intensity, the light guides were positioned 10 cm away from each pycnogonid, and the power on the illuminator was set at maximum. To determine whether epibionts could produce significant amounts of photosynthetic oxygen, we measured oxygen levels under epibionts in both well-lighted (as mentioned above) and dark conditions (no light; covered by black paper). Oxygen levels at the cuticle surfaces were given 1–2 min to stabilize between light treatments. Because the duration of each measurement varied greatly (40 s–5 min), oxygen concentrations were averaged over the final 30–40 s only. The variation in oxygen measurements was due to the thickness of the epibionts in the patches being measured; thicker epibiont layers tended to produce more oxygen over a longer time interval.

### Manipulation of grooming

To test whether *Achelia* spp. use their ovigers to control epibionts, we haphazardly selected 16 animals and separated them into two groups, restricted ovigers and controls (unrestricted ovigers). Pycnogonids from both groups were placed individually in chambers with approximately 2 g of hydroids as a food source. The chambers were designed to prevent pycnogonids from escaping while allowing for adequate water flow. Three holes (2–3-cm diameter) were cut into 60-ml round plastic containers with snap-top lips (Ziploc) fitted with nylon mesh (mesh openings approximately 1 mm$^2$). The chambers were suspended from the docks at Friday Harbor Labs, and submerged at a depth of 0.5–1 m for two weeks.

In the experimental group, ovigers were restricted by applying Loctite marine epoxy (Henkel Corp., Düsseldorf, Germany) to their distal ends, thereby gluing them together. Twenty-four hours later, ovigers were examined and, if the glue and/or epoxy was gone, another attempt was made. To avoid potential adverse effects of epoxy handling, individuals requiring more than two applications of epoxy were excluded from the experiment. At the end of the experiment, all individuals survived and the ovigers remained disabled. However, one pycnogonid from the experimental group lost a single oviger. Because this individual seemed healthy

otherwise, and its epibiont coverage was not different from the others in the group, it was included in the analysis.

Percent cover by macroepibionts (estimating coverage by microepibionts was impossible *via* standard microscopy) was estimated from photographs taken before and after the experiment. Images (dorsal view) were taken under a stereomicroscope fitted with a Nikon D7100 digital camera and stereomicroscope adapter. Images were analyzed using ImageJ software (v1.49) (Rasband, 2014). Individual patches of epibionts were outlined, summed, and divided by the total area of the pycnogonid (Chung *et al.*, 2007). Change in percent cover was then calculated for each individual by subtracting the percent cover at the beginning of the experiment from the percent cover at the end. The individual animals that we collected from the wild were not completely free of epibionts at the beginning of the experiment. By estimating the change in cover, we corrected for some of this initial variation, and better estimated how much colonization and growth occurred.

### Cuticular wax extraction

We tested the effect of cuticular waxes on epibiont cover by cutting each of 16 pycnogonids longitudinally down the center of its trunk and separating the halves into two groups: an experimental group, in which waxes were removed, and a control group, in which the waxes were left intact. Only individuals visibly free of epibionts were used in this assay. Cuticle pieces in the experimental group were soaked in a methanol:chloroform (1:1; a solvent used for general lipid extraction) treatment (30 min at 21 °C), then glued with Loctite marine epoxy (at the trunk) to a microscope slide, with legs suspended freely. The slides were then placed in individually marked, 50-ml Falcon tubes. Two 2 × 4 cm windows were cut on opposite sides of the tubes and fitted with 1-mm$^2$ nylon mesh. These windows permitted water to flow across the samples, but prevented access by larger organisms. The tubes were then hung off of the FHL dock, submerged to a depth of 0.5–1 m for two weeks. After recovery, percent epibiont cover was estimated, using the methods described above in *Manipulation of grooming*.

### Cuticle wettability

We estimated wettability by measuring contact angles of small water droplets placed on the cuticle. Higher contact angles indicate hydrophobic surfaces (*i.e.,* low wettability) and low-contact angles denote hydrophilic surfaces (*i.e.,* high wettability) (Yuan and Lee, 2013). Live sea spiders were gently centrifuged for 1 s at low speeds in a 1.0-ml microcentrifuge tube, packed with a small piece of KimWipe (Kimberly-Clark Corp., Irving, TX), which removed excess water from the cuticle. We used only individuals that had no visible epibionts. It is possible that bacterial biofilms were present on the cuticle, which would

affect our estimate of cuticle wettability, although it is not clear how (Thomas and Muirhead (2009) found that biofilms increased wettability; Epstein *et al*. (2011) found that they decreased it). However, the individuals likely had, at most, sparsely distributed individual bacteria (not biofilms), as revealed by images (using scanning electron microscopy, SEM) of areas of clean cuticle from individuals in the group with restricted ovigers (images not shown).

To test whether wettability varied across the cuticle, droplets (approximately 50 nl) of fresh tap water were placed on cuticle using a Drummond Nanoject nanoliter injector (Drummond Scientific Co., Broomall, PA), and the droplets were immediately imaged from the side by a stereomicroscope fitted with a digital camera (Nikon D7100). Images were analyzed in ImageJ. Contact angles were obtained from the femur, first tibia, second tibia, and trunk of eight individuals.

We also tested whether there was an association between local wettability and the presence of epibionts on different parts of the cuticle. We measured the percent cover of epibionts on the legs *versus* the trunk of the eight control individuals from the oviger restriction experiment. Percent cover was estimated as described above in *Manipulation of grooming*.

### Scanning electron microscopy and maximum epibiont thickness

Individuals from the grooming experiment were fixed in 2% cacodylate-buffered glutaraldehyde at 4 °C for 24 h, then washed with cacodylate buffer (pH 7.0) for 5 min and rinsed in deionized water. Samples were dehydrated in a graded ethanol series (50%, 70%, 90%, 95%, 100% ($\times$2)) for 10 min each, followed by 20 min in a 1:1 mixture of hexamethyldisilazane (HMDS) and ethanol. Samples were moved to 100% HMDS and left to air-dry in a fume hood overnight. Samples were sputter coated with gold (Denton Desk-V sputtercoater; Denton Vacuum, Inc., Moorestown, NJ), then viewed with an S-4700 Hitachi-model scanning electron microscope at the University of Montana.

To estimate thickness of the epibiont layers on the most heavily fouled individuals, we focused on the areas of greatest colonization from SEM images (*e.g.,* on the femur in Fig. 1D). Thickness was measured from the surface of the cuticle to the top of the epibionts. Images were analyzed in ImageJ (v1.49) (Rasband, 2014). Maximum epibiont thickness was used as an estimate of maximum possible fouling.

### Statistical analyses

Mean values ($\pm$ standard error) were calculated for each of the above-mentioned variables. Unless otherwise stated, Type I error was set at 0.05; all statistical analyses were performed in R (v3.0.2) (R Core Team, 2013).

Oxygen concentration at the bottom of the epibionts in the light cycle was compared against the dark cycle, using a paired *t*-test. These data were log-transformed to normality, which was confirmed using an Anderson-Darling test.

Oxygen concentrations between the bulk water, control group, and epibionts in the dark cycle were assessed by Kruskal-Wallis test, because the data were non-normal and had unequal variances among groups. We chose to compare differences between the dark epibiont group, bulk water, and control group because there was no apparent photosynthesis on the pycnogonid cuticle in the control group.

To assess the role of ovigers in epibiont control, a Wilcoxon signed-rank test was conducted; this test was chosen because the data were not normal and had an upper bound of 100%. These parameters violate the assumptions of a parametric test, and the values could not be normalized by transforming them. Similarly, the function of cuticle waxes in epibiont control and the concentration of epibionts on the trunk *versus* the legs were evaluated with a related-samples Wilcoxon signed-rank test (the observations were paired). These data also were not normal, and they had an upper bound of 100%. In the cuticle wax assay, however, the Q-Q plots were not definitive in detecting nonnormality. Therefore, we also transformed the original data using arcsin, a process typical for percentage data (Sokal and Rolf, 1981), and analyzed them, using a paired *t*-test in addition to a related-samples Wilcoxon signed-rank test.

Variation in cuticle wettability across body location was assessed using repeated measures analysis of variance followed by a pairwise *t*-test for multiple comparisons, with *P*-values adjusted using a Bonferroni correction. Normality of the data was confirmed with an Anderson-Darling test.

### Results

### Epibiont oxygen assay

Oxygen concentrations at the surface of the cuticle and in the bulk water did not differ significantly in the presence or absence of epibionts ($\chi^2 = 5.099$, d.f. $= 2$, $P = 0.078$) (Figs. 1 and 2). However, exposure to light in the presence of epibionts caused oxygen concentrations to rise significantly ($t = 3.937$, d.f. $= 7$, $P = 0.006$) (Figs. 2 and 3). In the experimental group, epibionts consisted primarily of algae and diatoms, forming layers approximately 0.25-mm thick (Fig. 1). Maximum epibiont thickness averaged 240 $\pm$ 42 $\mu$m ($n = 9$), with a peak thickness of 565 $\mu$m seen on one individual.

### Grooming analysis

Change in percent epibiont cover did not vary significantly with experimental (restricted ovigers) and control (unrestricted ovigers) pycnogonids ($Z = 37$, d.f. $= 15$, $P = 0.645$) (Fig. 4). Change in percent cover in the unrestricted ovigers group averaged 81.9% $\pm$ 3.6% compared to 74.8% $\pm$ 9.1% in the restricted ovigers group.

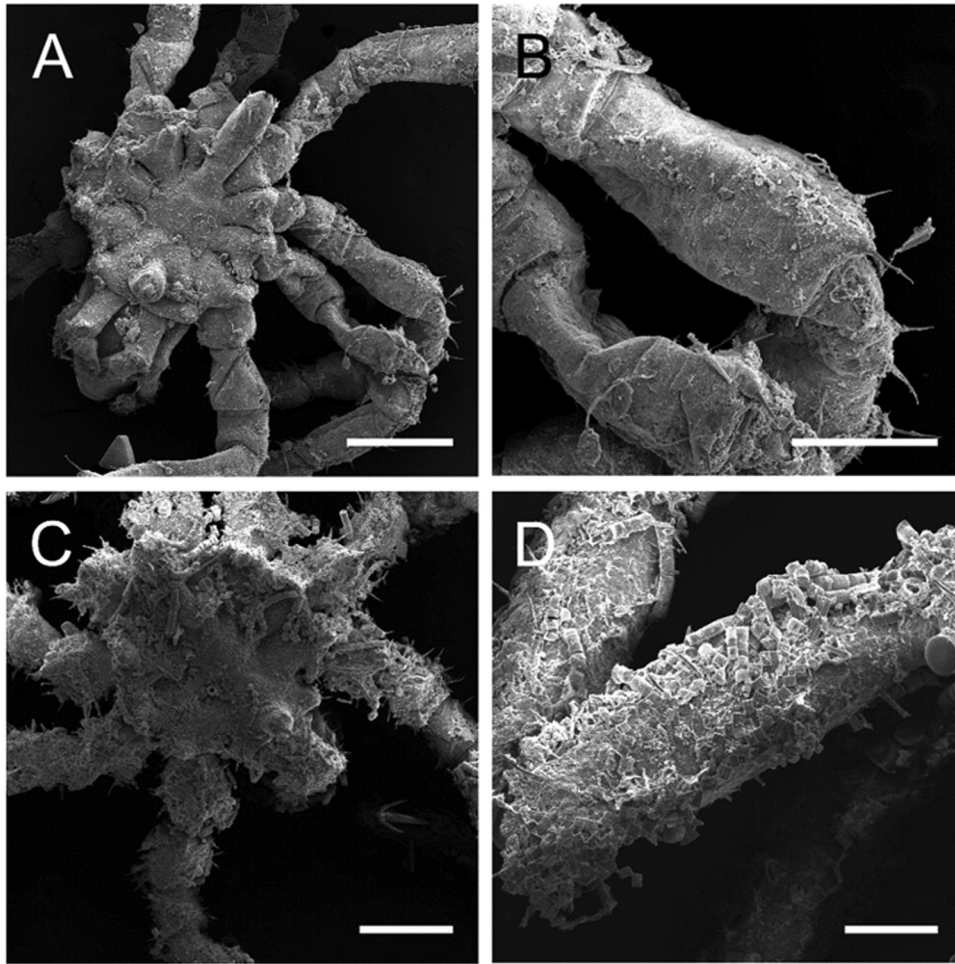**Figure 1.** Scanning electron micrographs of *Achelia* spp. (A) Trunk of a pycnogonid with relatively few epibionts (scale bar = 500 $\mu$m; total magnification = 40$\times$); (B) higher magnification view of femur from (A) (scale bar = 250 $\mu$m; total magnification = 110$\times$); (C) trunk of substantially fouled individual from the oviger-use experiment (scale bar = 500 $\mu$m; total magnification = 35$\times$); (D) higher magnification view of femur from (C) (scale bar = 250 $\mu$m; total magnification = 70$\times$).

### Wettability

Contact angles varied depending on where on the body they were measured, but all of these angles were low, indicating that the cuticle was fairly wettable ($F = 25.8$, d.f. = 24, $P < 0.001$) (Fig. 5). The contact angles of the femur and first and second tibias averaged 65.9 $\pm$ 2.0, 68.7 $\pm$ 2.9, and 64.8 $\pm$ 1.4 degrees, respectively. The trunk cuticle had higher wettability, as its contact angle was 45.8 $\pm$ 1.6 degrees. Pairwise comparisons indicated there were no differences in the contact angles among the leg segments, but each segment differed from that of the trunk. Although contact angles differed between the trunk and legs, epibiont percent cover did not differ significantly at these locations: 78.9% $\pm$ 5.5% and 75.7% $\pm$ 7.0%, respectively ($Z = 11$, d.f. = 7, $P = 0.383$) (data not shown).

### Cuticular wax analysis

The change in epibiont percent cover after wax extraction averaged 35.0% $\pm$ 7.3%, and percent cover averaged 18.7% $\pm$ 3.0% in the intact wax group (Fig. 4). A related-samples Wilcoxon rank-sum test indicated no significant difference between the groups ($Z = 35$, d.f. = 31, $P = 0.093$). However, our paired $t$-test, using arcsin-transformed data, showed that the wax-extracted group had a significantly higher percent coverage of epibionts than the intact wax group ($t = -2.34$, d.f. = 15, $P = 0.033$).

### Discussion

In bright light, epibionts on pycnogonids produced high levels of oxygen locally. In the dark, however, epibionts had no negative effect on local oxygen supply (Figs. 2 and 3).
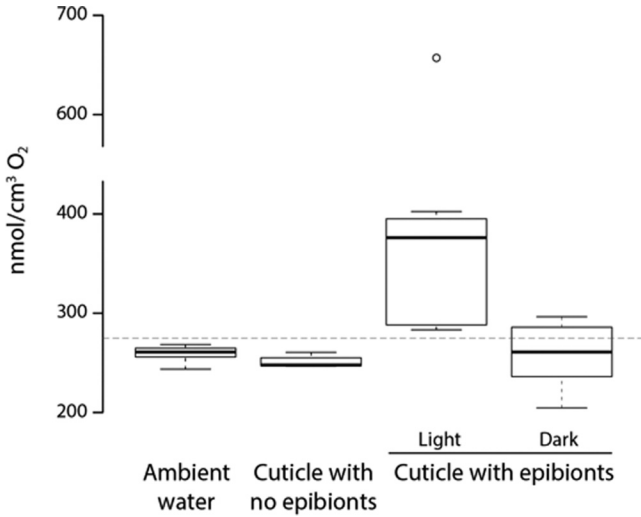
**Figure 2.** Oxygen concentrations in ambient water, at the surface of the cuticle in unfouled pycnogonids (see Fig. 1A, C), and at the surface of the cuticle under a layer of epibionts in light and dark treatments (see Fig. 1B, D) ($n = 8$ per group). The dashed line represents the theoretical oxygen concentration in air-saturated seawater at the experimental temperature (10 °C). Bold lines indicate medians, boxes indicate quartiles, and lines represent minimum (min) and maximum (max) extremes.

This result differed from the findings of Cohen and Strathmann (1996) and Woods and Podolsky (2007), who studied oxygen profiles in the gelatinous egg masses of gastropods. Those masses often contained dense populations of microalgae and cyanobacteria, which produced substantial photosynthetic oxygen when illuminated. In the dark, oxygen levels fell almost to zero in central parts of the gel matrix due to respiration by the eggs, and possibly also by the



**Figure 4.** Change in percent cover of epibionts on pycnogonids from the oviger use assay ($n = 8$ per group) and from the wax assay ($n = 16$ per group). Changes occurred over two weeks. Bold lines indicate the median, boxes indicate quartiles, and lines represent minimum (min) and maximum (max) extremes.

unicells. In our study, the relatively high levels of oxygen in darkness may have reflected the location and arrangement of epibionts on the cuticle, where they were exposed directly to moving water. They may also have reflected the low metabolic rate of the epibionts on the pycnogonids, or the pycnogonids themselves relative to the gastropod egg masses.

How important is oxygen production by epibionts in nature? The answer depends on available levels of light, which, in our study, varied significantly across collection sites. We collected some pycnogonids at depths of 20–30 m and on the undersides of submerged concrete blocks—sites that likely received very little light and would support very



**Figure 3.** Representative trace of oxygen concentration through epibionts. From the origin, the first two arrowheads indicate measurements made above and below epibionts during the light treatment, and the third arrowhead marks the transition to the dark treatment. The first arrowhead marks the oxygen level at the top of the epibiont layer; the second arrowhead marks the oxygen level at bottom of epibionts. The dashed line indicates baseline oxygen level of ambient water.
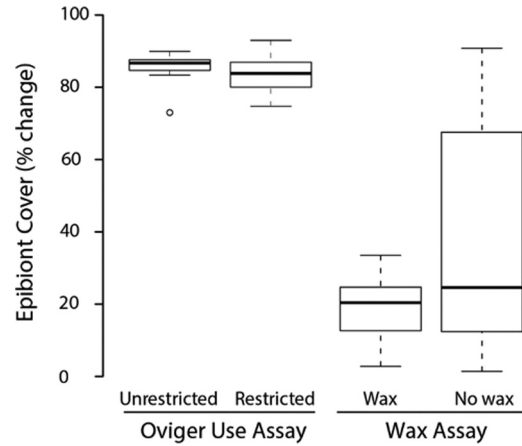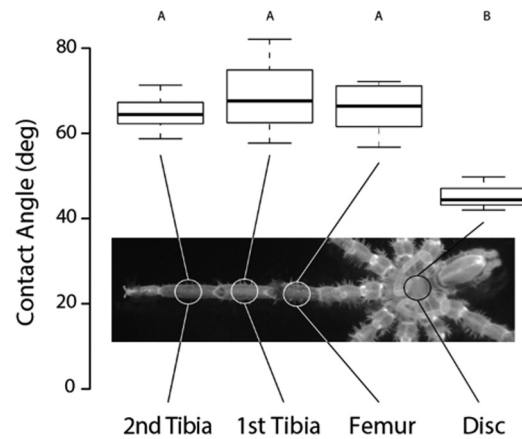


**Figure 5.** Cuticle wettability for different leg segments and body. Groups that do not share a letter are significantly different ($n = 8$ per group), repeated-measures analysis of variance. Bold lines indicate the median, boxes indicate quartiles, and lines represent minimum (min) and maximum (max) extremes.

low levels of photosynthesis. For example, at 25 m, red (700 nm) is completely attenuated, blue (420 nm) is 90% of value at the surface, and ultraviolet (326 nm) is about 50% of surface level (Denny, 1993). We collected other pycnogonids at just 1–2-m depth, which were well-lighted during daylight hours. At these depths, blue and ultraviolet are virtually unchanged, and red is attenuated to approximately 60% to 70% of its value in air (Denny, 1993). These are the locations in which photosynthesis could play a significant role in altering local levels of oxygen.

Several species of pycnogonids have been reported to use their ovigers to groom their cuticles (King, 1973; Arnaud and Bamber, 1987; Davenport *et al.*, 1987; Bamber, 2007). Our study, however, is the first to experimentally test the role of the ovigers in grooming. Here two species of *Achelia* showed no increase in epibiont coverage after two weeks when their ovigers were disabled (Fig. 4). Pycnogonid ovigers can be classified into two types: those with compound spines and those without; compound spines appear to be necessary for grooming (Bamber, 2007). Species within the genus *Achelia* lack compound spines on their ovigers. Our results, therefore, are consistent with the hypothesis that pycnogonids lacking compound spines do not groom (Bamber, 2007). A more powerful test of this hypothesis would experimentally test the effectiveness of grooming in species that do possess compound spines.

In many marine invertebrates, waxes alter cuticular wettability by rendering the cuticle more hydrophobic, which has been hypothesized to make it more difficult for epibionts to attach (Finlay *et al.*, 2002; Dahlström *et al.*, 2004; Sun *et al.*, 2012). The attachment hypothesis leads to several specific predictions, namely, cuticle wettability should in general be low, epibiont coverage should vary positively with wettability, and experimental increases in wettability should stimulate the growth of epibionts. Our results largely do not support these predictions. In *Achelia*, cuticle wettability was high (contact angles $< 90°$; Fig. 5) and, although it varied between legs and trunk, the densities of epibionts did not. Similarly, removing waxes gave inconclusive results. There was some evidence that waxes (or chemicals present in those waxes; see Fahrenbach, 1994, and Melzer *et al.*, 1996) on pycnogonids prevent epibiont attachment (Fig. 4; paired *t*-test), but our nonparametric analysis did not support this conclusion. Furthermore, like pycnogonids, decapod crustaceans had low contact angles and no covariation between contact angle and density of epibionts (Becker *et al.,* 2000). Together, these results suggest that the wettability-attachment hypothesis should be discarded, at least for marine arthropods.

This is the first study to assess how macroepibionts affect gas exchange in adult marine invertebrates. Using two species of temperate pycnogonids, we have shown that macroepibionts do not restrict local oxygen availability, and, in some cases, they may raise local oxygen levels. However,

epibionts may incur other negative effects not explored here. For example, encrusting epibionts can restrict movement of their hosts, which may make them more prone to predation; these effects have been suggested to occur in pycnogonids (Key *et al.*, 2013). Indeed, heavily fouled individuals in our study appeared less mobile due to algae wrapped around their legs. Increased weight and drag could also make the host more likely to be dislodged from the hydroids on which it lives. Furthermore, epibionts growing on the pycnogonids' eyes, palps, or sensory setae could interfere with finding food and mates, or sensing predators. In our study, many of the pycnogonids were only lightly fouled when they were initially brought into the lab.

Therefore, these animals must in some way prevent epibiont growth and attachment. Future experiments will explore other potential mechanisms of control, including molting (Thomas *et al.*, 1999), taking advantage of strong currents to remove loosely attached epibionts (Wolff, 1959), and nocturnality, which can reduce the growth of algae (Becker and Wahl, 1996). Future studies should also determine whether pycnogonids structure their cuticles to recruit epibionts—for camouflage or to control infections (Armstrong *et al.*, 2000; Dougherty and Russell, 2005). Perhaps pycnogonids frequently support epibionts because the positive effects derived from them are stronger than previously suspected.

## Literature Cited

**Armstrong, E., K. G. Boyd, and J. G. Burgess. 2000.** Prevention of marine biofouling using natural compounds from marine organisms. *Biotechnol. Annu. Rev.* **6:** 221–241.

**Arnaud, F., and R. N. Bamber. 1987.** The biology of pycnogonida. *Adv. Mar. Biol.* **24:** 1–96.

**Bamber, R. N. 2007.** A holistic re-interpretation of the phylogeny of the Pycnogonida Latreille, 1810 (arthropoda). Pp. 295–312 in *Linnaeus Tercentenary: Progress in Invertebrate Taxonomy (Zootaxa 1668)*, Z.-Q. Zhang and W. A. Shear, eds. Magnolia Press, Auckland, NZ.

**Bauer, R. T. 1981.** Grooming behavior and morphology in the decapod crustacea. *J. Crustac Biol.* **1:** 153–173.

**Bauer, R. T. 2013.** Adaptive modification of appendages for grooming (cleaning, antifouling) and reproduction in the Crustacea. Pp 337–375 in *Functional Morphology and Diversity*, L. Watling and M. Thiel, eds. Oxford University Press, New York.

Becker, K., and M. Wahl. 1996. Behaviour patterns as natural antifouling mechanisms of tropical marine crabs. *J. Exp. Mar. Biol. Ecol.* **203:** 245–258.

Becker, K., T. Hormchong, and M. Wahl. 2000. Relevance of crustacean carapace wettability for fouling. *Hydrobiologia* **426:** 193–201.

Bers, A. V., and M. Wahl. 2004. The influence of natural surface microtopographies on fouling. *Biofouling* **20:** 43–51.

Burnett, L. E., J. D. Holman, D. D. Jorgensen, J. L. Ikerd, and K. G. Burnett. 2006. Immune defense reduces respiratory fitness in *Callinectes sapidus*, the Atlantic blue crab. *Biol. Bull.* **211:** 50–57.

Callow, M. E., A. R. Jennings, A. B. Brennan, C. E. Seegert, A. Gibson, L. Wilson, A. Feinberg, R. Baney, and J. A. Callow. 2002. Microtopographic cues for settlement of zoospores of the green fouling alga *Enteromorpha*. *Biofouling* **18:** 229–236.

Carlton, J. T., ed. 2007. *The Light and Smith Manual: Intertidal Invertebrates from Central California to Oregon*, 4th ed. University of California Press, Berkeley, CA. 1019 p.

Chung, K. K., J. F. Schumacher, E. M. Sampson, R. A. Burne, P. J. Antonelli, and A. B. Brennan. 2007. Impact of engineered surface microtopography on biofilm formation of *Staphylococcus aureus*. *Biointerphases* **2:** 89–94.

Cohen, C. S., and R. R. Strathmann. 1996. Embryos at the edge of tolerance: effects of environment and structure of egg masses on supply of oxygen to embryos. *Biol. Bull.* **190:** 8–15.

Cole, L. J. 1904. Pycnogonida of the west coast of North America. *Harriman Alaska Expedition* **10:** 249–330.

Dahlström, M., H. Jonsson, P. R. Jonsson, and H. Elwing. 2004. Surface wettability as a determinant in the settlement of the barnacle *Balanus improvisus* (DARWIN). *J. Exp. Mar. Biol. Ecol.* **305:** 223–232.

Davenport, J., N. Blackstock, D. A. Davies, and M. Yarrington. 1987. Observations on the physiology and integumentary structure of the Antarctic pycnogonid *Decolopoda australis*. *J. Zool.* **211:** 451–465.

Davis, A. R., N. M. Targett, O. J. McConnell, and C. M. Young. 1989. Epibiosis of marine algae and benthic invertebrates: natural products chemistry and other mechanisms inhibiting settlement and overgrowth. *Bioorg. Mar. Chem.* **3:** 85–114.

Denny, M. W. 1993. *Air and Water: The Biology and Physics of Life's Media*. Princeton University Press, Princeton, NJ. 341 p.

Dougherty, J. R., and M. P. Russell. 2005. The association between the coquina clam *Donax fossor* Say and its epibiotic hydroid *Lovenella gracilis* Clarke. *J. Shellfish Res.* **24:** 35–46.

Dyrynda, P. E. J. 1986. Defensive strategies of modular organisms. *Philos. Trans. R. Soc. Lond. B Biol. Sci.* **313:** 227–243.

Epstein, A. K., B. Pokroy, A. Seminara, and J. Aizenberg. 2011. Bacterial biofilm shows persistent resistance to liquid wetting and gas penetration. *Proc. Natl. Acad. Sci. USA* **108:** 995–1000.

Fahrenbach, W. H. 1994. Microscopic anatomy of Pycnogonida: I. Cuticle, epidermis, and muscle. *J. Morphol.* **222:** 33–48.

Feifarek, B. P. 1987. Spines and epibionts as antipredator defenses in the thorny oyster *Spondylus americanus* Hermann. *J. Exp. Mar. Biol. Ecol.* **105:** 39–56.

Finlay, J. A., M. E. Callow, M. P. Schultz, G. W. Swain, and J. A. Callow. 2002. Adhesion strength of settled spores of the green alga *Enteromorpha*. *Biofouling* **18:** 251–256.

Gil-Turnes, M. S., M. E. Hay, and W. Fenical. 1989. Symbiotic marine bacteria chemically defend crustacean embryos from a pathogenic fungus. *Science* **246:** 116–118.

Hilton, W. A. 1939. A preliminary list of pycnogonids from the shores of California. *J. Entomol. Zool.* **31:** 27–35.

Key, M. M., Jr., J. B. Knauff, and D. K. A. Barnes. 2013. Epizoic bryozoans on predatory pycnogonids from the South Orkney Islands, Antarctica: "If you can't beat them, join them:" fouled pycnogonids from Antarctica. Pp. 137–153 in *Bryozoan Studies 2010*, Lecture Notes in Earth System Sciences 143, A. Ernst, P. Schäfer, and J. Scholz, eds. Springer, Heidelberg.

King, P. E. 1973. *Pycnogonids*. Hutchinson, London. 144 p.

Kozloff, E. N., and L. H. Price. 1996. *Marine Invertebrates of the Pacific Northwest.* University of Washington Press, Seattle, WA. 539 p.

Larkum, A. W. D., E.-M. W. Koch, and M. Kühl. 2003. Diffusive boundary layers and photosynthesis of the epilithic algal community of coral reefs. *Mar. Biol.* **142:** 1073–1082.

Melzer, R. R., M. Heβ, C. Dunkel, P. Ludwig, and U. Smola. 1996. Fine structure of the "slit organs" of the pycnogonid *Anoplodactylus petiolatus* (Anoplodactylidae). *Acta Zool.* **77:** 167–171.

Pipe, A. R. 1982. Epizoites on marine invertebrates: with particular reference to those associated with the pycnogonid *Phoxichilidium tubulariae* Lebour, the amphipod *Caprella linearis* (L.) and the decapod *Corystes cassivelaunus* (Pennant). *Chem. Ecol.* **1:** 61–74.

R Core Team. 2013. *R: A Language and Environment for Statistical Computing* [Online]. R Foundation for Statistical Computing, Vienna, Austria. Available: http://www.R-project.org/ [2015, June 1].

Rasband, W. S. 2014. *ImageJ* [Online]. U. S. National Institutes of Health, Bethesda, MD. Available: http://imagej.nih.gov/ij/ [2015, June 1].

Richmond, M. D., and R. Seed. 1991. A review of marine macrofouling communities with special reference to animal fouling. *Biofouling* **3:** 151–168.

Roberts, R. D., N. P. Revsbech, and L. R. Damgaard. 2007. Effect of water velocity and benthic diatom morphology on the water chemistry experienced by postlarval abalone. *J. Shellfish Res.* **26:** 745–750.

Russell, F. E. 1984. Marine toxins and venomous and poisonous marine plants and animals (invertebrates). *Adv. Mar. Biol.* **21:** 59–217.

Satuito, C. G., K. Shimizu, and N. Fusetani. 1997. Studies on the factors influencing larval settlement in *Balanus amphitrite* and *Mytilus galloprovincialis*. *Hydrobiologia* **358:** 275–280.

Scardino, A., R. De Nys, O. Ison, W. O'Connor, and P. Steinberg. 2003. Microtopography and antifouling properties of the shell surface of the bivalve molluscs *Mytilus galloprovincialis* and *Pinctada imbricata*. *Biofouling* **19:** 221–230.

Scholnick, D. A., K. G. Burnett, and L. E. Burnett. 2006. Impact of exposure to bacteria on metabolism in the penaeid shrimp *Litopenaeus vannamei*. *Biol. Bull.* **211:** 44–49.

Shine, R., F. Brischoux, and A. J. Pile. 2010. A seasnake's colour affects its susceptibility to algal fouling. *Proc. R. Soc. Lond. B Biol. Sci.* **277:** 2459–2464.

Sokal, R. R., and F. J. Rohlf. 1981. *Biometry: The Principles and Practice of Statistics in Biological Research,* 2nd ed. W. H. Freeman, San Francisco.

Smirnov, N. N. 2014. *Physiology of the Cladocera*. Academic Press, London. 352 p.

Sun, M., A. Liang, G. S. Watson, J. A. Watson, Y. Zheng, and L. Jiang. 2012. Compound microstructures and wax layer of beetle elytral surfaces and their influence on wetting properties. *PLoS One* **7(10):** e46710.

Thomas, E., and D. Muirhead. 2009. Impact of wastewater fouling on contact angle. *Biofouling* **25:**445–454.

Thomas, F., R. Poulin, T. de Meeüs, J.-F. Guégan, and F. Renaud. 1999. Parasites and ecosystem engineering: what roles could they play? *Oikos* **84:** 167–171.

Wahl, M. 1989. Marine epibiosis. I. Fouling and antifouling: some basic aspects. *Mar. Ecol. Prog. Ser.* **58:** 175–189.

Wahl, M., and B. Banaigs. 1991. Marine epibiosis. III. Possible antifouling defense adaptations in *Polysyncraton lacazei* (Giard) (Didemnidae, Ascidiacea). *J. Exp. Mar. Biol. Ecol.* **145:** 49–63.

Wahl, M., and F. Lafargue. 1990. Marine epibiosis. II. Reduced fouling on *Polysyncraton lacazei* (Didemnidae, Tunicata) and proposal of an antifouling potential index. *Oecologia* **82:** 275–282.

**Wahl, M., and H. Sönnichsen. 1992.** Marine epibiosis. IV. The periwinkle *Littorina littorea* lacks typical antifouling defences: why are some populations so little fouled? *Mar. Ecol. Prog. Ser.* **88:** 225–235.

**Wahl, M., F. Goecke, A. Labes, S. Dobretsov, and F. Weinberger. 2012.** The second skin: ecological role of epibiotic biofilms on marine organisms. *Front. Microbiol.* **3:** 292. doi: 10.3389/fmicb.2012.00292.

**Wicksten, M. K. 1980.** Decorator crabs. *Sci. Am.* **242:** 116–122.

**Witman, J. D., and T. H. Suchanek. 1984.** Mussels in flow: drag and dislodgement by epizoans. *Mar. Ecol. Prog. Ser.* **16:** 259–268

**Wolff, T. 1959.** Epifauna on certain decapod crustacea. Pp. 1060–1061 in *Proceedings of the 15th International Congress of Zoology, London,* H. R. Hewer and N. D. Riley, eds. International Congress of Zoology, London.

**Woods, H. A., and R. D. Podolsky. 2007.** Photosynthesis drives oxygen levels in macrophyte-associated gastropod egg masses. *Biol. Bull.* **213:** 88–94.

**Yuan, Y., and T. R. Lee. 2013.** Contact angle and wetting properties. Pp. 3–34 in *Surface Science Techniques*, Springer Series in Surface Sciences 51, G. Bracco and B. Holst, eds. Springer, Heidelberg.

**Chapter 4:** Costs of epibionts on Antarctic sea spiders

Steven J. Lane[1], Bret W. Tobalske[1], Amy L. Moran[2], Caitlin M. Shishido[2], and H. Arthur Woods[1]

[1]Division of Biological Sciences, University of Montana, Missoula, MT 59812, USA

[2]Department of Biology, University of Hawai'i at Mānoa, Honolulu, HI 96822, USA

**Abstract**

Nearly all marine animals harbor epibionts, organisms colonizing their body surfaces. Depending on where they occur on their host, epibionts can impose costs or provide benefits. For example, epibionts attached to the gills of marine arthropods can alter available oxygen levels via photosynthesis or respiration. Additionally, macroepibionts (e.g., kelp or barnacles) attached to host's limbs or body can increase the weight and drag of the host, which may increase costs of locomotion or make the host more prone to dislodgement by hydrodynamic forces. We examined the effects of macroepibionts on gas exchange, locomotion, and drag of three species of Antarctic sea spiders (pycnogonids). Epibionts had only minor effects on surface oxygen levels, but epibionts reduced the functional diffusion coefficient of oxygen through the cuticle by about half. Although these effects are significant locally and may be severe in individuals with high coverage by epibionts, the total coverage on most individuals was not high enough to significantly alter oxygen fluxes into the animal. Epibionts had no effect on host walking speeds, but they did double or triple the drag experienced by host sea spider. This likely increases the energetic costs of walking and increases the chance of being dislodged and swept into the water column by high currents. These results suggest that epibionts can impose a number of costs to their hosts but only in subtle ways that depend on total epibiont coverage of the host and rates of water flow.

**Introduction**

In marine environments, sessile organisms often colonize the surfaces of other organisms and are referred to as epibionts (Wahl, 1989). Common epibionts include bryozoans (Key et al., 1996), barnacles (Christie and Dalley, 1987), mussels (Poulter et al., 2017), and microorganisms, such as bacteria, diatoms, and microalgae (Wahl, 1989). These epibionts can impose numerous costs on their hosts, and their impact largely depends on where they occur on the host.

Epibionts growing on their host's respiratory structures, for example, can alter oxygen transport in a number of ways. Epibionts attached to gills may reduce respiratory surface area, or reduce external oxygen levels by taking up oxygen before it has a chance to enter the host's body (Gannon and Wheatly, 1992; Wahl and LaFargue, 1990). Bacteria within the gill chamber of crustaceans reduce host respiratory function by reducing oxygen levels and impeding hemolymph flow to the gills, which results in lower whole-body metabolism (Burnett et al., 2006; Scholnick et al., 2006). Mussels and barnacles are often found in crustacean and horseshoe crab gill chambers, but whether they impede gas exchange by their host is unknown (Botton, 2009; Jeffries et al., 1982). Not all effects are negative, however. Photosynthetic epibionts on external respiratory structures can increase available oxygen for gas exchange and may be beneficial (Lane et al., 2016). For example, photosynthesis by algal epibionts on sea snakes prolong dives by increasing the amount of oxygen the snakes absorb through cutaneous respiration (Shine et al., 2010).

Epibionts growing on their host's trunk or appendages can also increase their host's weight and drag (Watling and Thiel, 2013). For example, algal epibionts increase, by 2- to 6-fold, the local water velocity experienced by mussels, both by extending out of the mussel's boundary layer and into faster flow velocities and by increasing the mussels' projected surface area (Witman and Suchanek, 1984). Mussels with algal epibionts are most likely to be dislodged by high flows (Witman and Suchanek, 1984). Larger weight and higher drag can also influence how animals move and the costs of that movement. For instance, heavy loads of algal epibionts increase drag on sea snakes by disrupting the laminar flow of water across its body, resulting in substantially reduced swimming speeds (Avolio et al., 2006; Shine et al., 2010). Similarly, barnacles growing on snails more than triple the weight of their host and greatly reduces the host's crawling speed (Buschbaum and Reise, 1999). Increased weight may also raise energy

expenditure. Fouled snails have reduced growth rates, likely due to resource allocation from growth to locomotion (Wahl, 1996; 1997).

Sea spiders (class Pycnogonida) have long been observed to harbor epibionts (Gordon, 1932) but little is known about their effects (Pipe, 1982, Key et al. 2013; Lane et al., 2016) and only one study has explored their physiological effects (Lane et al., 2016). Sea spiders may be especially prone to the negative effects of epibionts because they lack gills and rely on the diffusion of oxygen across their cuticle (Davenport et al., 1987; Lane et al., *in review*). Epibionts may have multiple effects on sea spider behavior and physiology. Here, we predict that relatively large epibiotic barnacles increase drag, while encrusting epibionts impede gas exchange by blocking oxygen from diffusing across the cuticle (Fig. 1). Here, we tested these ideas by focusing on how macroepibionts influence host drag, locomotion, and gas exchange in three species of Antarctic sea spiders.

**Methods**

Animals were collected via SCUBA between 5 and 36 m depth in McMurdo Sound, Antarctica (77° 85' S, 166° 84' E) in October and November 2015 and 2016. Animals were returned to McMurdo Station and kept in seawater tables (-1 to 0 °C) until used in experiments, typically within two weeks.

Laboratory experiments were conducted on three species of sea spiders: *Ammothea glacialis*, *Colossendeis megalonyx*, and *Nymphon australe*. In the field and in video analyses, tests were conducted on animals within the genera *Ammothea* and *Colossendeis*. Due to subtle differences between species within each genus, we did not attempt to identify individuals to species in the field or in video analyses.

*Epibiont coverage in the wild*

We estimated the occurrence and percent coverage of macroepibionts (e.g., algae, bryozoans, barnacles) on *Ammothea*, *Colossendeis*, and *Nymphon* from videos and collections taken in the field. Individuals used in the scatter tests (see *Locomotion and Drag* section below for experimental details) were also counted for the presence or absence of any macroepibionts. Forty-four individual *Nymphon* and an additional 20 *Colossendeis* individuals were haphazardly collected from the field and their epibiont coverage was recorded. The percent cover of

macroepibionts was estimated by calculating the surface area of just the dorsal side of the animal in imageJ (v1.49) (Rashband 2014), and dividing by the total surface area of epibionts on the same side of the host. Measuring the percent of epibionts on the dorsal side was justified because barnacles were only found on the dorsal side and bryozoans and algae wrapped around the entire body area (e.g., leg segment) in a congruent manner, where they covered similar surface area on the dorsal and ventral sides. The percent coverage was then averaged across every individual for each species (regardless of collection site) (n = 38 *Ammothea*, 107 *Colossendeis*, 44 *Nymphon australe*).

*Oxygen levels through epibionts*

Oxygen levels through epibionts were measured following the methods of Lane et al. (2016). Living sea spiders were strapped to a piece of nylon to prevent movement and held underwater in a plastic container. Temperature within the container varied between -1 and 2 °C. Effects of temperature change on oxygen concentration were monitored and corrected based on measured oxygen levels in the ambient seawater. Because barnacles only appeared on the trunk of the sea spider, it is not likely that they effect the sea spider's gas exchange. Here, we only focused on sea spiders that were fouled with bryozoans and algae. We measured oxygen concentration in three locations: at the surface of unfouled sea spider cuticle, fouled cuticle (advancing the electrode tip through macroepibionts), and in the bulk water about 1 cm away from the sea spider. Oxygen concentrations at the surface of unfouled and fouled cuticle were measured in both dark and light conditions. Dark conditions were created by covering the testing chamber with black cloth and a box, while the light conditions were created using a Fiber-lite 180 illuminator (Dolan-Jenner Industries, Inc., Boxborough, MA) equipped with light guides (EKE 21 Volt, 150-watt lamp; Ushido America, Cypress, CA) with a color temperature of 3250 K. The light guides were set 15 cm from each individual, and the illuminator power was set to maximum. Measurements were made at three different clean or fouled sites that were haphazardly chosen along each sea spider. These measurements were then averaged together per site and per individual (n = 8 individuals per species).

We measured oxygen levels using a Clark-style $O_2$ microelectrode (50-µm glass tip; Unisense) connected to a picoammeter (PA2000; Unisense). The data were recorded once per second by a UI-2 acquisition interface (Sable Systems) controlled by Expedata software (v1.8.4,

Sable Systems). At the beginning of each test, the electrode was calibrated at the measurement temperature using air-bubbled and $N_2$-bubbled seawater.

*Diffusion coefficients*

Oxygen moves across sea spider cuticle via diffusion (Lane et al. 2017). Because distance is a key parameter affecting flux in diffusive systems (Dejours, 1981), it is likely that thick encrusting epibionts (e.g. bryozoans) restrict the diffusion of oxygen across the cuticle (Fig. 1 C-D). To test this, we measured the *functional* diffusion coefficients of oxygen through clean and fouled sea spider cuticle following the methods of Lane et al. (2017). In brief, diffusion coefficients of oxygen in cuticle were measured using step-change experiments, where internal oxygen levels within a leg segment were monitored as external $PO_2$ was altered (Lane et al., 2017; Woods and Moran, 2008). Leg segments were prepared and functional diffusion coefficients of oxygen in cuticle were estimated following the methods of Lane et al. (2017). Leg segments were haphazardly chosen based on presence or absence of macroepibionts. We measured functional diffusion coefficients from a clean and a fouled leg segment from eight different *A. glacialis* and nine different *C. megalonyx* and *N. australe* individuals.

*Locomotion and drag*

Escape-walking speeds of *Ammothea* and *Colossendeis* species with and without macroepibionts were measured in the field using a GoPro 3+ or GoPro 4 camera set to take an image every 10 s, with images recorded at 5 megapixels. Radial and tangential distortions imposed by the GoPro lens were removed from these images using Argus software (v1.0; Jackson et al. 2016) and de-distortion coefficients obtained using the Camera Calibrator app, Computer Vision Toolbox 8.0 in MatLab (v. 9.3; The Mathworks, Inc., Natick, MA, USA). We used a 50-cm scale placed in the center of the field of view before the trials to calibrate the images. The camera was mounted on a tripod approximately 1 m off the bottom and the area in view was illuminated using a dive light (SeaLife Sea Dragon 1500). Sea spiders with and without macroepibionts were placed by hand within the field of view. Sea spiders appeared to be photophobic and spontaneously walked away from the light. We digitized the movement of each sea spider using a custom script (DLTdv5, Hedrick, 2008) in Matlab and calculated locomotor speeds (cm s$^{-1}$) in IGOR Pro (v6, Wavemetrics, Inc., Beaverton, OR, USA). For each individual,

we calculated mean and maximum walking speed as it left the field of view, with an average walking distance per individual of approximately 50 cm. The mean and maximum velocities were averaged by epibiont condition (present or absent) and by genus. Seawater flow conditions and substrate type only varied slightly among testing locations (current $< 4$ cm s$^{-1}$ and the components of the substrate (e.g., rocks) had a diameter $< 5$ mm), so individuals from same genus were averaged across all sites. To adjust for any influence of animal size on walking speed, we divided average and maximum walking speeds by animal leg span. We measured escape locomotor speeds on 15 *Ammothea* (5 clean and 10 fouled) and 18 *Colossendeis* (12 clean and 6 fouled).

To test the effects of epibionts on host sea spider drag, we conducted drop tests using *Ammothea and C. megalonyx* with and without epibionts. A drop test consisted of dropping an individual sea spider in the water column approximately 2 m in front of a GoPro 3+ camera sampling at 30 frames s$^{-1}$ with a narrow view (1080 x 720 pixels). Drop tests were conducted within a 1 m deep aquarium tank at McMurdo station. GoPro videos were de-distorted, digitized and analyzed as described. The animals descended at constant velocity almost immediately after beginning descent. At terminal velocity, absolute drag is equal to the animal's underwater weight (Denny, 1993).

Drop tests were conducted on eight *Ammothea* and *C. megalonyx* individuals with relatively high epibiont (bryozoans and algae) loads (55.3 $\pm$ 1.7 (s.e.m.) and 27.8 $\pm$ 7.5 % cover, respectively) and 17 *Ammothea* and 33 *C. megalonyx* with clean cuticle. Additionally, we conducted drop tests on four *Ammothea* and four *Colossendeis* with barnacles and on those same individuals after the barnacles were physically removed (Fig. 1 A-B). Individuals harbored between 5 and 20 individual barnacles (*Litoscalpellum aurorae*).

*Statistical analyses*

Mean values ($\pm$ s.e.m.) are given for each variable. All statistical analyses were performed in R (v3.0.2; R Core Team 2016); type I error was set at 0.05.

External PO$_2$ at the surface of clean cuticle and through the epibionts on fouled cuticle in both light and dark conditions were compared using a linear mixed effects model with individual set as a random effect. Post-hoc comparisons were conducted using a Tukey Test.

The diffusion coefficients of oxygen through clean and fouled cuticle of *C. megalonyx* were compared using a paired t-test. Data from *A. glacialis* and *N. australis* did not meet the parametric test assumptions, so their means were compared using a Wilcoxon signed-rank test.

The effects of epibionts on host drag were compared within species, and the test varied with epibiont composition. Species of *Ammothea* and *Colossendeis* with barnacles and with barnacles removed were grouped together (due to small sample sizes) and compared using a paired Wilcoxon signed-rank test. A non-parametric test was chosen because it does not take into account variance, and therefore, the contribution of phylogeny to variance is ignored. *A. glacialis* and *C. megalonyx* individuals with encrusting epibionts (such as bryozoans) were compared to separate individuals with clean cuticle of the same species using a t-test.

Escape walking speeds, adjusted for animal leg span, of clean and fouled *Ammothea* or *Colossendeis* were compared using a t-test. Average velocity of *Ammothea* did not meet the t-test assumptions, so the means were compared using a Wilcoxon signed rank test.

## Results

### *Occurrence of fouled sea spiders*

Macroepibionts occurred on 12 of 38 (32 %) *Ammothea* individuals collected. The percent cover of epibionts on fouled individuals averaged $16.3 \pm 4.7$ %. Macroepibionts occurred on only 14 of 107 (13 %) *Colossendeis* collected, and macroepibionts covered $16.0 \pm 5.0$ % of their bodies. Lastly, macroepibionts occurred on 64 % (28 of 44) *Nymphon australe*, but only $7.3 \pm 2.4$ % of their bodies were covered. In *A. glacialis* and *C. megalonyx*, macroepibionts consisted primarily of bryozoans and algae, while in *N. australe* macroepibionts consisted only of algae.

### *Oxygen levels through macroepibionts*

In all three species, exposing epibionts to light increased external $PO_2$ compared to epibionts in the dark and control conditions (Table 1; Figure 2). Only on *C. megalonyx* did epibionts in the dark reduce external $PO_2$ conditions compared to the controls.

### *Diffusion coefficients*

Macroepibionts on the surface of the cuticle reduced the functional diffusion coefficient of oxygen through the cuticle in all three species (Figure 3). In *A. glacialis*, fouled cuticle

reduced the diffusion coefficient by 40 % ($7.71 \times 10^{-7} \pm 9.02 \times 10^{-8}$ and $1.88 \times 10^{-6} \pm 2.47 \times 10^{-7}$ cm s$^{-1}$, respectively) ($W_8 = 36$, $P = 0.014$). Similarly, in *C. megalonyx*, fouled cuticle had a diffusion coefficient 50% that of clean cuticle ($6.39 \times 10^{-7} \pm 1.49 \times 10^{-7}$ and $1.22 \times 10^{-6} \pm 1.59 \times 10^{-7}$ cm s$^{-1}$, respectively) ($t_8 = 2.934$, $P = 0.019$). Finally, in *N. australe*, fouled cuticle also reduced the diffusion coefficient of the cuticle by 50 % compared to clean cuticle ($5.93 \times 10^{-7} \pm 6.88 \times 10^{-8}$ and $1.14 \times 10^{-6} \pm 1.64 \times 10^{-7}$ cm s$^{-1}$, respectively) ($W_9 = 43$, $P = 0.011$).

*Locomotion and drag*

Average and maximum escape walking speeds did not vary between clean and fouled individuals of *Ammothea* or *Colossendeis* (Table 2).

Encrusting epibionts, like algae and bryozoans, increased the absolute drag for both *Ammothea* and *Colossendeis* (Table 2; Figure 4). Epibiotic barnacles also greatly increased the absolute drag for all host sea spiders (Table 2; Figure 4).

**Discussion**

We hypothesized that macroepibionts affect sea spider gas exchange, locomotion, and drag. Our data suggest that epibionts only have small effects on surface oxygen levels. We found no significant draw down of oxygen on the sea spider surface for most animals, only a modest decrease in *C. megalonyx*. While we could experimentally increase oxygen levels using an artificial light source, it is not clear that there is enough light *in situ* for most species to benefit from increased external oxygen levels, except for very shallow-water animals in bright sunlit conditions. Additionally, epibionts had no effect on sea spider walking speeds. We did, however, find that epibionts significantly reduce the functional diffusion coefficient of oxygen across the cuticle and increase the drag the sea spiders experience, and these results are discussed in more detail below.

Macroepibionts significantly reduced the diffusion coefficient of oxygen, by about half, across all three species. The reduced diffusion coefficient likely reduces the total oxygen flux across the cuticle and can have substantial negative effects on oxygen uptake (Dejours, 1981; Lane et al., 2017). Locally, therefore, the effects of epibionts on oxygen diffusion are quite profound, but how costly is a reduction in the diffusion coefficient to oxygen uptake for the whole animal? Davenport et al. (1987) showed that when half of the sea spider's legs are covered

68

with rubber tubes, oxygen uptake is reduced by 30 %. When all of the limbs are covered, oxygen uptake is reduced by 50 %. Although the diffusion coefficient in the Davenport et al. study was effectively zero, this research suggests that severe fouling can impose costs on sea spider respiration.

Sea spiders are, however, largely free of macroepibionts. In our sample, the majority of *Colossendeis* and *Ammothea* were free of macroepibionts, and, in those that were fouled, only a small percentage of their surface area was covered. Similarly, although most *N. australe* possessed some macroepibionts, it was only a small fraction of their surface area. Only 10 individuals had fouling on over 50 % of their body surfaces (the three most fouled individuals, one *N. australe* and two *C. megalonyx*, were ~ 65 % fouled). Sea spiders, therefore, must have some mechanism for controlling macroepibionts to keep them from covering too much of their cuticle. Previous studies have hypothesized that sea spiders use specialized appendages, called ovigers, to groom their cuticle and prevent the colonization and growth of epibionts (Arnaud and Bamber, 1987). Alternatively, sea spiders periodically molt their cuticle (King, 1973), which is a common mechanism of control for many marine arthropods (Thomas et al., 1999). Because sea spiders appear to be largely unfouled by epibionts, future studies should focus their efforts on determining the mechanisms with which they keep their cuticle clean.

Macroepibionts doubled to tripled the amount of drag the host sea spiders experience. Although the increase in drag had no apparent effect on mean or maximum walking speeds, increased drag could increase the chance of dislodgement due to high flow conditions, which may limit the movement of fouled sea spiders to times of low flow as has been shown in other marine invertebrates (Lau and Martinez 2003; Martinez 1996). We know very little about the flow conditions in the benthos around the Southern Ocean. Along the benthos (at 29 m deep) at one of our field sites, Turtle Rock, current averages 3-4 cm s$^{-1}$ over the year but reaches peak flows of 27 cm s$^{-1}$ (unpublished data). During these periods of peak flow, macroepibionts likely increase the risk of dislodgement which would have a number of ecological consequences. For example, risk of dislodgement may restrict mobility which limits the animal's foraging and mating patterns (Lau and Martinez, 2003). Epibionts could also influence sea spider habitat selection by limiting fouled hosts to areas of low flow or to areas with favorable substrate types to which the sea spider can cling (Lau and Martinez, 2003). Future studies should measure the behavioral response of sea spiders with and without macroepibionts to different flow regimes to

directly measure sea spider behavior and the likelihood of dislodgement across various substrates.

In conclusion, we found that epibionts can limit local oxygen flux across the cuticle but have little effect on surface oxygen levels. Additionally, we found that epibionts increase the drag the sea spider experiences but did not affect host walking speeds. Epibionts could have other indirect effects not studied here. Barnacles on the sea spider trunk could prevent the sea spiders from achieving the correct position for copulation. Additionally, we often observed bryozoans and algae covering the sea spider's gonopores, which could interfere with laying and fertilization, as has been reported for some snails (Buschbaum and Reise 1999). These snails also have reduced growth rates as resources are allocated from growth to locomotion (Wahl, 1996; 1997). Therefore, the relatively low costs to epibionts shown here may be the results of resource allocation from other systems to that of gas exchange and locomotion. Little is known about how epibionts alter community structure within the Antarctic, and understanding the physiological effects of epibionts on individual hosts is an important first step in attempting to explain the role of epibionts on populations and the community structure of the ecosystem (Wahl, 2008; Seaborn, 2014).

## Ethical approval

All applicable international, national, and/or institutional guidelines for the care and use of animals were followed. All procedures performed in studies involving animals were in accordance with the ethical standards of the institution or practice at which the studies were conducted.

## References

Avolio C, Shine R, Pile AJ (2006) The adaptive significance of sexually dimorphic scale rugosity in sea snakes. Am Nat 167, 728–738.

Barry JP, Dayton PK (1988) Current patterns in McMurdo Sound, Antarctica and their relationship to local biotic communities. Polar Biol 8: 367-376.

Botton ML (2009) The ecological importance of horseshoe crabs in estuarine and coastal communities: a review and speculative summary. In *Biology and conservation of horseshoe crabs*. Springer US. pp. 45-63.

Burnett, LE, Holman JD, Jorgensen DD, Ikerd JL, Burnett KG (2006). Immune defense reduces respiratory fitness in *Callinectes sapidus*, the Atlantic blue crab. Biol Bull 211: 50–57.

Buschbaum C, Reise K (1999) Effects of barnacle epibionts on the periwinkle *Littorina littorea* (L.). Helgo Mar Re*s* 53: 56-61.

Botton ML (2009) The ecological importance of horseshoe crabs in estuarine and coastal horseshoe crabs in estuarine and coastal communities: a review and speculative summary. communities: a review and speculative summary. In: *Biology and conservation of Horseshoe Crabs* (Eds. J.T. Tanacredi, M.L. Botton and D. Smith). Springer, USA. pp. 45-63.

Christie AO, Dalley R (1987). Barnacle fouling and its prevention. In *Barnacle Biology* (ed. A. J. Southward), pp. 419-433. Rotterdam: A. A. Balkema.

Davenport J, Blackstock N, Davies DA, Yarrington M (1987) Observations on the physiology and integumentary structure of the Antarctic pycnogonid *Decolopoda australis*. J Zool 211: 451–465.

Dejours P (1981) *Principles of comparative respiratory physiology*, p. 265. Amsterdam, The Netherlands: Elsevier/North-Holland Biomedical Press.

Denny MW (1993) *Air and Water: The Biology and Physics of Life's Media*. Princeton University Press, Princeton, NJ. 341 p.

Gannon AT, Wheatly MG (1992) Physiological effects of an ectocommensal gill barnacle, *Octolasmis muelleri*, on gas exchange in the blue crab *Callinectes sapidus*. J Crustacean Biol 12: 11-18.

Gordon I (1932) *Pycnogonida*. Discovery Reports 6: 1-138.

Hedrick TL (2008) Software techniques for two- and three-dimensional kinematic measurements of biological and biomimetic systems. Bioinspir Biomim 3: 1-6.

Jeffries WB, Voris HK, Yang CM (1982) Diversity and distribution of the pedunculate barnacle *Octolasmis* in the seas adjacent to Singapore. J Crustacean Biol 2: 562

Key MM Jr, Jeffries WB, Voris HK, Yang CM (1996) Epizoic bryozoans, horseshoe crabs, and other mobile benthic substrates. *Bull Mar Sci* 58: 368-384.

Key MM Jr, Knauff JB, Barnes DKA (2013) Epizoic bryozoans on predatory pycnogonids from the South Orkney Islands, Antarctica: "If you can't beat them, join them:" fouled pycnogonids from Antarctica. Pp. 137–153 in *Bryozoan Studies 2010*, Lecture Notes in Earth System Sciences 143, A. Ernst, P. Schäfer, and J. Scholz, eds. Springer, Heidelberg.

Lane SJ, Shishido CM, Moran AL, Tobalske BW, Woods HA (2016) No effects and no control of epibionts in two species of temperate pycnogonids. Biol Bull 230: 165-173.

Lane SJ, Shishido CM, Moran AL, Tobalske BW, Arango CP, Woods HA (2017) Upper limits to body size imposed by respiratory–structural trade-offs in Antarctic pycnogonids. Proc R Soc B 284: 20171779.

Lau WWY, Martinez MM (2003) Getting a grip on the intertidal: flow microhabitat and substratum type determine the dislodgement of the crab *Pachygrapsus crassipes* (Randall) on rocky shores and in estuaries. J Exp Mar Bio Ecol 295: 1-21.

Martinez MM (1996) Issues for aquatic pedestrian locomotion. Amer Zool 36: 619-627.

Pipe AR (1982) Epizoites on marine invertebrates: with particular reference to those associated with the pycnogonid *Phoxichilidium tubulariae* Lebour, the amphipod Caprella linearis (L.) and the decapod *Corystes cassivelaunus* (Pennant). Chem Ecol 1: 61–74.

Poulter R, Oliver PG, Hauton C, Sanders T, Ciotti BJ (2017) Infestation of shore crab gills by a free-living mussel species. Mar Biodiv 1-6.

R Core Team (2016) *R: A Language and Environment for Statistical Computing* [Online]. R Foundation for Statistical Computing, Vienna, Austria.

Rasband WS (2014) *ImageJ* [Online]. U. S. National Institutes of Health, Bethesda, MD.

Scholnick DA, Burnett KG, Burnett LE (2006) Impact of exposure to bacteria on metabolism in the penaeid shrimp *Litopenaeus vannamei*. Biol Bull 211: 44–49.

Seaborn T (2014) Limpets and their algal epibionts: costs and benefits of *Acrosiphonia* spp and *Ulva lactuca* growth. J Mar Biol 2014: 1-7.

Shine R, Brischoux F, Pile AJ (2010) A seasnake's colour affects its susceptibility to algal fouling. Proc R Soc Lond B Biol Sci 277: 2459–2464.

Thomas F, Poulin R, de Meeüs T, Guégan J-F, and Renaud F (1999) Parasites and ecosystem engineering: what roles could they play? Oikos 84: 167–171.

Wahl M, Goecke F, Labes A, Dobretsov S, Weinberger F (2012) The second skin: ecological role of epibiotic biofilms on marine organisms. Front Microbiol 3: 292. doi: 10.3389/fmicb.2012.00292.

Wahl M, Lafargue F (1990) Marine epibiosis. II. Reduced fouling on *Polysyncraton lacazei* (Didemnidae, Tunicata) and proposal of an antifouling potential index. Oecologia 82: 275–282.

Wahl M (1989) Marine epibiosis. I. Fouling and antifouling: some basic aspects. Mar Ecol Prog Ser 58: 175–189.

Wahl M (2008) Ecological lever and interface ecology: epibiosis modulates the interactions between host and environment. Biofouling 24: 427-438.

Watling L, Thiel M (2013) *Functional morphology and diversity*. Vol. 1. Oxford University Press, New York.

Wahl M (1996) Fouled snails in flow: potential of epibionts on *Littorina littorea* to increase drag and reduce snail growth rates. Mar Ecol Prog Ser 138, 157–168.

Wahl M (1997) Increased drag reduces growth of snails: comparison of flume and in situ experiments. Mar Ecol Prog Ser 151, 291–293.

Witman JD, Suchanek TH (1984) Mussels in flow: drag and dislodgement by epizoans. Mar Ecol Prog Ser 16: 259–268

Woods HA, Moran AL (2008) Oxygen profiles in egg masses predicted from a diffusion-reaction model. *J. Exp. Biol.* 211, 790–797. (doi:10.1242/jeb.014613)

**Table 1**. Linear mixed effects model results for factors affecting external $PO_2$: epibiont condition (fouled/unfouled) and light level (light or dark) on *Ammothea glacialis*, *Colossendeis megalonyx*, and *Nymphon australe*.

| Species | Variable (d.f.) | *F* | *P* |
|---|---|---|---|
| *Ammothea glacialis* | | | |
| | Epibiont condition (1) | 6.847 | 0.016 |
| | Light level (1) | 6.694 | 0.017 |
| | Interaction (1) | 9.330 | 0.006 |
| *Colossendeis megalonyx* | | | |
| | Epibiont condition (1) | 0.999 | 0.329 |
| | Light level (1) | 24.536 | < 0.001 |
| | Interaction (1) | 26.488 | < 0.001 |
| *Nymphon australe* | | | |
| | Epibiont condition (1) | 9.623 | 0.005 |
| | Light level (1) | 5.297 | 0.032 |
| | Interaction (1) | 4.439 | 0.047 |

**Table 2**. Average and maximum escape locomotor speeds, normalized for individual leg span, as well as absolute drag measurements on *Ammothea* and *Colossendeis* with fouled or clean cuticle.

| Variable | Condition | mean | ± s.e.m. | d.f. | *t*-value | *P*-value |
|---|---|---|---|---|---|---|
| Average Velocity / legspan | | | | | | |
| *Ammothea* | Fouled | 0.009 | 0.002 | 13 | 14* | 0.343 |
| | Clean | 0.006 | 0.001 | | | |
| *Colossendeis* | Fouled | 0.007 | 0.002 | 16 | 1.646 | 0.119 |
| | Clean | 0.015 | 0.003 | | | |
| Maximum Velocity / legspan | | | | | | |
| *Ammothea* | Fouled | 0.014 | 0.002 | 13 | -0.284 | 0.781 |
| | Clean | 0.013 | 0.001 | | | |
| *Colossendeis* | Fouled | 0.015 | 0.005 | 16 | 1.133 | 0.274 |
| | Clean | 0.023 | 0.004 | | | |
| Absolute Drag | | | | | | |
| *Ammothea* | Fouled | 0.0010 | 0.0001 | 23 | 122* | 0.002 |
| | Clean | 0.0003 | 0.0001 | | | |
| *Colossendeis* | Fouled | 0.0015 | 0.0001 | 39 | 220.5* | 0.004 |
| | Clean | 0.0008 | 0.0001 | | | |

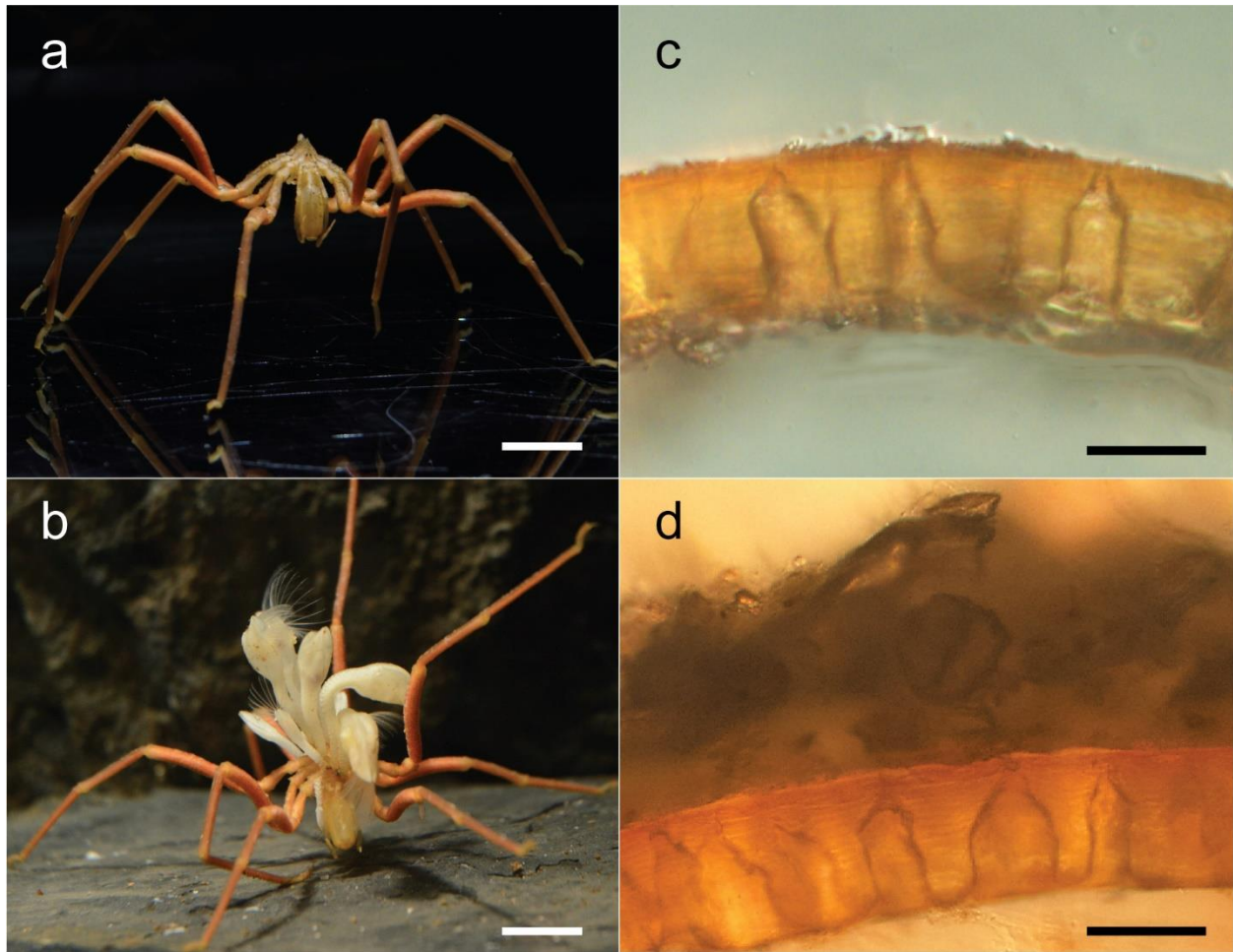| | | | | | | |
|---|---|---|---|---|---|---|
| Absolute Drag | | | | | | |
| all species | Barnacles | 0.0017 | 0.0003 | 14 | 36* | 0.008 |
| | No barnacles | 0.0006 | 0.0001 | | | |

*Wilcoxon signed rank test *W* value



**Figure 1.** Representative unfouled (A) and barnacle-fouled (B) *Ammothea glacialis* and unfouled (C) and bryozoan-fouled (D) cuticle from *Colossendeis megalonyx*. Scale bar equals 1 cm in A and B, and 100 µm in C and D. Photo credit to S.J.L. and Timothy Dwyer.
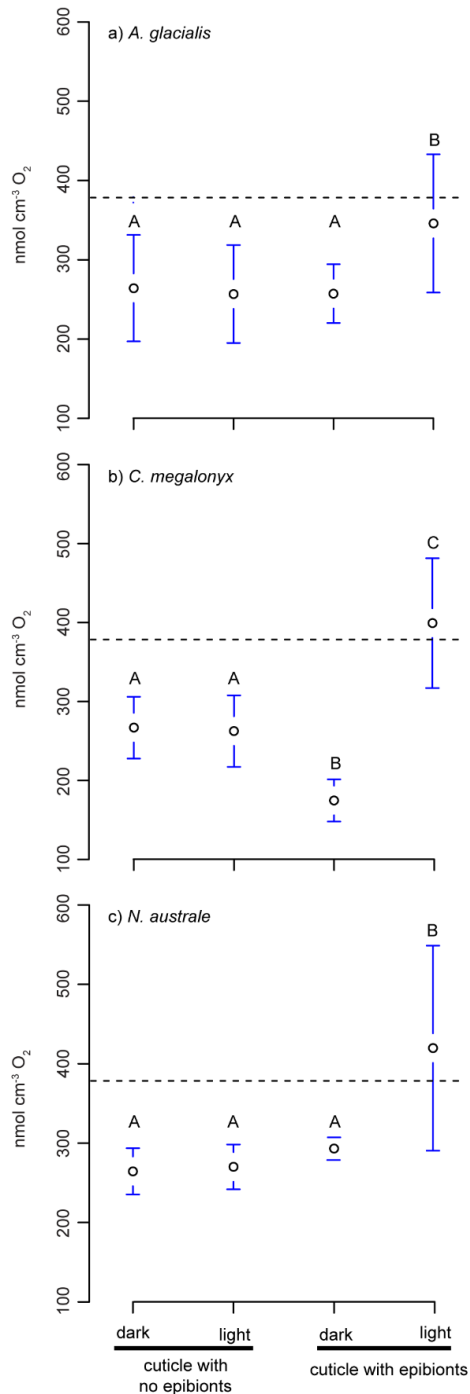
**Figure 2.** Oxygen concentration at cuticle surface on clean and at bottom of epibiont on layer fouled sea spiders in dark and light conditions for A) *Ammothea glacialis* (n = 8), B) *Colossendeis megalonyx* (n = 8), and C) *Nymphon australe* (n = 8). The dashed line represents the oxygen concentration of seawater at -1 °C. Means that do not share a letter are significantly different. Error bars represent s.e.m.
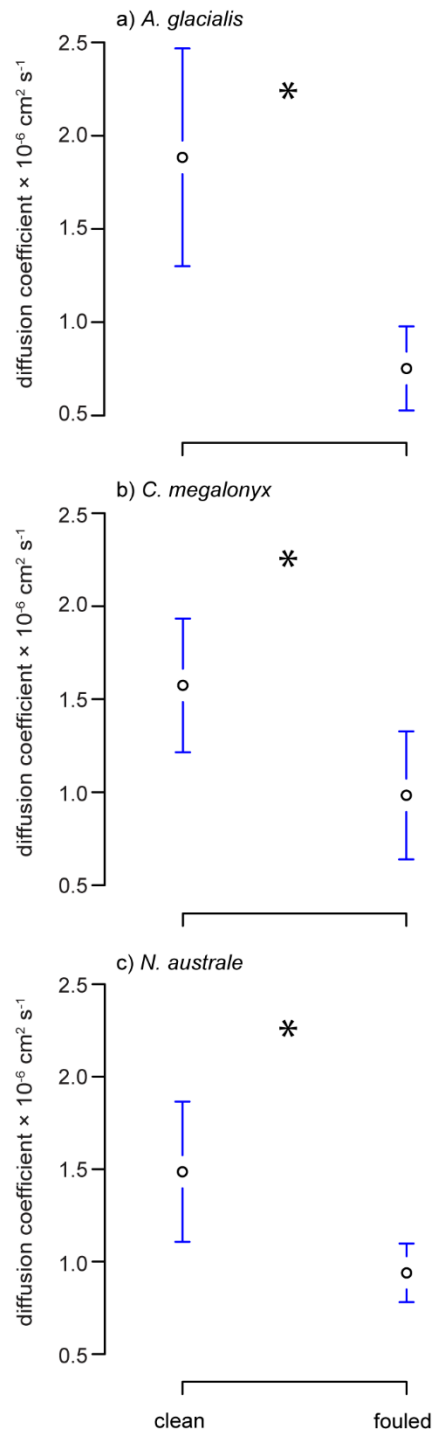
**Figure 3.** Functional diffusion coefficients of oxygen through clean and fouled cuticle for A) *Ammothea glacilias* (n = 8), B) *Colossendeis megalonyx* (n = 9), and C) *Nymphon australe* (n = 9). "*" indicates p-value < 0.05. Error bars represent s.e.m.
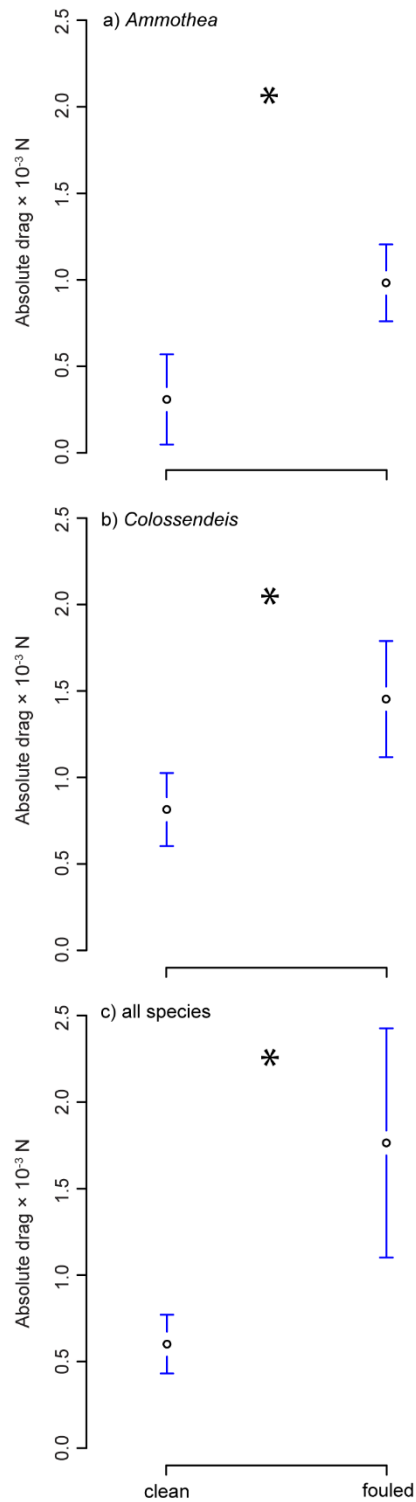
**Figure 4**. Absolute drag for clean and fouled cuticle for A) *Ammothea* (n = 25), B) *Colossendeis* (n = 41), and C) all species (n = 16). See Table 2 for description of "fouled" for each analysis. "*" indicates p-value < 0.05. Error bars represent s.e.m.